DISS. ETH NO 25663

TRAPPED: DEVELOPING AN UNBIASED APPROACH TO IDENTIFY EPOXIDE HYDROLASE SUBSTRATES *IN VIVO*

A thesis submitted to attain the degree of

DOCTOR OF SCIENCES of ETH ZURICH

(Dr. sc. ETH Zurich)

presented by

MONIKA DENGLER

MSc in Pharmaceutical Sciences, ETH Zurich

born on 18.08.1988

citizen of Oberegg AI

accepted on the recommendation of

Prof. Dr. Hanns Ulrich Zeilhofer

Prof. Dr. Ursula Quitterer and Prof. Dr. Michael Arand

2019

Für Emily und Levin

PREAMBLE

The main project entitled “Deciphering the (patho)physiologic role of epoxide hydrolases by *ex vivo* cartography of their substrate landscape” was a joint project conducted by me and Bettina Hew. Initially, it was planned that after the establishment of the trapping method in cooperation, I would focus on the three enzymes mEH, Cif and MEST and Bettina would focus on sEH, EH3 and EH4. Application of the method was not successful and a separation of the project by enzymes was not possible. During method development, I had the lead in the mass spectrometry part and Bettina Hew in the virus production and application, but the experiments and data analysis was performed with equal contribution. In my doctoral thesis I focused on the mass spectrometry analysis but to provide complete information about the project, I included the necessary results from virus production, which are described in Bettina Hew’s doctoral thesis in detail, as well. For the second project, “Kinetic analysis of Cif”, I performed all experiments and data analysis.

SUMMARY

Epoxide hydrolases (EHs) of the α/β hydrolase fold enzyme family hydrolyze epoxides to the corresponding vicinal diols. In mammals, epoxides are mainly formed within the body through epoxidation of xenobiotic or endogenous substrates by cytochrome P450-dependent monooxygenases (CYPs). Two of the five known mammalian EHs are well characterized. The microsomal epoxide hydrolase (mEH) is primarily involved in detoxification of carcinogenic epoxides derived from xenobiotic compounds and the soluble epoxide hydrolase (sEH) primarily regulates endogenous signaling epoxides derived from fatty acids. Although some substrates are known for the epoxide hydrolase 3 (EH3), its function remains unclear. For the epoxide hydrolase 4 (EH4) and mesoderm specific transcript (MEST) no substrates are known, but knockout of MEST in mice leads to growth retardation and a behavioral phenotype. Another EH with activity in the human body is the CFTR inhibitory factor (Cif), a virulence factor secreted by the opportunistic pathogen *Pseudomonas aeruginosa*. Cif reduces the surface expression of the chloride channel CFTR in human airway endothelial cells, resulting in increased mucus viscosity facilitating bacterial colonization. The enzyme activity of Cif is crucial for the effect on CFTR but the molecular target remains to be identified.

In this project, we aimed to identify the physiologically relevant substrate(s) of the aforementioned EHs. For the bacterial EH Cif, a substrate screening was performed using recombinantly expressed enzyme, but kinetic analysis suggested that the found substrates 14,15-epoxyeicosatrienoic acid (14,15-EET), 17,18-epoxyeicosatetraenoic acid, and 19,20-epoxydocosapentaenoic acid are not relevant *in vivo*. To identify relevant substrates *in vivo*, an unbiased approach was developed that takes advantage of the characteristic two-step reaction mechanism of α/β hydrolase fold EHs. By introducing a point mutation, trapping mutants of the six EHs were constructed which are able to nucleophilically attack and bind their substrates but cannot perform the second hydrolytic step, thus trapping their substrates with a covalent ester bond. Using adeno-associated viruses (AAVs), these trapping mutants were expressed in mice, where they should encounter and bind their substrates in a physiologic environment. For expression in peripheral organs of mice, the serotype AAV-rh10 was used, while the serotype AAV-PHP.B was used to target the brain after the intravenous injection of the virus into the tail vein. Successful expression in the liver was confirmed for all trapping EHs except EH3, and in the brain for mEH, sEH and EH4 by western blot analysis.

Mass spectrometry was used to identify the substrates that were trapped by the enzymes. For this, mouse tissue was lyzed and the virally expressed trapping mutants were enriched using His-tag affinity

chromatography. After digestion with trypsin, the samples were analyzed on a TripleTOF mass spectrometer using SWATH, a data independent scan mode which provides time-resolved recording of the fragment ions of all precursors. Since the sequence and therefore the mass of the peptide which carries the trapped substrate is known, the mass of the substrate can be determined.

With mass spectrometry we confirmed the presence of virally expressed mEH, sEH, Cif and MEST in the liver and mEH and sEH in the brain by detecting peptides specific for these enzymes. However, no substrate modified peptide was detected for any enzyme in any of the tissues. As proof of principle, the peptide-substrate complex of recombinantly expressed sEH incubated with 14,15-EET was detected in an *in vitro* trapping experiment confirming that the ester intermediate is stable enough for detection by mass spectrometry.

Analysis of the sample preparation procedure with synthetic peptides revealed a selective and substantial loss of the sEH, EH3, and EH4 peptides. This was probably the main problem in the analysis of the sEH expressing tissue. For mEH and MEST, only the unmodified peptide was detected, indicating that the trapping mutants were not able to bind their substrates, probably due to protein misfolding. EH3, EH4, and Cif peptides were likely not detected due to their low tissue concentrations, probably caused by a shorter half-life of these proteins. Nevertheless, successful trapping and analysis was shown *in vitro* and required measures to improve the method were identified. Establishment of the *in vivo* trapping approach and identification of EH substrates could bring fundamental insights into the role of EHs in mammalian physiology and new strategies for therapeutic intervention.

Unexpectedly, mice expressing trapping mEH in the brain developed a striking trembling phenotype which was milder in mEH KO mice and absent when wild type instead of trapping mEH was expressed. Further analysis is required but preliminary experiments suggest a loss of dopaminergic cells in the substantia nigra causing a Parkinson's disease-like pathology.

ZUSAMMENFASSUNG

Epoxidhydrolasen (EHs) der α/β hydrolase fold Enzymfamilie hydrolysieren Epoxide zu korrespondierenden Diolen. In Säugetieren werden Epoxide hauptsächlich durch Epoxidierung von Fremdstoffen oder körpereigenen Stoffen durch Cytochrom P450-abhängige Monooxigenasen (CYPs) gebildet. Zwei der fünf bekannten EHs in Säugetieren sind gut untersucht. Die mikrosomale EH (mEH), die hauptsächlich für die Entgiftung krebserregender Epoxide verantwortlich ist und die lösliche EH (sEH), die vorwiegend Fettsäureepoxide abbaut, die vom Körper als Signalstoffe verwendet werden. Von der EH3 kennt man einige Substrate, die Funktion dieses Enzyms ist jedoch noch unklar. Von der EH4 und dem mesoderm specific transcript (MEST) sind keine Substrate bekannt, MEST KO Mäuse zeigen aber eine verlangsamte Entwicklung und einen Verhaltensphänotyp. Eine weitere für den Menschen relevante EH ist der CFTR inhibitoy factor (Cif), ein Virulenzfaktor des opportunistischen Krankheitserregers *Pseudomonas aeruginosa*. Cif reduziert die Menge des Chloridkanals CFTR auf der Oberfläche von Lungenepithelzellen des Menschen, was zur Erhöhung der Mukusviskosität führt und die Kolonisierung durch Bakterien vereinfacht. Die EH-Aktivität von Cif ist relevant für diesen Effekt aber der molekulare Mechanismus ist nicht bekannt.

Das Ziel dieses Projekts war es, physiologisch relevante Substrate der sechs EHs zu finden. Für die bakterielle EH Cif wurde ein Substratscreening mit rekombinant exprimiertem Enzym durchgeführt. Kinetische Analysen mit den gefundenen Substraten 14,15-Eepoxyeicosatriensäure (14,15-EET), 17,18-Epoxyeicosatetraensäure und 19,20-epoxydocosapentaensäure deuten jedoch darauf hin, dass dies keine relevanten *in vivo* Substrate von Cif sind. Um relevante Substrate zu finden, haben wir einen unvoreingenommenen Ansatz entwickelt, der auf dem typischen, zweistufigen Reaktionsmechanismus von α/β hydrolase fold EHs basiert. Durch eine Punktmutation haben wir die EHs so verändert, dass sie ihr Substrat nicht umsetzen, sondern nur einfangen (Trappingmutanten). Die Mutanten können das Substrat nukleophil angreifen und binden, aber der zweite Schritt des Reaktionsmechanismus, die Hydrolyse und Freisetzung des Produkts, ist unterbunden und das Substrat bleibt durch eine kovalente Esterbindung ans Enzym gebunden. Mit Hilfe von Adeno-assoziierten Viren (AAVs) wurden die Trappingmutanten in Mäusen exprimiert, wo sie ihr physiologisch relevantes Substrat einfangen sollten. Für die Expression in peripheren Organen wurde der Virusserotyp AAV-rh10 benutzt und für die Expression im Gehirn der Serotyp AAV-PHP.B. Mit Western Blot Analysen wurde die virale Expression von mEH, sEH und EH4 im Gehirn und aller Trapping-EHs ausser EH3 in der Leber bestätigt.

Die gebundenen Substrate wurden mit Massenspektrometrie analysiert. Dazu wurde das Mausgewebe lysiert und die Trappingmutanten über His-tag Affinitätschromatographie angereichert. Nach proteolytischem Verdau mit Trypsin wurden die entstandenen Peptide auf einem TripleTOF Massenspektrometer mit SWATH gemessen. SWATH ist ein datenunabhängiger Scanmodus, der alle Vorläuferionen und alle Fragmente aufzeichnet. Da die Sequenz und dadurch die Masse des Peptids, an die das Substrat gebunden ist, bekannt ist, kann die Masse des gebundenen Substrats bestimmen werden.

Die virale Expression von mEH, sEH, Cif und MEST in der Leber und mEH und sEH im Gehirn konnte mit Massenspektrometrie bestätigt werden indem für diese Enzyme spezifische Peptide gemessen wurden. Ein eingefangenes Substrat konnte jedoch nicht gefunden werden, in keinem der untersuchten Gewebe. Um das Prinzip zu verifizieren, wurde ein *in vitro* Versuch durgeführt, bei dem rekombinant exprimierte sEH mit 14,15-EETs inkubiert wurde und der Peptid-Substrat-Komplex identifiziert werden konnte. Dieser Versuch bestätigt, dass der Peptid-Substrat-Komplex für die Analyse stabil genug ist.

Mit synthetischen Peptiden konnte gezeigt werden, dass die Peptide von sEH, EH3 und EH4 während der Probenaufarbeitung selektiv und in grossem Umfang verloren gingen. Dies war vermutlich das Hauptproblem bei der Analyse von sEH aus dem Gewebe. Die Peptide von mEH und MEST konnten gemessen werden, aber sie hatten kein Substrat gebunden. Dies deutet darauf hin, dass die mEH und MEST Trappingenzyme das Substrat nicht binden konnten, vermutlich aufgrund von Proteinfehlfaltung. Die Peptide von EH3, EH4 und Cif konnten in den Gewebeproben nicht detektiert werden, was vermutlich mit ihrer tiefen Konzentration, verursacht durch eine kürzere Halbwertszeit, zusammenhängt. Die Etablierung dieser Substrateinfangmethode *in vivo* und die Identifizierung von EH Substraten würde einen fundamentalen Einblick in die Rolle von EHs in der Säugetierphysiologie bringen und könnte zur Entwicklung von neuen therapeutischen Strategien führen.

Die Mäuse, die die Trapping-mEH Mutante im Gehirn exprimiert haben, haben unerwarteterweise einen Phänotyp gezeigt. Die Tiere entwickelten ein Zittern am ganzen Körper, welches sich über die Zeit verstärkte. Das Phänomen war in mEH KO Mäusen verlangsamt und trat bei Mäusen, bei denen das wildtyp mEH Enzym im Gehirn exprimiert wurde, überhaupt nicht auf. Weitere Untersuchungen werden benötig, um die Grundlage dieses Phänotyps zu verstehen. Die Daten deuten jedoch darauf hin, dass der Phänotyp durch Untergang von dopaminergen Zellen in der Substantia nigra verursacht wird, was eine Parkinson-ähnliche Pathologie hervorruft.

TABLE OF CONTENTS

GLOSSARY

AA	arachidonic acid
AAV	adeno-associated virus
ABHD	α/β-hydrolase domain-containing
ABHD7	obsolete gene name of EPHX4
ABHD9	obsolete gene name of EPHX3
ACN	acetonitrile
AEBS	microsomal antiestrogen binding site
Ala or A	alanine
Arg or R	arginine
Asn or N	asparagine
Asp or D	aspartic acid
AUC	area under the curve
B[*a*]P	benzo[*a*]pyrene
BK_{Ca}	large conductance calcium-activated potassium channel
bp	base pair(s)
CA2	region of the hippocampus
CatNuc	catalytic nucleophile
CF	cystic fibrosis
CFTR	cystic fibrosis transmembrane conductance regulator
ChEH	cholesterol epoxide hydrolase
CID	collision induced dissociation
Cif	cystic fibrosis transmembrane conductance regulator inhibitory factor
Cif HQ	Cif trapping mutant with point mutation H297Q
COPD	chronic obstructive pulmonary disease
COX	cyclooxygenase
CV	coefficient of variation
CYP	cytochrome P450-dependent monooxygenase
Cys or C	cysteine
DHA	docosahexaenoic acid
DHET	dihydroxyeicosatrienoic acid
DIA	data independent acquisition
EET	epoxyeicosatrienoic acids
EH	epoxide hydrolase
EH3	epoxide hydrolase 3
EH3 HQ	epoxide hydrolase 3 trapping mutant with point mutation H337Q
EH3 KO	epoxide hydrolase 3 knockout
EH3k	epoxide hydrolase 3 missing the N-terminal membrane anchor
EH4	epoxide hydrolase 4
EH4 HQ	epoxide hydrolase 4 trapping mutant with point mutation H336Q
EH4k	epoxide hydrolase 4 missing the N-terminal membrane anchor
ENaC	epithelial sodium channel
eNOS	endothelial nitric oxide synthase
EPA	eicosapentaenoic acid

EpDPA	epoxydocosapentaenoic acid
EpETEs	epoxyeicosatetraenoic acids
EPI	enhanced product ion
ER	endoplasmic reticulum
ESA	epoxystearic acid
ESI	electron spray ionization
EST	expression sequence tag
FA	formic acid
FASP	filter aided sample preparation
FRET	Foerster resonance energy transfer
G3BP1	Ras-GAP SH3 domain binding protein-1
GFP	green fluorescent protein
Gln or Q	glutamine
Glu or E	glutamic acid
Gly or G	glycine
HETE	hydroxyeicosatetraenoic acids
His or H	histidine
HPLC	high pressure liquid chromatography
HxA3	hepoxilin A3
HxB3	hepoxilin B3
i.v.	intravenous
IC_{50}	half maximal inhibitory concentration
IDA	information dependent acquisition
IgA	immunoglobulin A
IHC	immunohistochemistry
IMAC	immobilized metal affinity chromatography
ITR	inverted terminal repeat
kb	kilobase
k_{cat}/K_m	catalytic efficiency
K_m	Michaelis constant, substrate concentration at which the reaction rate is half maximal
KO	knockout
LC-MS/MS	liquid chromatography tandem mass spectrometry
LD	lipid droplet
LIT	linear ion trap
LOX	lipoxygenase
LPLD	familial lipoprotein lipase deficiency
LTA_4	leukotriene A_4
LTB_4	leukotriene B_4
LXA_4	lipoxin A_4
Lys or K	lysine
m/z	mass-to-charge ratio
mEH	microsomal epoxide hydrolase
mEH HQ	microsomal epoxide hydrolase trapping mutant with point mutation H431Q
mEH KO	microsomal epoxide hydrolase knockout
MEST	mesoderm specific transcript (also known as peg1)

MEST HQ	mesoderm specific transcript trapping mutant with point mutation H314Q
MEST KO	mesoderm specific transcript knockout
MOI	multiplicity of infection
MPTP	1-methyl-4-phenyl-1,2,3,6-tetrahydropyridine, neurotoxin
MRM	multiple reaction monitoring, also called selected reaction monitoring (SRM)
mRNA	messenger RNA
MS	mass spectrometer/mass spectrometry
OMV	outer membrane vesicle
ORF	open reading frame
PCR	polymerase chain reaction
Peg1	paternally expressed gene 1, see MEST
PPARγ	peroxisome proliferator-activated receptor gamma
PUFA	poly-unsaturated fatty acid
Q1, Q2, Q3	quadrupole mass filter 1, 2, 3
Qtrap	triple quadrupole linear ion trap
RPLC	reversed phase liquid chromatography
RT-PCR	reverse transcription polymerase chain reaction
SAR	scaffold attachment region
SDS-PAGE	sodium dodecyl sulfate polyacrylamide gel electrophoresis
sEH	soluble epoxide hydrolase
sEH HQ	soluble epoxide hydrolase trapping mutant with point mutation H524Q
sEH KO	soluble epoxide hydrolase knockout
Ser or S	serine
SNP	single-nucleotide polymorphism
SPE	solid phase extraction
SRM	selected reaction monitoring, alternative name for MRM
SWATH	sequential window acquisition of all theoretical spectra
TFA	trifluoroacetic acid
TOF	time-of-flight
Tyr or T	tyrosine
USP10	ubiquitin specific peptidase-10
Val or V	valine
VEGF	vascular endothelial growth factor
vg	viral genomes
V_{max}	maximal rate of enzyme catalyzed reaction
WB	western blot
WT	wild type

1. INTRODUCTION

1.1. Epoxides in the human body

An epoxide is a three-membered ring of one oxygen and two carbon atoms. Due to the electronegativity of the oxygen atom and tension in the ring, the carbon atoms possess electrophilic reactivity. Epoxide hydrolases (EHs) hydrolyze epoxides to their corresponding vicinal diol by the addition of a water molecule (Figure 1).

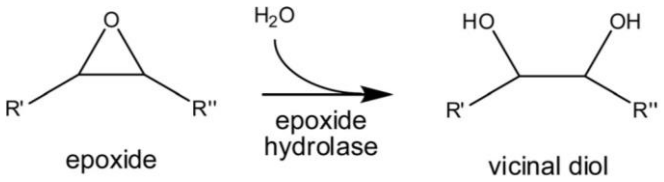

Figure 1: Epoxide hydrolysis to vicinal diol by epoxide hydrolase (EH).

In mammals, epoxides can be taken up from the environment as such but most often they are formed within the body during xenobiotic (foreign compound) metabolism, mainly in the liver. In phase I of xenobiotic metabolism, the compounds are functionalized. Different enzymes oxidize, reduce or hydrolyze xenobiotics which can then be conjugated in phase II to hydrophilic endogenous molecules such as glutathione, sulfate, glycine, or glucuronic acid, creating more hydrophilic compounds that can be excreted. The functionalization in phase I can lead to reactive intermediates, for example the epoxidation of aromatic ring systems or alkenes by cytochrome P450-dependent monooxygenases (CYPs). The generated epoxides are electrophilically reactive and potentially react with proteins and DNA bases leading to toxic or carcinogenic effects. EHs generally protect the body by hydrolyzing these epoxides to the less reactive and more water-soluble diols.

Besides xenobiotic epoxides, the body produces epoxides with important signaling function. These signaling molecules are mainly derived from fatty acids and have little genotoxic potential. A well characterized group of signaling epoxides are the epoxyeicosatrienoic acids (EETs), which are generated in the arachidonic acid cascade. (For further details about their functions see chapter 1.2.2.2.) Hydrolysis of these epoxides to the corresponding diol typically leads to the termination of the signaling function. Other endogenous epoxides found in the body are hepoxilin A3 and B3 (chemoattractants involved in neutrophil recruitment (Mrsny *et al.*, 2004)), leukotoxin and

isoleukotoxin (9,10-epoxide and 12,13-epoxide of linoleic acid generated by neutrophils during oxidative burst (Kosaka *et al.*, 1994)), leukotriene A_4 (precursor of the chemoattractant leukotriene B_4), cholesterol-5,6-epoxide, cholesterol-24,25-epoxide, and epoxides generated from eicosapentaenoic acid (EPA) and docosahexaenoic acid (DHA).

1.2. Mammalian epoxide hydrolases

In mammals, five epoxide hydrolases have been described: microsomal EH (mEH), soluble EH (sEH), epoxide hydrolase 3 (EH3), cholesterol EH (ChEH), and the leukotriene A_4 (LTA_4) hydrolase. Structural analysis further proposed that epoxide hydrolase 4 (EH4) and mesoderm-specific transcript (MEST, also known as paternally expressed gene 1 (Peg1)) also act as epoxide hydrolases but no substrate has been found to proof their activity (Kaneko-Ishino *et al.*, 1995; Decker *et al.*, 2012). Previously, it had been reported that hepoxilins were hydrolyzed by the hepoxilin hydrolase but it was shown that this turnover is performed by sEH and not by a distinct hepoxilin hydrolase (Cronin *et al.*, 2011). Among the mammalian EHs, mEH and sEH have been studied intensively over the last decades. mEH is mainly involved in xenobiotic metabolism protecting the body from reactive epoxide whereas sEH is the key player in the metabolism of signaling fatty acid-epoxides but it also complements the detoxification selectivity of mEH.

mEH, sEH, EH3, EH4, and MEST belong to the same enzyme superfamily, the α/β hydrolase fold enzymes (Arand *et al.*, 1994; Decker *et al.*, 2012). In contrast, LTA_4 hydrolase and ChEH do not belong to this enzyme superfamily. The LTA_4 hydrolase, which converts LTA_4 to LTB_4, is a member of the superfamily of zinc metallohydrolases, and epoxide hydrolysis does not result in the formation of a vicinal diol but in two hydroxyl groups that are separated by eight carbon atoms. This enzyme shows besides its epoxide hydrolase activity also zinc-dependent aminopeptidase activity (Vo *et al.*, 2018). The identity of ChEH was unknown for a long time and comparison of ChEH and mEH concerning substrate turnover and reaction mechanism suggested that ChEH belongs to a different enzyme family (Muller *et al.*, 1997). In 2010, the ChEH was identified when it was shown that ChEH activity is carried out by the microsomal antiestrogen binding site (AEBS). The enzyme is fully inhibited by AEBS ligands including tamoxifen (de Medina *et al.*, 2010).

The enzymes from the family of the α/β hydrolase fold enzymes have diverged from a common ancestor and share structural similarities along with a typical catalytic triad (Ollis *et al.*, 1992). The core of these enzymes consists of eight central β-strands connected by several α-helices (Figure 2). This α/β hydrolase fold is covered by a variable lid domain that is inserted between strand β6 and β7. The substrate binding pocket is located between the core domain and the lid domain and harbors the common catalytic triad which consists of a catalytic nucleophile (Ser, Cys or Asp), a base (His) and an

acid (Asp or Glu). In the primary sequence, these three residues are separated by a variable number of amino acids but are always in the order nucleophile – acid – histidine and in the tertiary structure they lie in close proximity (Ollis *et al.*, 1992).

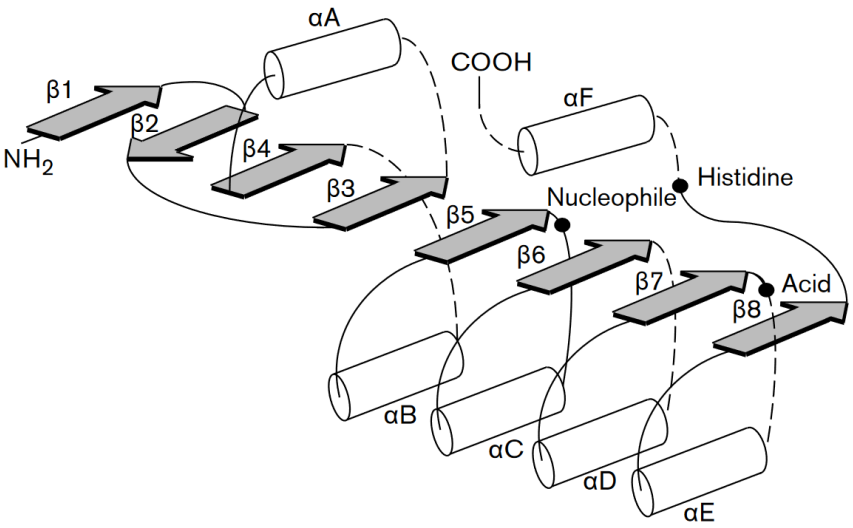

Figure 2: Secondary structure of the α/β- hydrolase fold. α-Helices are represented by white cylinders and β-strands by grey arrow. The location of the residues forming the catalytic triad is indicated by black dots. Dashed lines indicate the location of possible insertions. Figure adapted from (Nardini & Dijkstra, 1999).

The nucleophile is located in a sharp turn, the nucleophile elbow, making it accessible for the substrate. The histidine is the only residue that is absolutely conserved among the family members (Nardini & Dijkstra, 1999). Further Insertions of a few amino acid residues or even complete extra domains in the α/β hydrolase fold are possible while maintaining a conserved catalytic machinery, shaping the substrate binding site for the respective substrates (Nardini & Dijkstra, 1999).

Enzymes with different functions and very different substrates belong to the α/β hydrolase fold enzyme family, including esterases, lipases, proteases, haloalkane dehalogenases and EHs. EHs invariably use an aspartic acid as catalytic nucleophile. The feature that distinguishes EHs from other members of the α/β hydrolase fold enzyme family are two conserved tyrosine residues located in the lid domain which are important for the epoxide activation and orientation in the catalytic pocket (Nardini *et al.*, 1999). The following reaction mechanism depicted in Figure 3, which all EHs from the α/β hydrolase fold enzyme family have in common, was first proposed based on similarities to the bacterial haloalkane dehalogenase (Arand *et al.*, 1994). The two tyrosine residues from the lid domain position the epoxide in the catalytic pocket via hydrogen bonds which increases electron withdrawal from the carbon atoms adjacent to the oxygen, thus increasing their reactivity. In the first catalytic step, the oxygen of the aspartic acid attacks one of the electrophilic carbons of the epoxide and forms an ester bond resulting in opening of the ring structure. In the second catalytic step, this ester intermediate is hydrolyzed by a water molecule which is activated through proton abstraction by the

His-Asp/Glu charge relay system. This releases the diol product and the transfer of the proton from the catalytic nucleophile to the tyrosine reconstitutes the enzyme.

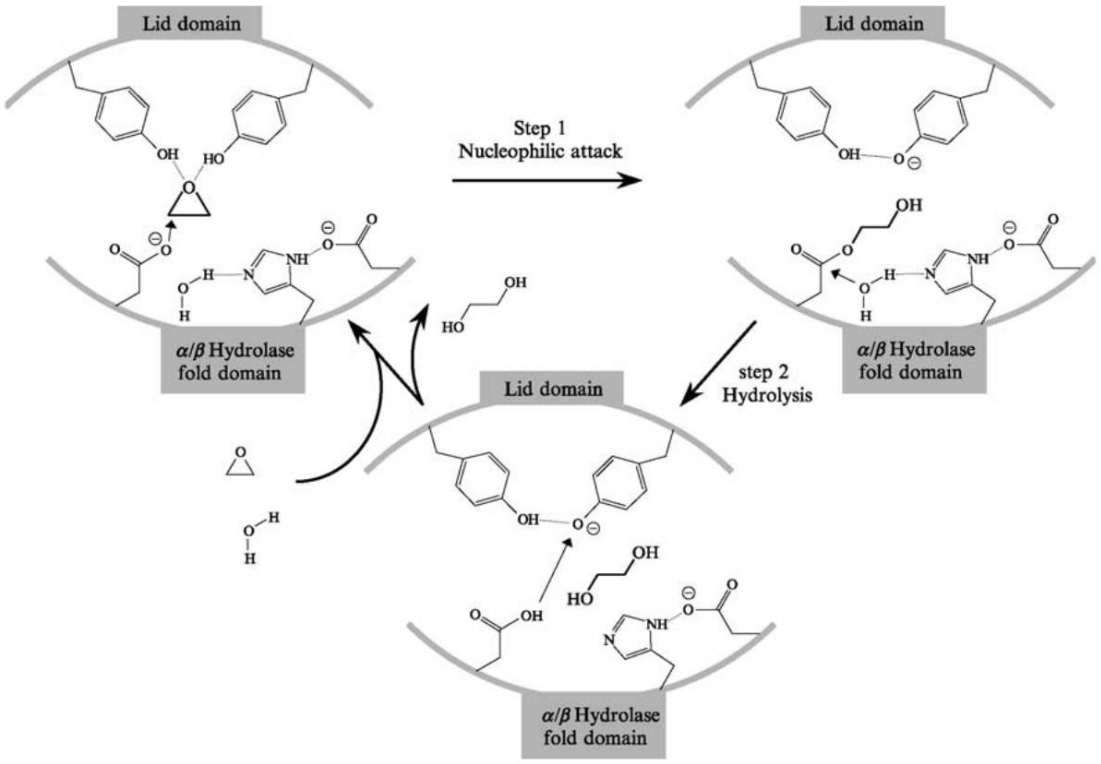

Figure 3: Enzymatic mechanism of α/β hydrolase fold epoxide hydrolases. Detailed description in the text. Figure adapted from (Arand *et al.*, 2005).

Lacourciere and Armstrong could proof the formation of the covalent enzyme-substrate intermediate with a mEH turnover experiment in $H_2{}^{18}O$. In a single-step reaction, the labelled oxygen of water would be incorporated into the product but in the mEH turnover, ^{18}O was incorporated into the protein (Lacourciere & Armstrong, 1993). Further studies showed that the first step, the formation of the ester intermediate, proceeds by several orders of magnitude faster than the second, hydrolyzing step which therefore is the rate-limiting step (Laughlin *et al.*, 1998).

1.2.1. Microsomal epoxide hydrolase

mEH, encoded by the gene EPHX1, is an endoplasmic reticulum (ER) resident enzyme consisting of 455 amino acids. The catalytic triad is formed by Asp226, Glu404, and His431 and the two tyrosine residues involved in catalysis are Tyr299 and Tyr374 (Saenz-Mendez *et al.*, 2017). Its N-terminal membrane anchor spans the ER membrane and its catalytic domain is located on the cytoplasmic side of the ER (Friedberg *et al.*, 1994; Holler *et al.*, 1997). Crystallization of a mammalian mEH has not been successful, however, a crystal structure of the related *Aspergillus niger* EH is available (Arand *et al.*,

1999b; Zou *et al.*, 2000). mEH is widely expressed in different organs with highest expression in the liver, mainly in hepatocytes, followed by the pancreas and other glands (Coller *et al.*, 2001). The expression in the brain was studied in more detail in the mouse and was found in vascular cells, in the choroid plexus epithelial cells and in some specific neuronal populations of the hippocampus, striatum, amygdala, and cerebellum, as well as in a fraction of astrocytes (Marowsky *et al.*, 2009a).

1.2.1.1. Role in xenobiotic metabolism

mEH is regarded as the major player in xenobiotic metabolism and the detoxification of reactive and potentially genotoxic epoxides. Its high expression in the liver and its broad substrate selectivity of *cis*-substituted epoxides of various sizes are supporting its position as a detoxifying enzyme. mEH hydrolyses epoxides derived from chemicals, for example styrene (Oesch, 1974; Herrero *et al.*, 1997), 1,3-butadiene (Wickliffe *et al.*, 2003), benzene (Snyder *et al.*, 1993), or polycyclic aromatic hydrocarbons (PAHs) (Shimada, 2006) and epoxides derived from pharmaceuticals such as carbamazepine (Bellucci *et al.*, 1987) or oprozomib (Wang *et al.*, 2017). This broad substrate specificity is combined with a comparatively low hydrolysis rate, for most of its substrates smaller than 1 s^{-1}. However, mEH is still a rapid detoxifier due to its two-step reaction mechanism. The first step, the formation of the ester intermediate, is sufficient to abolish the reactive potential of a toxic epoxide and thus detoxify it. Due to the up to three orders of magnitude higher rate constant of the first step compared to the second step, the consumption of the substrate is much faster than the formation of the diol product. If mEH is in excess over toxic epoxides, which can be expected from the high mEH expression in the liver, the substrate is eliminated quickly in the first step resulting in rapid detoxification (Oesch *et al.*, 2004).

In certain cases, mEH metabolism increases the carcinogenic potential of xenobiotics instead of reducing it. One example is the activation of benzo[*a*]pyrene (B[*a*]P), a compound produced by incomplete combustion of organic matter (Figure 4). CYPs epoxidize B[*a*]P which is subsequently hydrolyzed by mEH. The resulting dihydrodiol is still a substrate of CYPs and is either conjugated by phase II enzyme or epoxidized again. If the first epoxidation and subsequent hydrolysis takes place at position 7,8 and this compound is epoxidized again, B[*a*]P-7,8-dihydrdiol-9,10-epoxide is produced. This reactive bay region dihydrodiol epoxide is no longer a substrate of mEH due to steric hindrance and can only be detoxified by phase II metabolism (Shimada, 2006), which is insufficient to protect the body from its potent mutagenic effects.

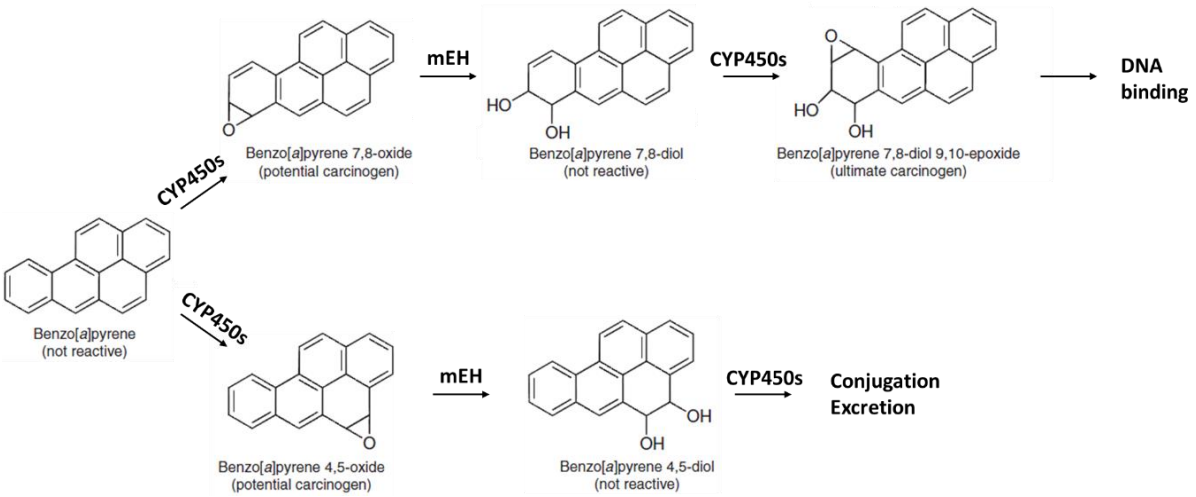

Figure 4: Selected pathways of benzo[*a*]pyrene metabolism. Formation of the benzo[*a*]pyrene 7,8-diol and subsequent epoxidation leads to an epoxide, benzo[*a*]pyrene 7,8-diol 9,10-epoxide, which is no substrate of mEH and possesses reactivity towards DNA. Epoxidation at other sites leads to metabolites that are rapidly turned over by mEH and can be conjugated and excreted.

The role of mEH in detoxification and toxification was also studied with mEH knockout (KO) mice. mEH deficient mice showed reduced carcinogenicity of 7,12-dimethylbenz[*a*]anthracene versus control animals in a skin tumorigenicity model (Miyata *et al.*, 1999) and also the toxicity of naphthalene was decreased in mEH KO mice in some locations of the lung compared to wild type (WT) mice (Carratt *et al.*, 2016). A protective effect of mEH was shown for example for 1,3-butadien. mEH deficient mice had significantly higher mutation frequencies in the Hprt reporter gene than exposed WT mice of the same strain (Wickliffe *et al.*, 2003). In general, mEH can activate some carcinogenic compounds, but it is predominantly a detoxifying enzyme.

1.2.1.2. Role in physiology

The role of mEH in xenobiotic metabolism has been studied in detail but its role in the turnover of endogenous epoxides is not yet fully understood. Endogenous substrates for mEH are some steroid epoxides, such as estroxide or androstene oxide, and epoxy-fatty acids, particularly arachidonic acid derived EETs. However, kinetic analysis showed that mEH hydrolyzes EETs less efficient than sEH, suggesting that sEH is the relevant enzyme in EETs turnover (Morisseau, 2013).

Targeted depletion of mEH in mice was used to further study the role of mEH in physiology. mEH KO mice exhibited no differences in weight, development, fertility, and behavior, and histological examination revealed no differences between mEH KO and wild type mice, indicating that mEH is not a critical requirement of normal development and physiology (Miyata *et al.*, 1999). In humans, two high frequency polymorphisms of mEH are reported at position 113 (either Tyr or His) and at position 139 (either His or Arg). No effect on enzyme kinetics has been determined but the His113/His139

haplotype is reported to have a slightly reduced half-life (Laurenzana *et al.*, 1998). The His113 variant has been associated with lower risk and a less severe course of preeclampsia (Groten *et al.*, 2014) and with a protective effect for COPD in smokers and former smokers (Brogger *et al.*, 2006). The cause of these effects is not known but a role in signaling cascades cannot be excluded (Sari *et al.*, 2017).

Recent studies support the hypothesis that mEH plays a significant role in the turnover of endogenous signaling epoxides. sEH was generally shown to hydrolyze EETs faster than mEH but they have different region-preference profiles concerning V_{max}. Fastest hydrolysis with sEH is obtained with 14,15-EET whereas mEH prefers 11,12-EET (Decker *et al.*, 2012). Analysis with plasma from mEH KO mice showed that mEH contributes substantially to the turnover of 8,9-EET and leukotoxin (Marowsky *et al.*, 2017). In addition, mEH and sEH differ in their expression pattern and subcellular localization. In the liver of mice, mEH but not sEH was detected in Kupffer cells and endothelial cells (Marowsky *et al.*, 2017). In the brain, mEH is present in specific neuronal populations in different regions and sEH is almost exclusively expressed in astrocytes (Marowsky *et al.*, 2009b). Furthermore, mEH is ER resident and very recent reports suggest a physical interaction of mEH with the epoxide forming CYP enzymes leading to substrate channeling between these two enzymes (Orjuela Leon *et al.*, 2017). Taken together, these results suggest distinctive roles of both mEH and sEH in the turnover in the endogenous fatty acid epoxides.

1.2.2. Soluble epoxide hydrolase

sEH, encoded by the gene EPHX2, consists of 554 amino acids and is present in the cell cytosol and, in some tissues such as hepatocytes and renal proximal tubules, as well in peroxisomes (Arand *et al.*, 1991; Enayetallah *et al.*, 2006). The catalytic triad consists of Asp333, His524 and Asp495 and is supported in substrate turnover by the tyrosines Tyr381 and Tyr465. A crystal structure of human sEH is available (Gomez *et al.*, 2004). In contrast to the other mammalian EHs, sEH is a bi-functional enzyme with two catalytic domains. The C-terminal domain harbors the epoxide hydrolase activity, whereas the N-terminal domain shows phosphatase activity (Cronin *et al.*, 2003). The two domains are linked by a proline-rich linker (Figure 5). The enzyme forms a homodimer where the N-terminal domain interacts with the C-terminal domain of the other monomer (Argiriadi *et al.*, 1999).

sEH is widely expressed in many different organs including liver, kidneys, heart, brain and lungs with highest activity in the liver followed by the kidneys (Pacifici *et al.*, 1988; Enayetallah *et al.*, 2004). In the mouse brain, sEH is primarily expressed in astrocytes in all areas of the brain, particularly in the cortex, hippocampus, amygdala and striatum. Neuronal expression was only found in the central amygdala (Marowsky *et al.*, 2009b).

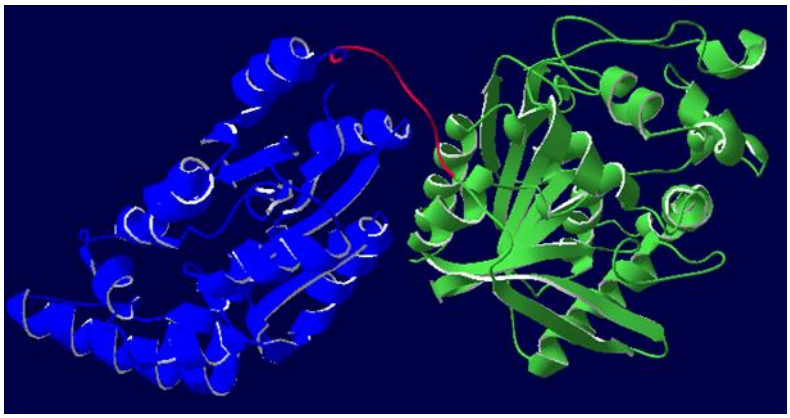

Figure 5: Three-dimensional structure of a human sEH monomer. The N-terminal phosphatase domain is shown in blue, the C-terminal EH domain in green, and the linker in red.

1.2.2.1. Role in xenobiotic metabolism

The EH that is mainly associated with xenobiotic metabolism is the mEH. However, sEH complements the substrate specificity of mEH as it is able to hydrolyze *trans*-substituted epoxides that are not too bulky. Examples are *trans*-stilbene oxide or *trans*-ethyl styrene oxide (Arand *et al.*, 2003c).

1.2.2.2. Role in physiology

It has been well established that the major function of sEH is the metabolism and control of fatty acid derived epoxides. Substrates of sEH are all regioisomeres of EET, epoxides of other PUFAs, leukotoxin, LTA_4 and hepoxilin A3 and B3 (Newman *et al.*, 2005; Cronin *et al.*, 2011). Early reports show clinical relevance of sEH in the turnover of leukotoxin to leukotoxin-diol which has been reported to be a strong mediator of acute respiratory distress syndrome (ARDS) characterized by a widespread inflammation in the lungs after severe stress conditions such as extensive body burn (Moghaddam *et al.*, 1997). Of major clinical relevance is, however, the hydrolysis of EETs. EETs are produced from arachidonic acid (AA) which is released from membrane phospholipids by phospholipase A2 upon different stimuli, such as growth factors, hormones or cytokines. AA is the precursor for three main metabolic pathways, the cyclooxygenase (COX) pathway producing prostaglandins, the lipoxygenase (LOX) pathway producing leukotriene, lipoxins and hydroxyeicosatetraenoic acids (HETEs), and the CYP pathway producing EETs and HETEs (Harizi *et al.*, 2008). The CYP pathway is perhaps the least explored eicosanoid pathway. Four possible regioisomeres of EET are formed from AA mainly by CYPs of the CYP2C and CYP2J subfamily (Figure 6).

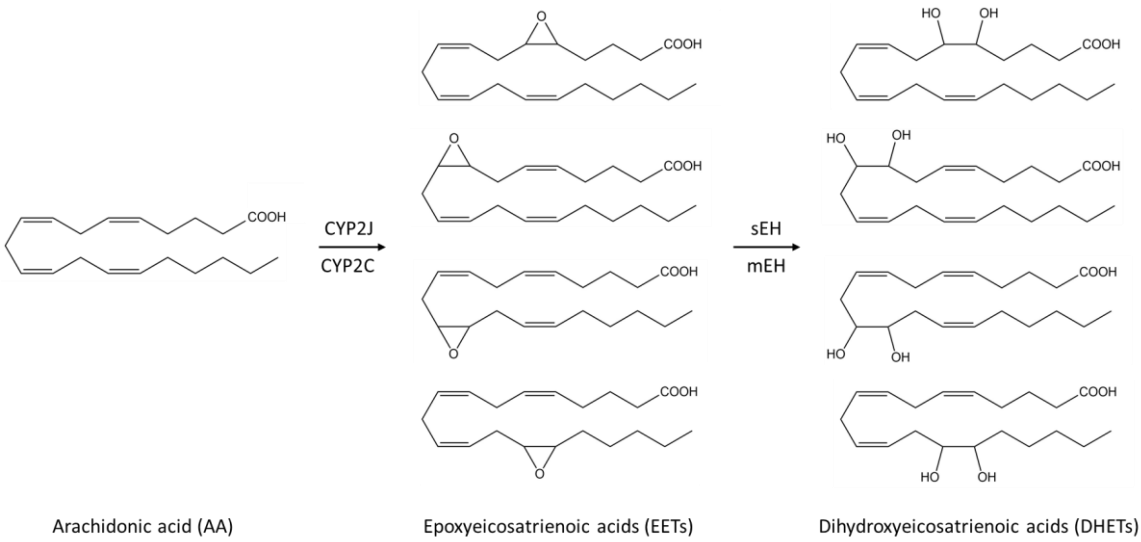

Figure 6: Synthesis of the four regioisomeres of EET from AA by CYP epoxygenases and hydrolysis by epoxide hydrolases.

The resulting EETs act as local, autocrine, or paracrine mediators and have important physiological effects such as anti-inflammation, vasodilation, analgesia, angiogenesis, antithrombotic effects, cardioprotection, and antidiabetic effects (Decker *et al.*, 2009; Campbell *et al.*, 2017). The mechanism how EETs produce their effects is not understood yet. Multiple EET targets have been identified, for example activation of large conductance calcium-activated potassium channel (BK_{Ca}) which leads to hyperpolarization and relaxation of smooth muscle cells, or inhibition of the epithelial sodium channel (ENaC) which results in increased sodium excretion in the kidney. Other targets are the IκB kinase (IKK) involved in NF-κB translocation, K_{Ca} channels and TRPA1 and TRPV4 (Sisignano *et al.*, 2012; Campbell *et al.*, 2017). Some low affinity EET receptors have been proposed, for example peroxisome proliferator-activated receptor gamma (PPARγ), however, a high affinity EET receptor has not been identified (Liu *et al.*, 2005). Different studies showed that EET actions are GTP-dependent and Gαs mediated which suggests a G-protein coupled EET receptor (Campbell *et al.*, 2017).

EET hydrolysis by sEH (or mEH) to the less active dihydroxyeicosatrienoic acids (DHETs) is thought to terminate the mostly beneficial effects. Based on this, sEH was established as a drug target and numerous studies tested the effect of sEH inhibition on inflammatory disease, neurodegenerative diseases, stroke, cardiovascular diseases, COPD, pain, metabolic syndrome, and diabetes (Morisseau & Hammock, 2013; Wagner *et al.*, 2017). For example, sEH inhibitors reduced blood pressure in angiotensin II hypertensive rats (Imig 2002) and chronic inhibition of sEH showed cardioprotective effects (Neckar *et al.*, 2012). Anti-inflammatory effects of sEH inhibition were shown in a mouse model of chronic active inflammatory bowel disease (Zhang *et al.*, 2012) and, in a different study, sEH inhibitors reduced tobacco-smoke induced lung inflammation in rats (Smith *et al.*, 2005). However, not all effects of EETs are beneficial. Panigrahy et al. analyzed the role of EETs in cancer and showed that

EETs promote metastasis by triggering secretion of VEGF by the endothelium at the secondary (metastasis) site. Furthermore, sEH inhibition promoted primary tumor growth and metastasis in mice which could lead to severe side effects in clinical use of sEH inhibitors (Panigrahy *et al.*, 2012).
Many sEH inhibitors were generated that usually carry a urea moiety as the pharmacophore. The urea was postulated to mimic the reaction intermediate resulting in a high affinity to the active site of sEH. Modern compounds show low-nanomolar to picomolar potency and exhibit good pharmacokinetics (Morisseau & Hammock, 2013). Different inhibitors went to clinical tests, for example the compound GSK2256294 was tested for COPD (Yang *et al.*, 2017) and AR9281 for hypertension and type 2 diabetes (Chen *et al.*, 2012). However, no sEH inhibitor has been approved for human applications so far.

1.2.2.3. sEH polymorphism and knockout mice

In humans, six sEH polymorphisms have been identified, Lys55Arg, Arg103Cys and Cys154Tyr in the phosphatase domain and Arg287Gln, Val422Ala and Glu470Gly in the EH domain. The Arg287Gln and Arg103Cys variant showed decreased EH activity and the double mutant had a 10-fold decreased catalytic efficiency compared to the WT enzyme combined with a reduced stability (Przybyla-Zawislak *et al.*, 2003). The two SNPs also decreased the phosphatase activity whereas Lys55Arg, Cys254Tyr increased phosphatase activity *in vitro*. The Arg287Gln was associated with increased risk for coronary artery calcification in African-American but not Caucasian (Fornage *et al.*, 2004), increased risk for ischemic stroke in white Europeans (Gschwendtner *et al.*, 2008) and insulin resistance in Japanese type 2 diabetic patients (Ohtoshi *et al.*, 2005). In patients with IgA nephropathy, Arg287Gln was associated with a positive effect on kidney survival (Lee *et al.*, 2011).
sEH KO mice showed no obvious phenotype and developed and reproduced normally. The first sEH KO mouse line produced exhibited reduced systolic blood pressure in male but not female animals (Sinal *et al.*, 2000). In contrast, a second sEH KO line did not show a difference in baseline blood pressure (Luria *et al.*, 2007). In both studies, the epoxy fatty acid metabolism was impaired in sEH deficient mice.

1.2.2.4. sEH phosphatase domain

The role of the sEH phosphatase domain is not fully understood. Substrates are threo-9/10-phosphonooxy-hydroxy-octadecanoic acid, polyisoprenyl phosphates, sphingosine-1-phosphate and lysophosphatidic acid (Kramer & Proschak, 2017). A role in cholesterol metabolism was suggested, as in mice cholesterol levels were elevated by the phosphatase domain and lowered by the EH domain of sEH (EnayetAllah *et al.*, 2008). Another theory is that sEH phosphatase is involved in the regulation of

endothelial nitric oxid synthease (eNOS) activity which is a key regulator of vascular tone (Hou *et al.*, 2012).

1.2.3. Epoxide hydrolase 3 and 4

EH3 and EH4 were discovered by Decker and colleagues through a sequence similarity search with a 16 amino acid sequence motif that is highly conserved among EHs (Decker *et al.*, 2012). The identified genes ABHD9 and ABHD7 were renamed to EPHX3 and EPHX4, respectively. The primary sequence of both enzymes predicts an N-terminal membrane anchor. EH3 consists of 360 amino acids and the residues involved in catalysis are Asp173, His337, Asp307, Tyr220, and Tyr281. Quantitative RT-PCR indicated strongest EH3 expression in mice in lung, skin, and upper gastro-intestinal tract. Substrates of EH3 are 9,10-epoxystearic acid, EETs and leukotoxin. EH3 hydrolyses EETs and leukotoxin with higher specific activity than sEH or mEH but also higher K_m, resulting in a catalytic efficiency in the range of sEH (Decker *et al.*, 2012).

The substrate specificity of EH3 implies a role in signaling molecule processing. However, genetic disruption of EPHX3 in mice showed no significant effects on the metabolism of EETs or leukotoxin *in vivo* and no other overt phenotype (Hoopes *et al.*, 2017). A study which predicted disease genes by human-mouse conserved co-expression analysis suggested a role of EH3 in ichthyosis (Ala *et al.*, 2008). Based on this and the expression pattern of EH3 it was speculated that EH3 plays a role in skin barrier formation (Decker *et al.*, 2012).

EH4 is a 362 residue protein and is mainly expressed in the brain (Lord *et al.*, 2013). The predicted catalytic triad is Asp169, His336 and Asp307 and one of the involved tyrosines is likely Tyr281. No epoxide substrate is known for EH4 but the high sequence identity of 45% with EH3 highly suggests identity as an EH. Recently, EH4 was shown to be associated with lipid droplets (LD) in sebaceous gland cells and siRNA-mediated downregulation of EH4 increased LD size (Dahlhoff *et al.*, 2015).

1.2.4. Mesoderm specific transcript

Mest is an imprinted gene and only the paternally inherited allele is expressed. The maternally inherited gene is silenced by CpG-methylation in the promoter during development and in adult tissue (Kobayashi *et al.*, 1997). The MEST protein consists of 335 amino acids and has a predicted N-terminal membrane anchor. The catalytic triad consists of Asp147, His314 and Asp284. MEST belongs to the α/β-hydrolase fold family and is postulated to be an epoxide hydrolase due to its sequence similarity and a proposed conserved epoxide-coordinating tyrosine Tyr254 (Kaneko-Ishino *et al.*, 1995; Decker *et al.*, 2012). However, no substrate has been identified so far to proof EH activity.

MEST is highly conserved in mammalian species (Sado *et al.*, 1993). For example, the primary sequence of human and rat MEST differs in only 5 of the total 335 amino acids. Throughout development it is widely expressed, particularly in mesodermal tissue and areas of the developing brain (Kaneko-Ishino *et al.*, 1995). There is limited information about the expression in adult tissue. The expression sequence tag (EST) profile[1] identified high numbers of Mest transcripts in various tissues. MEST protein expression was shown in neuron-enriched areas in brain and spinal cord (Lefebvre *et al.*, 1998), placenta (Mayer *et al.*, 2000) and adipose tissue (Takahashi *et al.*, 2005).

Targeted disruption of the Mest gene in mice led to a phenotype. Knockout mice were viable and fertile but peri- and postnatal lethality was increased, and pups were smaller at birth and showed growth retardation. Furthermore, adult Mest KO females showed abnormal maternal behavior. They were unable to care properly for delivered pups and often failed to free them from their extra-embryonic tissue in preparation of feeding (Lefebvre *et al.*, 1998).

More recently, a correlation of MEST with adipose tissue expansion has been established. In mice with a positive energy balance, MEST expression in adipose tissue was induced and levels correlated with expansion of fat mass (Nikonova *et al.*, 2008). Additionally, when Mest was depleted in adipose tissue or globally, fat mass accumulation with high fat diet was reduced compared to WT (Anunciado-Koza *et al.*, 2017).

1.3. The bacterial EH Cif

Bacteria use EHs for different purposes, for example in catabolism to exploit carbon and energy sources (van der Werf *et al.*, 1998), in the defense against toxic epoxides (Chownk *et al.*, 2017) or in the synthesis of, for instance, mycolic acids which are found in the cell wall of mycobacteria (Madacki *et al.*, 2018).

One bacterial EH that belongs to the α/β hydrolase fold enzyme family, the cystic fibrosis transmembrane conductance regulator (CFTR) inhibitory factor (Cif), is of particular interest because it directly affects the human host. Cif is a virulence factor secreted from the opportunistic pathogen *Pseudomonas aeruginosa* (Swiatecka-Urban *et al.*, 2006; MacEachran *et al.*, 2007). The enzyme consists of 319 amino acids and the residues Asp129, His297, and Glu153 build the catalytic triad. However, the crystal structure of Cif revealed that the enzyme differs in typical EH motifs. Instead of two tyrosine residues involved in epoxide positioning, Cif possesses a tyrosine and a histidine, Tyr239 and His177 (Bahl *et al.*, 2010). Substrates of Cif are epibromohydrin and *cis*-stilbene oxide as well as

[1] https://www.ncbi.nlm.nih.gov/UniGene/ESTProfileViewer.cgi?uglist=Hs.270978, December 14th, 2018

endogenous fatty acid-epoxides 14,15-EET, epoxyeicosatetraenoic acids (EpETEs) and epoxydocosapentaenoic acid (EpDPAs) (Bahl *et al.*, 2010; Flitter *et al.*, 2016; Hvorecny *et al.*, 2017).

Cif was first identified in a study where they analyzed why *P. aeruginosa* is particularly successful at colonizing and chronically infecting lungs of patients with cystic fibrosis (CF). CFTR-mediated transepithelial Cl^- secretion, which is already impaired in CF patients, was reduced by a cell free filtrate of *P. aeruginosa* in polarized human airway epithelial cells (Swiatecka-Urban *et al.*, 2006). Further studies identified Cif as the responsible factor and gave more insight in the action on CFTR. Cif is secreted by *P. aeruginosa* in outer membrane vesicles and enters the cytosol of human airway epithelial cells upon fusion of the vesicles with the plasma membrane. In the host cell, Cif reduces the abundance of CFTR on the apical membrane leading to a reduction of transepithelial Cl^- and indirectly Na^+ and water flux. In consequence, the airway superficial fluid dehydrates, and its viscosity increases which impairs mucociliary clearance, the first line of host defense (Hvorecny *et al.*, 2018).

The molecular mechanism of Cif is only partially understood (Figure 7). In healthy lung epithelial cells, CFTR is continuously ubiquitinated and internalized by endocytosis. Most of the CFTR is then deubiquitinated by the ubiquitin specific peptidase-10 (USP10) and recycled back to the apical cell membrane. Cif inhibits the deubiquitination by stabilizing an inhibitory effect of Ras-GAP SH3 domain binding protein-1 (G3BP1) on USP10, thereby inhibiting the recycling of CFTR and redirecting it to the lysosome, where it is degraded (Bomberger *et al.*, 2011). The epoxide hydrolase activity of Cif is necessary for the reduction of CFTR. Inactive Cif mutants had no effect on the apical membrane abundance of CFTR (Bahl *et al.*, 2015). Up to now, the link between EH activity and deubiquitination of CFTR remains unknown (Bahl *et al.*, 2015), and no role for an epoxide or diol in the recycling of CFTR has been established.

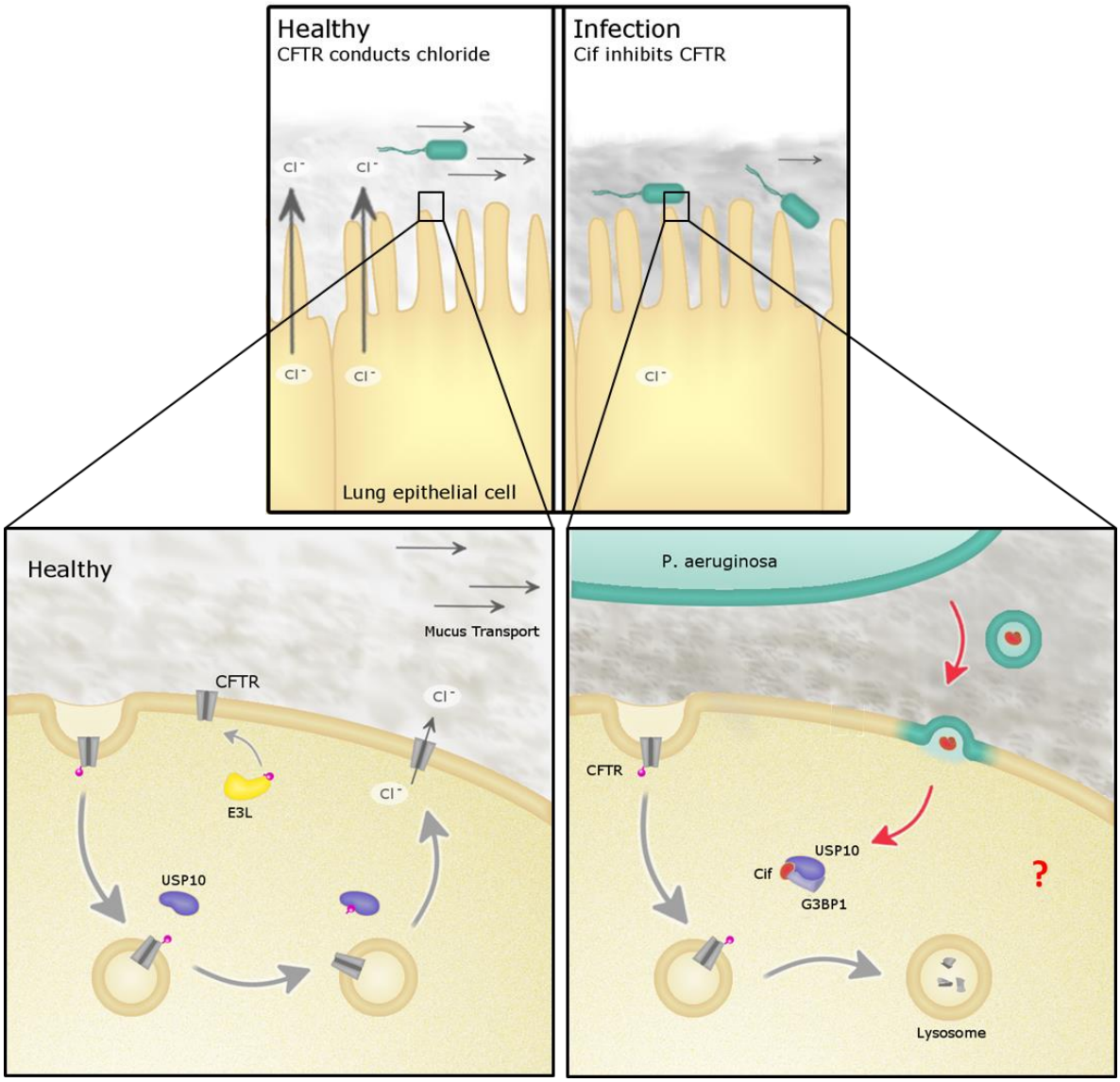

Figure 7: Proposed effect of Cif on airway epithelial cells. In healthy lung epithelial cells, CFTR is constitutively ubiquitinated, internalized in the endosome, and recycled back to the apical plasma membrane. Cif, which is delivered from *P. aeruginosa* via outer membrane vesicles, blocks the deubiquitination by ubiquitin specific peptidase-10 (USP10) and redirects CFTR from the recycling pathway to the degradative pathway, decreasing its expression on the apical membrane. It was proposed that Cif stabilizes an inhibitory interaction between USP10 and Ras-GAP SH3 domain binding protein-1 (G3BP1) but the exact molecular mechanism remains to be determined. The reduced apical membrane abundance of CFTR reduces Cl^- and indirectly H_20 and Na^+ flux, leading to dehydration of airway superficial fluid and impaired mucociliary clearance.

This data showed that Cif is a potential drug target for the treatment of *P. aeruginosa* infections and Cif inhibitors were developed. The first identified Cif inhibitor, tiratricol, was not useful for *in vivo* applications due to thyroid hormone-like activity. A series of rationally designed Cif inhibitors displayed IC_{50} in the sub-micromolar range and 27-fold selectivity over sEH and 50-fold selectivity over mEH toward Cif. However, the inhibitors showed high plasma protein binding (>99%) and short half-lives of 5.7-29 min determined with human liver microsomes (Kitamura *et al.*, 2016).

More recent studies propose an additional effect of Cif on neutrophilic inflammation in the lung. Cif was shown to hydrolyze 14,15-EET produced by airway epithelial cells which decreases the generation of pro-resolving 15-epi LXA_4 by neutrophils. This contributes to a robust, damaging inflammation which is typical for *P. aeruginosa* infection in cystic fibrosis (Flitter *et al.*, 2016; Hvorecny *et al.*, 2018). Besides 14,15-EET, Cif can also hydrolyze other fatty acid epoxides including EpDPAs and EpETEs. The highest hydrolytic activity was found towards 19,20-EpDPA and 17,18-EpETE when tested individually. However, in a mixed substrate approach of EETs, EpETEs, and EpDPAs, which better represents the *in vivo* situation, only EpDPAs and 14,15-EET were hydrolyzed (Hvorecny *et al.*, 2017). Also in this model, the highest turnover was achieved with 19,20-EpDPA outperforming the previously described turnover of 14,15-EET which has been connected to neutrophilic inflammation *in vivo* (Flitter *et al.*, 2016). Further studies are required to, on one hand, identify the link between Cif's epoxide hydrolase activity and the downregulation of CFTR and, on the other hand, evaluate the role of Cif in the hydrolysis of fatty acid epoxides produced by the host.

1.4. Classical approaches to study enzyme substrates

An important step to understand the role of an enzyme is to identify its substrate(s). Without this information, the role of an enzyme can be studied by structural comparison to related enzymes, by pharmacological inhibition or by knockout mouse models but to confirm the results, the molecular mechanism including the substrate are required.

Classical approaches to identify enzyme substrates include substrate screenings and kinetic analysis to evaluate the relevance of a found substrate. This is usually done in an *in vitro* system with purified enzyme under standardized conditions. The limitations of these studies are that the substrate selection depends on the availability of the compounds and on the choice of the researcher. Furthermore, the study conditions might not represent the conditions *in vivo*, requiring confirmation of the results *in vivo* to avoid false conclusions. For example, with classical approaches, no substrate could have been identified for EH4 and MEST yet (Decker *et al.*, 2012). If a substrate screening is negative, it is not clear whether the true substrate was not offered, the used enzyme was inactive, or the conditions were not appropriate.

The substrate landscape of mEH and sEH is well established. Kinetic analyses indicated that sEH is the main enzyme involved in the turnover of endogenous epoxides, such as EETs. However, even though sEH hydrolyzes EETs more efficiently (Zeldin *et al.*, 1993; Decker *et al.*, 2012), there is gaining evidence that mEH is also involved in EETs turnover in the body (Marowsky *et al.*, 2009a; Marowsky *et al.*, 2017). A possible explanation is the difference in cellular and subcellular distribution of mEH and sEH. A recent study showed complex formation between mEH and CYP2J5, one of the enzymes that produces EETs

from arachidonic acid (Orjuela Leon *et al.*, 2017). This allows efficient substrate channeling and gives mEH an advantage that is lost in kinetic *in vitro* studies.

1.5. A novel trapping approach to identify EH substrates

To identify physiologically relevant substrates of EHs, a novel unbiased approach was developed which takes advantage of the two-step reaction mechanism of EHs (Figure 8A). By replacing the catalytic histidine (His) by glutamine (Gln, Q) or alanine (Ala, A), enzymes were created that can still perform the first catalytic step leading to a covalent intermediate between the enzyme and the substrate but cannot perform hydrolysis (Figure 8B). These enzymes are called trapping EHs or EH HQ/HA.

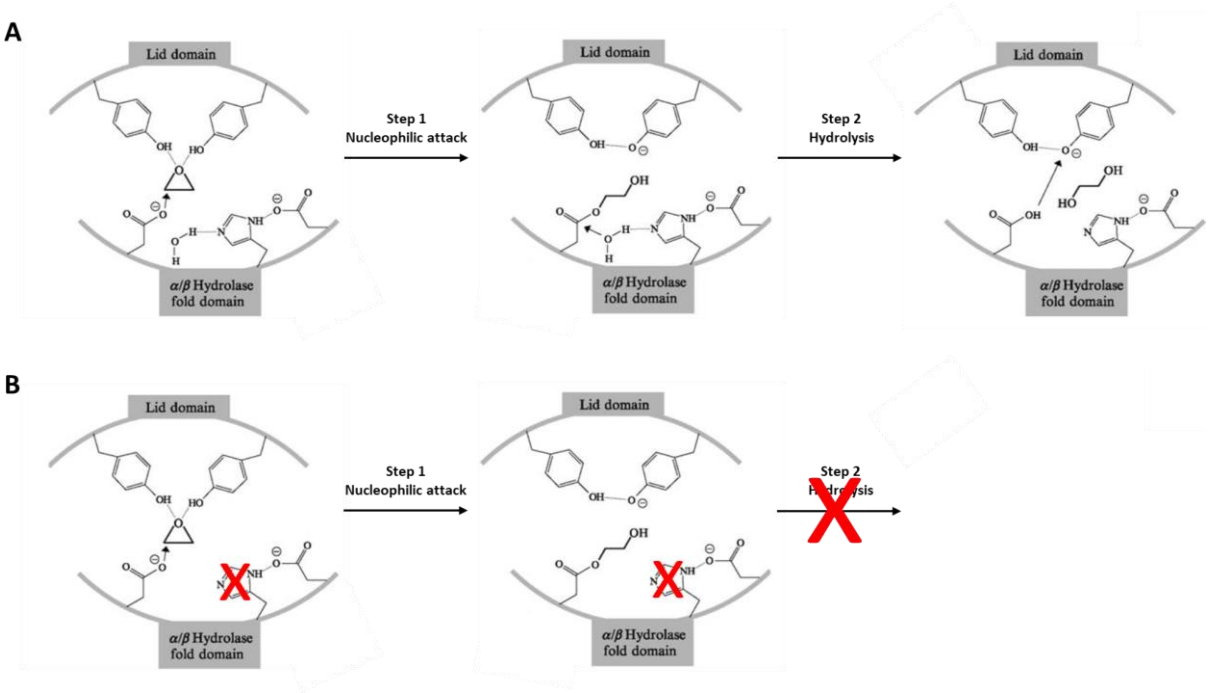

Figure 8: Modification of the EH mechanism to trap the substrate with a covalent ester bond. The typical two-step reaction mechanism of EHs of the α/β-hydrolase fold enzyme family shown in (**A**) was modified by site-directed mutagenesis of the catalytic histidine (His, H) which was replaced by glutamine (Gln, Q) or alanine (Ala, A) (**B**). Gln or Ala are not able to activate a water molecule, inhibiting the second hydrolytic step. The mutated enzyme, called trapping mutant, nucleophilically attacks its substrate but cannot release it, keeping it covalently bound to the catalytic nucleophile of the enzyme.

The trapping mutants of the different EHs were used to trap their substrates *in vivo*. With adeno-associated viruses (AAVs), the trapping enzymes were expressed in the living mouse which provides all possible substrate under physiological conditions, including compounds that have not been identified yet. To identify the bound substrates, the substrate-enzyme complex was enriched from the tissue by His-tag base affinity chromatography and analyzed by liquid chromatography tandem mass spectrometry (LC-MS/MS).

EH trapping mutants have been successfully used before for different purposes. In a study to identify the catalytic triad of the rat mEH, the purified trapping mutant H431Q was incubated with 9,10-epoxy[^{14}C]stearic acid. After intensive washing, autoradiography revealed covalent substrate binding to the mEH mutant (Arand *et al.*, 1999a). The same was shown with a recombinantly expressed H332Q mutant of rat sEH with [^{3}H]trans-stilbene oxide (Arand *et al.*, 1996). More recently, a purified Cif E153Q trapping mutant was used to trap the substrate epibromohydrin for crystallization to analyze the structure of the covalent intermediate (Bahl *et al.*, 2016). Finally, the trapping approach was tested in a preliminary experiment in our group. Purified rat sEH trapping mutant was incubated with epoxystearic acid (ESA) or 14,15-EET and the predicted modified peptide could be detected with LC-MS/MS. Additionally, alkaline hydrolysis was used to release the product which could be detected. Taken together, these experiments indicate that the substrate-enzyme intermediate obtained with the trapping mutants is stable enough for retrieval from the tissue and analysis with LC-MS/MS.

1.6. Epoxide hydrolase expression patterns and expected substrates

To trap relevant substrates, the trapping EHs have to be expressed in the same organs and cells where the wild type enzyme occurs. This is particularly important for mEH and sEH which have overlapping substrate specificities and the substrate turnover might be mainly influenced by their localization. For the other enzymes, the site of expression is less important as identification of any novel substrate would help to understand the role of these enzymes.

sEH is widely expressed throughout the body with highest expression in the liver in hepatocytes followed by kidneys, heart, brain and lungs (Pacifici *et al.*, 1988; Enayetallah *et al.*, 2004). Based on the well-established role in signaling molecule metabolism, we expect sEH to trap mainly EETs and other fatty acid epoxides (Decker *et al.*, 2009). In the liver, epoxides derived from xenobiotic precursors could be trapped as well, especially when animals are challenged with xenobiotic compounds.

mEH shows highest expression in the liver mainly in hepatocytes, where both metabolism of xenobiotic epoxides and endogenous signaling epoxides take place (Coller *et al.*, 2001). Due to its broader substrate specificity, mEH might trap many different epoxides derived from xenobiotic compounds but also endogenous epoxides. Another organ of interest for mEH is the brain where it is expressed in different cell types compared to sEH. mEH expression was reported in vascular cells, choroid plexus epithelial cells and neurons whereas sEH is mainly expressed in astrocytes (Marowsky *et al.*, 2009a). In the vascular and choroid plexus epithelial cells, a role of mEH in detoxification is expected and thus trapping of epoxides derived from xenobiotic compounds. However, in neurons we expect a role in

physiological processes probably mediated by EETs. The substrate spectrum trapped by mEH should give insight to the extent mEH is occupied with detoxification and what role the enzyme plays in the turnover of signaling molecules in different organs.

Expression of EH3 was found in lung, skin, and upper gastro-intestinal tract (Decker *et al.*, 2012). EH3 was shown to efficiently hydrolyze EETs and leukotoxin but the function of this turnover is unclear. A role of EH3 in skin barrier formation was proposed and trapping of an epoxyalcohol of a skin specific linoleate ceramide ester is possible (Yamanashi *et al.*, 2018).

The orphan enzymes EH4 and MEST are mainly expressed in the brain and in adipose tissue (Lefebvre *et al.*, 1998; Takahashi *et al.*, 2005; Lord *et al.*, 2013). For MEST the brain is of high interest as MEST KO mice showed a behavioral phenotype (Lefebvre *et al.*, 1998). For both enzymes the identification of a substrate would confirm their identity as EH.

The bacterial EH Cif has been reported to be expressed in airway endothelial cells upon infection by *P. aeruginosa*, therefore the target organ for substrate trapping is the lung. However, we expect every cell type expressing CFTR to contain the target epoxide of Cif. We hypothesize that Cif hydrolyzes an epoxide linked to CFTR recycling, but no such compound is known so far. 19,20-EpDPA and 14,15-EET were proposed to be the primary substrates of Cif (Hvorecny *et al.*, 2017).

1.7. Adeno-associated viral vectors for gene delivery

Adeno-associated viruses (AAV) are among the smallest viruses known and require co-infection with adenoviruses or other viruses to replicate. No pathologic effect has been associated with AAV infections. They have been studied intensively and are a widely used tool for mammalian gene delivery. Many AAV vectors have been used in clinical trials and the first AAV based gene therapy, alipogene tiparvovec, for the treatment of familial lipoprotein lipase deficiency (LPLD) was approved in Europe in 2012 (Scott, 2015; Naso *et al.*, 2017).

AAVs are non-enveloped, linear, single-stranded DNA viruses. Their genome of approximately 4.7 kb size contain *rep*, *cap* and *aap* genes which are flanked by inverted terminal repeats (ITRs). The *rep* genes encode proteins required for genome replication, virus assembly, and site-specific integration into the host genome upon infection. The capsid proteins are encoded by the *cap* genes and *aap* is required for the activation of assembly (Ojala *et al.*, 2015). The ITRs flanking these genes are the only *cis*-acting elements and are required for genome replication and packaging (Wu *et al.*, 2006).

To use recombinant AAVs as gene delivery tool, the viral genome between the ITRs is replaced by a transgene expression cassette containing the gene of interest, a mammalian promoter and a terminator. For virus production usually done in HEK cells, the expression cassette flanked by ITRs is provided on a plasmid. A second plasmid is used to provide the required *rep*, *cap* and *aap* genes lacking

ITRs to avoid packaging of these genes into the AAV capsid. The adenovirus genes necessary for AAV replication (E1a, E1b, E2a, E4Orf6, vaRNA) are supplied on a third plasmid or together with the *rep*, *cap* and *aap* genes on one single plasmid. Upon co-transfection of HEK cells with the plasmids, viral particles are produced and can be purified (Salganik *et al.*, 2015; Naso *et al.*, 2017).

Infection with the obtained viral particle does not lead to integration of the transgene into the host genome due to the lack of the *rep* genes. The transgene persists as episomes in the nucleus of transduced cells and leads to long-lasting expression in both dividing and non-dividing cells (Ojala *et al.*, 2015). An additional advantage of AAVs is low immunogenicity probably due to low transduction efficiency of antigen-presenting cells such as macrophages and dendritic cells (Salganik *et al.*, 2015).

Tissue tropism (which cells are infected by an AAV) depends on the virus serotype and the route of application. For example, after tail vein injection in mice, almost all the serotypes AAV1-AAV9 mediated transgene expression in the liver and muscle but only AAV8 and AAV9 could target the brain (Zincarelli *et al.*, 2008). A very promising candidate for high transgene expression is the more recently discovered serotype rh10. After i.v. injection, this serotype could transduce all organs and showed higher expression levels than serotypes AAV1-AAV9 (Hu *et al.*, 2010). A promising candidate to efficiently transduce the brain is the serotype PHP.B which was developed by Cre recombination-based AAV targeted evolution of AAV9 (Deverman *et al.*, 2016).

1.8. Liquid chromatography-tandem mass spectrometry

LC-MS/MS synergistically combines the separation capabilities of high-performance LC (HPLC) with the mass analysis potential of MS. For the data acquisition, the compounds are separated by HPLC prior to MS detection. The retention time, the time required to elute analytes from the solid stationary phase, is the first level of selectivity. The technique used here for LC separation of peptide analytes is reversed phase LC (RPLC). In RPLC, peptides are separated on a C18-HPLC column according to their lipophilicity. Thus, lipophilic peptides elute later than hydrophilic peptides. Before entering the MS, analytes are ionized, and the mobile phase is evaporated in the ionization source at the interface between LC and MS.

In the used LC-MS/MS systems, the ionization is based on electron spray ionization (ESI) (Fenn *et al.*, 1989). The liquid mobile phase coming from the LC is pumped through a fine metal capillary kept at 3-5 kV and nebulized at its tip. The fine spray of charged droplets is evaporated usually by heat under a stream of dry nitrogen and the resulting charged analytes are drawn into the mass analyzer by electrical force.

In the mass analyzer, molecules are separated according to their mass-to-charge ratio (*m/z*). Typical mass analyzers use the principles of time-of-flight analysis (TOF) or quadrupole-based separation. The MS systems used in this work are a triple quadrupole linear ion trap (QTrap) 4000 and a tripleTOF 6600.

1.8.1. QTrap 4000 MS technology

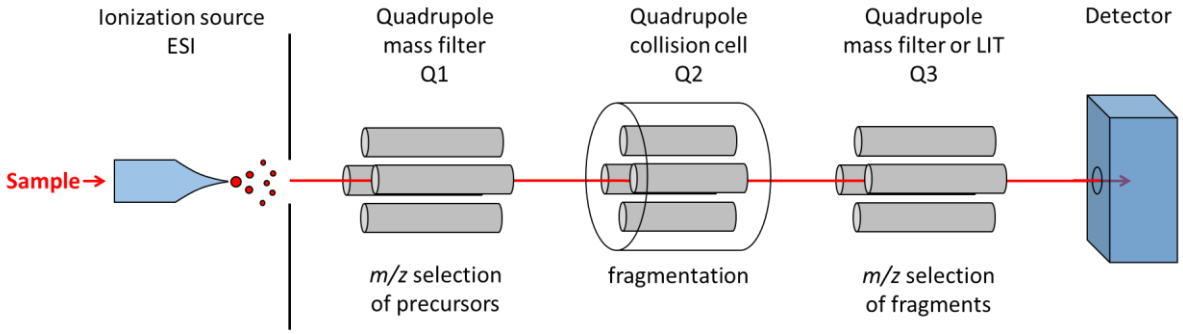

Figure 9: Principle of a QTrap MS. Visualization of the arrangement of the different modules in a QTrap device.

The QTrap MS system consists of an ESI source and a hybrid triple quadrupole linear ion trap (LIT). It is a tandem MS composed of two quadrupole mass filters (Q1 and Q3) connected via a quadrupole collision cell (Q2) (Figure 9). In a typical experiment, the mass filters are set to a certain *m/z* allowing only molecules with this *m/z* to pass. In Q1, the precursor ion (also called parent ion) is selected which then enters the collision cell Q2 where it is fragmented through a collision gas. The fragment ions enter the Q3 which either acts as a mass filter again or as a linear ion trap depending on the used scan type. In the multiple reaction monitoring (MRM) (also called selected reaction monitoring (SRM)) scan type, both quadrupoles act as mass filters selective for the precursor ion in Q1 and for a specific fragment of the molecule of interest in Q3. This transition (pair of precursor *m/z* and fragment *m/z*) is highly specific and allows the discrimination of two molecules that have similar or identical precursor *m/z*. The MS cycles through a series of transitions and records the signal as a function of time (HPLC elution) (Figure 10, upper panel). This scan type allows quantitative analysis of molecules in complex samples with very high sensitiviy. In the enhanced product ion (EPI) scan type, the Q3 acts as an ion trap acquiring a full scan spectrum of all fragments generated by the fragmentation of the precursor ion in the collision cell (Figure 10, lower panel). Sensitivity for the fragments is increased, as in the EPI scan mode the Q3 operates as a LIT, accumulating fragments before detecting them, thus giving a better signal-to-noise ratio for the detected spectra. The obtained fragment spectra contain further information about the detected molecules increasing the confindence in positive findings. In contrast to MRM, acquisition of EPI spectra takes more time, limiting the number of analytes that can be detected per run.

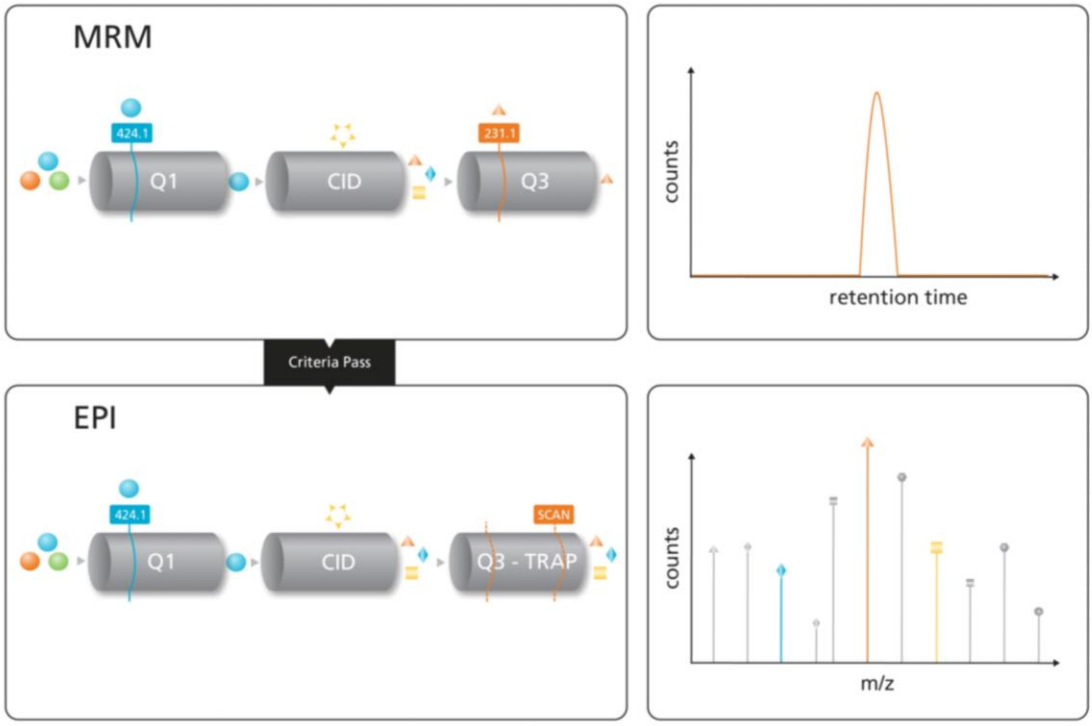

Figure 10: MRM EPI scan mode. In a first step, MRM acquisition is performed. If a transition (precursor-fragment ion pair) exceeds a certain threshold, the EPI acquisition is induced for the respective precursor ion and all fragments are trapped in the LIT and transferred to the detector. CID stands for collision-induced dissociation and represents Q2**.** Figure taken from Sciex user guide[2].

Using information dependent acquisition (IDA), these two scan types can be combined (Figure 10). MRM is used as the survey scan. Any MRM signal exceeding a certain threshold triggers the acquisition of an EPI scan. This combines the selectivity of MRM with the high information content obtained by EPI. MRM EPI (IDA) data provides a "fingerprint" of a compound, bearing the possibility to be compared to MS/MS mass spectral libraries for better identification (Sciex user guide[1]).

1.8.2. TripleTOF 6600 MS technology

The TripleTOF system combines quadrupole technology front-end with the accelerator TOF analyzer in the back. Like the triple quadrupole, it contains a Q1 quadrupole mass filter followed by a Q2 collision cell but instead of the Q3 mass filter/LIT, the TripleTOF 6600 has an accelerator TOF analyzer. In TOF analyzers, *m/z* of a fragment is determined by the time the ion takes to fly through a tube with a certain length under vacuum (Domon & Aebersold, 2006).

[2] https://sciex.com/Documents/brochures/qtrapMRM-EPI-lib-search_10160414.pdf, October 10th, 2018

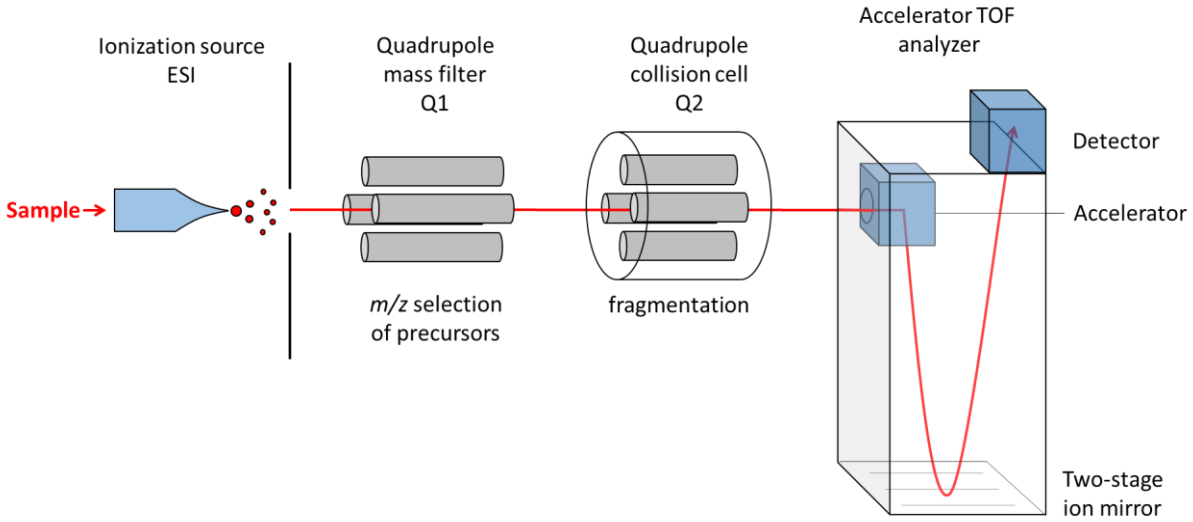

Figure 11: Principle of a TripleTOF MS. Visualization of the arrangement of the different modules in a TripleTOF device.

TripleTOF systems exhibit higher mass resolution in MS and MS/MS mode compared to QTrap devices. In the MS mode, Q1 acts as an ion guide to the accelerated TOF analyzer where the mass analysis takes place. In the MS/MS mode, the precursor ions are selected in Q1 and fragmented in the Q2 collision cell and the product ions are analyzed in the TOF analyzer. Due to the high resolution, the isotope pattern of multiply charged analytes can be resolved. Most elements have more than one stable isotope, most importantly, 1.1% of the carbon ions have a weight of 13 Da instead of 12 Da. For example, a molecule that contains 100 carbon atoms contains no ^{13}C with a chance of approximately 34%, one ^{13}C with a chance of 37%, two ^{13}C with a chance of 20% and more than two ^{13}C with a chance of 9%. In the mass spectrum, this translates to a typical isotope pattern with multiple peaks where the chance is reflected by the relative abundance of every species measured. Since the mass spectrum shows *m/z* and the isotope only affects *m*, the charge *z* can be derived from the isotope pattern which equals 1 divided by the *m/z* difference of two isotopes. (For example, if the peaks of different isotopes are separated by 0.25 Da then the charge z equals 1/0.25 = 4.)

1.8.3. SWATH scan mode

The TripleTOF 6600 used in this work is able to perform sequential window acquisition of all theoretical spectra (SWATH) (Gillet *et al.*, 2012). In contrast to the aforementioned IDA used on the QTrap 4000, SWATH is a data independent acquisition (DIA) mode, meaning that all precursor ions are fragmented independently of their signal in Q1 (Lambert *et al.*, 2013). In the SWATH scan mode, within 2-4 s cycle time, the MS steps through a set of precursor acquisition windows designed to cover 400-1200 *m/z* as a whole mass range. All precursors from the quadrupole isolation window (Q1) are fragmented in Q2 during each cycle and complete, high accuracy fragment ion spectra are recorded in the accelerated TOF analyzer (Figure 12).

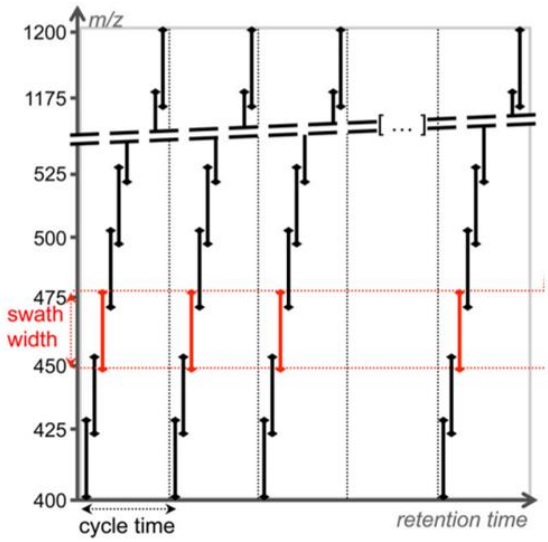

Figure 12: Schematic representation of SWATH acquisition. The MS steps through a set of precursor acquisition windows designed to cover 400-1200 *m/z* as a whole mass range within a certain cycle time. All precursors from the quadrupole isolation window (Q1) (e.g. 450-475 *m/z*, for 25 Da wide windows) are fragmented in Q2 during each cycle and fragment ion spectra are recorded in the accelerated TOF analyzer. The same precursor isolation window is fragmented repeatedly at each cycle during the whole chromatographic run. Figure taken from (Gillet *et al.*, 2012).

The same precursor isolation window is fragmented in every cycle during the whole chromatographic run, thus providing a time-resolved recording of the fragment ions of all precursors that enter the MS (Gillet *et al.*, 2012). SWATH MS data is therefore highly multiplexed and contains information about all analytes present above the detection limit. The data can be analyzed for any analyte in question, also post-acquisition, which is not possible with MRM or IDA data (see Figure 13).

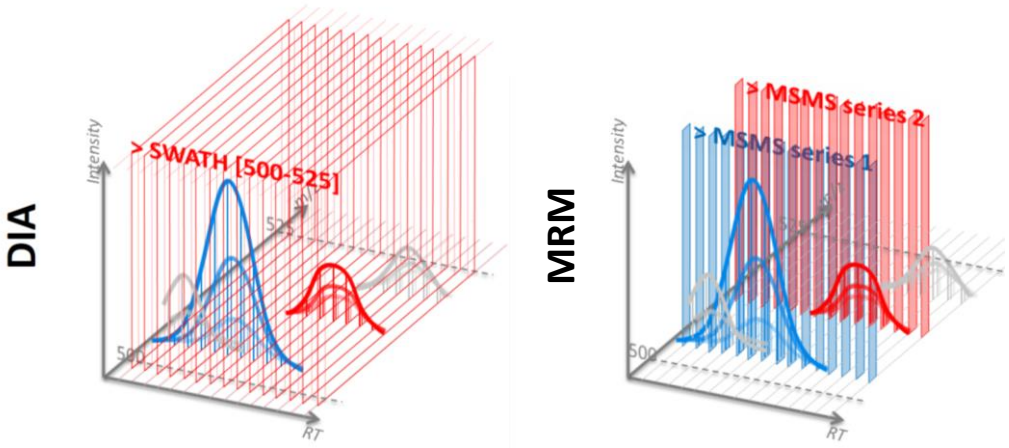

Figure 13: Data structure of the SWATH (DIA) and MRM acquisition mode. In DIA (left), the complete precursor mass range is selected for fragmentation in consecutive and contiguous precursor windows (e.g. 25 Da windows, as shown here for region 500–525 *m/z*) repeatedly during the LC separation. This enabels screening of the data for any compound or fragment present above the detection limit. In MRM (IDA) (right) only the peptides of interest (here blue and red) are selected for fragmentation repeatedly and with a given periodicity during the elution. Recorded data only includes MS/MS spectra of the specified transitions (precursor-fragment pairs). No information is recorded for compounds that were not included into the acquisiton method. Figures taken from (Gillet *et al.*, 2016).

1.9. Peptide analysis with mass spectrometry

Protein analysis typically includes digestion with a protease, with trypsin being the most frequently used and thus the one with the most comprehensive data in peptide libraries. The MS/MS spectra of the obtained peptides contain structural information about the peptide as they preferentially break at certain points along the backbone. Figure 14 shows the typical fragments that are produced from peptides.

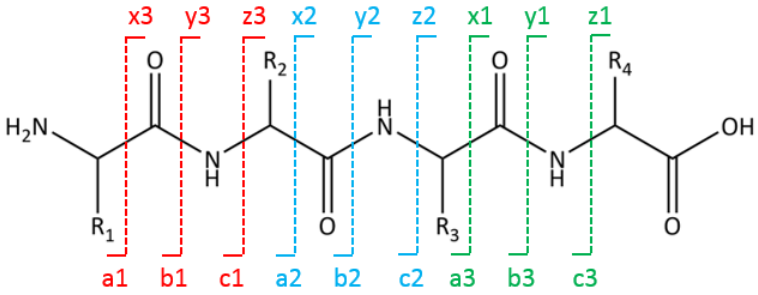

Figure 14: Nomenclature of fragments occurring during MS/MS analysis of peptides. N-terminal fragments are called a, b and c with the number indicating the number of amino acids. C-terminal fragments are called x, y and z.

The fragments will only be detected if they carry at least one charge. Using low energy CID (collision induced dissociation) which is the case for QTrap and TripleTOF, y and b fragments are generated predominantly. In a series of, for example, y fragments, the mass difference of y(n) to y(n-1) is the mass of amino acid n. This can be used for de-novo sequencing of the peptide but requires high quality

and complete spectra which are usually not available. Therefore, the obtained spectra are compared to databases that contain a limited pool of peptide sequences. The masses and fragments of peptides from known proteins are predicted *in silico* and the peptide sequence that matches the given spectrum best, is identified. If several spectra match multiple peptides of the same protein, the confidence that this protein is truly present is increased.

In contrast to classical large-scale proteomic approaches which aim to elucidate the entire content of proteins in a cell, organ, or organism, we are interested in one particular peptide of each of the six proteins under investigation. Although we know the amino acid sequences, the exact masses are unknown because these peptides will be modified by the substrates. However, the fragmentation pattern obtained in the MS/MS spectrum is predictable. This fingerprint of the target peptide is used to identify the parent mass of the substrate modified peptide. Since the mass of the unmodified peptide is known, the mass of the substrate can be calculated. This provides the first lead for further structural analyses to identify the caught substrate.

1.10. Aim of the study

The aim of the present project is to identify the preferred *in vivo* substrates of the six EHs mEH, sEH, EH3, EH4, MEST, and Cif to elucidate their physiologic functions. Besides classical substrate screening and kinetic analysis we aim to develop and use a novel *in vivo* substrate trapping approach. The major questions addressed are:

1) Which substrates are preferred *in vivo* by the well characterized sEH, mEH and EH3 in a tissue and treatment-specific manner?

2) What are the physiologic substrates of the hitherto orphan human EHs EH4 and MEST?

3) Which substrate is processed by the bacterial EH Cif and does this provide a lead to understand Cif's role in the pathophysiology of *P. aeruginosa* infection?

Answering these questions would boost the understanding of the role of EHs in mammalian/human physiology and thus create new leads for the development of novel therapeutic strategies. The development of the substrate trapping method itself would be a major breakthrough in identifying the real contribution of enzymes under investigation in the *in vivo* situation in an unbiased manner.

2. MATERIALS AND METHODS

2.1. Chemicals

If not indicated otherwise, all chemicals were obtained from Sigma-Aldrich (St. Louis, MO, USA) and Roth AG (Karlsruhe, Germany). Fatty acid derived epoxides were purchased from Cayman Chemicals (Michigan, USA).

2.2. Vectors and plasmids

Table 1: Plasmid constructs

Abbreviation	Full name	Purpose
pRSET	pRSET A	Expression of inclusion bodies in *E.coli*
pET	pET20b(+)	Expression of functional EHs in *E. coli*
pAM-CAG	pAM-CAG-pl-HisC-WPRE	AAV production and expression of EHs in HEK cells
pGEF	pGEFII-HisC	Expression of active Cif in *E. coli*
AAV-PHP.B	pUCmini-iCAP-PHP.B	AAV production (Deverman *et al.*, 2016)
AAV-rh10	pAAV2/rh10	AAV production (Gao *et al.*, 2003; Cearley *et al.*, 2008)
Helper plasmid	pBS-E2A-VA-E4	AAV production (Paterna *et al.*, 2000)

Adapted from Bettina Hew, ETH Diss. No. 25662, (Hew, 2019)

2.3. Primers

Table 2: Primers used to insert EHs into pRSET

Name	Sequence	Restric. site
mEHfor BamHI BstBI	*GATCGGATCCGCCGCC*ATGTGGCTAGAAATCCTCCTCAC	BamHI
mEHrev BamHI BstBI	*GATCTTCGAAGC*TTGCCGCTCCAGCACCGACAGGAA	BstBI
sEHfor BamHI BstBI	*GATCGGATCC*GCCGCCATGACGCTGCGCGCGG	BamHI
sEHrev BamHI BstBI	*GATCTTCGAAGC*CATCTTTGAGACCACCGG	BstBI
EH3for Cla BstBI	*GATCATCGATGCGGCCGC*GCCGCCATGGCGGAGCTGGTGGTGA	ClaI
EH3rev NotI BstBI	*GATCTTCGAAGC*GTCCAGCAGGTCTTGCAAGAAGG	BstBI
EH4for BamHI BstBI	*GATCGGATCCGCCGCC*ATGGCGAGGCTGCGGGATTGCCTG	BamHI
EH4rev BamHIBstBI	*GATCTTCGAAGC*ATCTTTTTTTCTTGTTTCTTCTTTTAGAAATGTCCATATCAA	BstBI
Mestfor KpnI BstBI	*GATCGGTACCGCGGCCGCGCCGCC*ATGGTGCGCCGAGATCGCCTCC	KpnI
Mestrev NotI BstBI	*GATCTTCGAAGC*GAAGGAGTTGATGAAGCCCAT	BstBI
Ciffor BamHI HindIII	*GATCGGATCCGCCG*CCATGGTCCTCGATAGACTTTGCCG	BamHI
Cifrev BamHI HindIII	*GATCAAGCTTATCGATGC*TAGATCTCCTCCGCGACCGCGG	HindIII

Cursive, non-complementary sequence; underlined, restriction site

Table 3: Mutagenesis primer

Name	Sequence
mEH D226A for	CTACATTCAAGGAGG***C***G***C***CTGGGGGTCCCTG
mEH D226A rev	CAGGGACCCCCAG***GC******G***CCTCCTTGAATGTAG
mEH H431A for	GGTTCGTGGGGGC***GC***CTTTGCGGCCTTTGAGG
mEH H431A rev	CCTCAAAGGCCGCAAAG***GC***GCCCCCACGAACC
mEH H431Q for	CGTGG***T***GGCCA***G***TTTGCGGCCTTTGAGGAG
mEH H431Q rev	CTCCTCAAAGGCCGCAAA***C***TGGCC***A***CCACG
sEH D335A for	CATTGGCCATG***CA***TGGGGTGGCATGCTGGTG
sEH D335A rev	CACCAGCATGCCACCCCA***TG***CATGGCCAATG
sEH H524A for	GACTGTGGG***GC***CTGGACACAGATGGAC
sEH H524A rev	GTCCATCTGTGTCCAG***GC***CCCACAGTC
sEH H524Q for	GGACACATTGAGGACTGTGGGCA***G***TGGACACAGATGGAC
sEH H524Q rev	GTCCATCTGTGTCCA***C***TGCCCACAGTCCTCAATGTGTCC
EH3 D173A for	GTGGCCCATG***CA***TGGGGTGCCCTCCTTG
EH3 D173A rev	CAAGGAGGGCACCCCA***TG***CATGGGCCAC
EH3 H337A for	GCCAGGCATAGGG***GC***TTG***T***ATCCCACAGAG
EH3 H337A rev	CTCTGTGGGAT***A***CAA***GC***CCCTATGCCTGGC
EH3 H337Q for	GCCAGGCATAGGGCA***G***TG***T***ATCCCACAGAG
EH3 H337Q rev	CTCTGTGGGAT***A***CA***C***TGCCCTATGCCTGGC
EH4 D169A for	GTTCTTATTGGCCATG***CA***TGGGGGGGCATGATTGCTTGG
EH4 D169A rev	CCAAGCAATCATGCCCCCCCA***TG***CATGGCCAATAAGAAC
EH4 H336A for	GTCAGAAGCCAGT***GC***TTGGCTGCAGCAAGACCAAC
EH4 H336A rev	GTTGGTCTTGCTGCAGCCAA***GC***ACTGGCTTCTGAC
EH4 H336Q for	GTCAGAAGCCAGTCA***G***TGGCT***G***CAGCAAGACCAAC
EH4 H336Q rev	GTTGGTCTTGCTG***C***AGCCA***C***TGACTGGCTTCTGAC
Mest D147A for	GGATCAACCTTCTTTCTCATG***CA***TATGGAGATATTGTTGCTCAGG
Mest D147A rev	CCTGAGCAACAATATCTCCATA***TG***CATGAGAAAGAAGGTTGATCC
Mest H314A for	GATGACCACATTAGC***GCT***TATCCACAGCTAGAGGATCCC
Mest H314A rev	GGGATCCTCTAGCTGTGGATA***AGC***GCTAATGTGGTCATC
Mest H314Q for	GACCACATTAGCCA***A***TATCCACAGCT***G***GAGG
Mest H314Q rev	CCTC***C***AGCTGTGGATA***T***TGGCTAATGTGGTC
Cif D129A for	CTGGTGGCCCACG***CG***ATCGGTATCTG
Cif D129A rev	CAGATACCGAT***CG***CGTGGGCCACCAG
Cif H297A for	GCTGTGGC***GC***CTGGCTGCCGGAAGAGTG
Cif H297A rev	CACTCTTCCGGCAGCCAG***GC***GCCACAGC
Cif H297Q for	GCTGTGGCCA***A***TGGCT***T***CCGGAAGAGTG
Cif H297Q rev	CACTCTTCCGG***A***AGCCA***T***TGGCCACAGC

Bold cursive, mutation; underlined, changed codon

Table 4: Primers to insert EHs into pAM-CAG vector

Name	Sequence	Restric. site
mEHfor BamHI BstBI	*GGATCCGCCGCC*ATGTGGCTAGAAATCCTCCTCAC	BamHI
mEHrev BamHI BstBI	*GATCTTCGAAGC*TTGCCGCTCCAGCACCGACAGGAA	BstBI
sEHfor BamHI BstBI	*GGATCC*GCCGCCATGACGCTGCGCGCGG	BamHI
sEHrev BamHI BstBI	*GATCTTCGAAGC*CATCTTTGAGACCACCGG	BstBI
EH3for NotI BstBI	*GCGGCCGC*GCCGCCATGGCGGAGCTGGTGGTGA	NotI
EH3rev NotI BstBI	*GATCTTCGAAGC*GTCCAGCAGGTCTTGCAAGAAGG	BstBI
EH4for BamHI BstBI	*GGATCCGCCGCC*ATGGCGAGGCTGCGGGATTGCCTG	BamHI
EH4rev BamHIBstBI	*GATCTTCGAAGC*ATCTTTTTTTCTTGTTTCTTCTTTTAGAAATGTCCATATCAA	BstBI
Mestfor NotI BstBI	*GCGGCCGC*GCCGCC*ATGGTGCGCCGAGATCGCCTCC	NotI
Mestrev NotI BstBI	*GATCTTCGAAGC*GAAGGAGTTGATGAAGCCCAT	BstBI
Ciffor BglII ClaI	*AGATCTGCCG*CCATGGTCCTCGATAGACTTTGCCG	BglII
Cifrev BglII ClaI	*ATCGATGC*TAGATCTCCTCCGCGACCGCGG	ClaI

Cursive, non-complementary sequence; underlined, restriction site

Table 5: Oligonucleotides

Name	Sequence
Polylinker pAM-CAG sense1	GATCCGCTAGCGGTACCTTCG
Polylinker pAM-CAG sense2	AATCGCGAACATCATCATCATCATCATCGCGAGTA
Polylinker pAM-CAG antisense1	AGCTTACTCGCGATGATGATG
Polylinker pAM-CAG antisense2	ATGATGATGTTCGCGATTCGAAGGTACCGCTAGCG
Polylinker pAM-CAG sense3	GATCCGCGGCCGCCTGCAGCTCGAGGAATT
Polylinker pAM-CAG antisense3	CGAATTCCTCGAGCTGCAGGCGGCCGCG

Table 6: Sequencing primer

Name	Sequence
AAV8-SAR120514	TGACGTCAATGGAAAGTCCC
AAV-pl-for	GTGGCTGCGTGAAAGCCTTGA
CAGfor	GCCCAGTACATGACCTTA
VP1.5	GGACTTTCCAAAATGTCG
XL39	CCACCAGCCTTGTCCTAATA

2.4. Antibodies

Table 7: Primary antibodies

Abbreviation	Supplier information
Anti-His-tag	Anti-6X Histag® antibody-ChIP Grade (ab9108), polyclonal, Abcam
Anti-GFP	GFP Polyclonal Antibody (A6455), polyclonal, Invitrogen
Anti-human mEH	Rabbit 2 Anti-mix mEH, polyclonal, in-house

Adapted from Bettina Hew, ETH Diss. No. 25662, (Hew, 2019)

Table 8: Secondary antibodies

Abbreviation	Supplier information
Anti-rabbit AP	Anti-Rabbit IgG (whole molecule), F(ab')2 fragment–Alkaline Phosphatase antibody produced in goat (A3937), Sigma Aldrich
Odyssey 680	IRDye® 680RD Donkey anti-Rabbit Antibody (926-68073), polyclonal, Li-Cor
Odyssey 800	IRDye® 800CW Donkey Anti-Rabbit IgG (H+L) (926-32213), polyclonal, Li-Cor
Cy3	Cy™3 AffiniPure Donkey Anti-Rabbit IgG (H+L) (711-165-152), polyclonal, Jackson Immuno Research

Adapted from Bettina Hew, ETH Diss. No. 25662, (Hew, 2019)

2.5. Microbiological methods

2.5.1. PCR

DNA fragments of interests were amplified by polymerase chain reaction (PCR) with the PCR reaction mix and PCR program summarized in

Table 9 using a Thermal Cycler T100 (Bio-Rad Laboratories, Inc., Hercules, CA, USA). PCR primers were obtained from Microsynth (Balgach, Switzerland) and were solubilized in water. 10 x dNTP mix contained 2.5 mM dNTPs (Thermo Fischer Scientific, Waltham, MA, USA) and 10 x PCR buffer consisted of 200 mM Tris, 100 mM $(NH_4)_2SO_4$, 100 mM KCl, 20 mM $MgSO_4$, 1% Triton X-100, 1 mg/mL BSA at pH 7.4. Homemade Pfu DNA polymerase, which can correct wrongly incorporated nucleotides by its 3'→5' exonuclease activity, was used. To avoid unspecific primer binding, the Pfu polymerase was added last to the PCR reaction mix, after heating up to 95 °C (hot-start PCR).

Table 9: PCR reaction mix and PCR program

PCR reaction mix		PCR program		
Plasmid DNA	40 ng	95 °C	5’	
Forward primer (25 µM)	0.5 µl	95 °C	30’’	┐
Reverse primer (25 µM)	0.5 µl	55 - 65 °C*	10’’	├ 30 cycles
10 x dNTP mix	5 µl	72 °C	2’	┘
10 x PCR buffer	5 µl	72 °C	5’	
Pfu polymerase, added last	1 µl			
Water	ad 50 µl			

* 3-5 tubes of the same reaction mix were processed in parallel with different annealing temperatures between 55-65 °C (gradient PCR)

2.5.2. Site-directed mutagenesis PCR

Site-directed mutagenesis PCR was performed to change up to three nucleotides in a plasmid construct. The complete plasmid was amplified by PCR using two complementary primers containing the desired mutations flanked by at least 10-15 bases on either side of the mutation(s). The PCR reaction mix and PCR program are summarized in Table 10 and a Thermal Cycler T100 (Bio-Rad Laboratories, Inc., Hercules, CA, USA) was used. Primers, dNTP mix, PCR buffer and Pfu polymerase were used as described in the previous chapter 2.5.1.

After the PCR, the template plasmid was digested by direct addition of 1 µl of the restriction endonuclease DpnI and incubation for 1 h at 37 °C. DpnI cleaves the sequence GATC in the methylated template plasmid of bacterial origin but not the amplified, mutated plasmid lacking methylation. After digestion, 0.5 - 2 µl of the plasmid solution was transformed into *E. coli* for amplification and analysis (see chapter 2.5.5. and 2.5.6.).

Table 10: Site-directed mutagenesis PCR reaction mix and PCR program

PCR reaction mix		**PCR program**		
Plasmid DNA	40 ng	95 °C	3’	
Forward primer (25 µM)	0.3 µl	95 °C	1’	
Reverse primer	0.3 µl	55-65 °C*	1’	30 cycles
10 x dNTP mix	3 µl	72 °C	10’	
10 x PCR buffer	3 µl	72 °C	15’	
ATP	0.5 µl			
Pfu polymerase	0.6 µl			
Water	ad 30 µl			

* 3-5 tubes of the same reaction mix were processed in parallel with different annealing temperatures between 55-65 °C (gradient PCR)

2.5.3. Cloning

The plasmid segment of interest was amplified by PCR with primers designed to introduce the required endonuclease restriction sites. The amplified DNA insert was purified using the QIAquick PCR Purification Kit (Qiagen, Hilden, Germany) according to the manufacturer’s protocol. The insert and up to 5 µg of target plasmid backbone were digested with the respective restriction endonucleases (New England Biolabs (NEB), Ipswich, MA, USA) using the suggested NEB buffer and, if required, BSA for 1 hr at 37 °C. If required, the backbone was dephosphorylated by addition of calf intestinal phosphatase (NEB) to the restriction endonuclease digest and incubation for 1 h at 37 °C. Both backbone and insert were separated by gel electrophoresis on a preparative 0.7-1% agarose gel and purified using the QIAquick Gel Extraction Kit (Qiagen, Hilden, Germany) according to the manufacturer’s protocol. The DNA concentration was quantified by Nanodrop.

For the ligation, 40-50 ng backbone was incubated with the insert in a molar ratio of 1:3 (backbone:insert) together with 1 µl of 10 x T4 ligation buffer and 0.2 µl T4 DNA ligase (both Thermo Fisher Scientific, Waltham, MA, USA) in a final volume 10 µl for 30 min in the dark. The ligase was inactivated by incubation for 10 min at 65 °C before up to 2 µl of the ligated plasmid was transformed into TOP10 or MDS42 *E. coli*.

2.5.4. Transformation of *E. coli*

Electroporation was used to transform electrocompetent *E. coli* (One Shot TOP10 Electrocomp *E. coli;* Thermo Fisher Scientific, Waltham, MA, USA) with a plasmid of interest. 0.5-2 µl plasmid were added to 40 µl thawed electrocompetent bacteria and incubated for 5 min on ice. The bacteria were then transferred to a pre-cooled electroporation cuvette with a gap width of 0.1 cm (Bio-Rad Laboratories, Inc., Hercules, CA, USA) and electroporated with one pulse of 5 ms at 1.35 kV with a Gene Pulser™ (Bio-Rad Laboratories). Subsequently, cells were suspended in 500 µl pre-warmed (37 °C) LB medium and incubated for 1 h at 37 °C and 220 rpm. 100 µl of the bacteria suspension was plated on LB agar dishes containing 0.1 mg/ml ampicillin and incubated overnight at 37 °C.

2.5.5. Plasmid amplification

A starter culture of 4 ml of LB medium containing 100 µg/ml ampicillin was inoculated with an *E. coli* colony containing the plasmid of interest and incubated overnight at 37 °C and 220 rpm. The starter culture was directly used to isolate the plasmid with QIAprep Spin Miniprep Kit (Qiagen, Hilden, Germany). For high plasmid amounts, the starter colony was used to inoculate a larger culture of 150-250 ml for isolation with the HiSpeed Plasmid Maxi Kit (Qiagen). Isolation was performed according to the manufacturer's protocol. DNA yield was quantified by Nanodrop.

2.5.6. Plasmid analysis and Sanger sequencing

200-500 ng plasmid DNA was digested with suitable restriction endonucleases (NEB, Ipswich, MA, USA) using the suggested NEB buffer and, if required, BSA for 1 h at 37 °C. The obtained DNA fragments were separated on a 1-2% agarose gel by gel electrophoresis and the size was determined by comparison to standards (GeneRuler DNA Ladder Mix; Thermo Fisher Scientific, Waltham, MA, USA). DNA sequence was determined by Sanger sequencing performed by Microsynth (Balgach, Switzerland) using the primers listed in Table 6.

2.6. Recombinant protein expression

pRSET plasmid constructs were used for the expression of inclusion bodies and pET and pGEF constructs were used for the expression of functional protein in *E. coli*. Expression of functional enzyme in HEK293T cells after transient transfection with pAM-CAG constructs is described in the doctoral thesis of Bettina Hew (Hew, 2019).

The expression vector was transformed into BL21-AI *E. coli* which contain an arabinose inducible T7 RNA polymerase. A starter culture of 4 ml of LB medium containing 100 µg/ml ampicillin was inoculated with an *E. coli* colony and incubated overnight at 37 °C and 220 rpm. The next day, the starter culture was centrifuged, and the bacteria were washed twice with LB medium before they were used to inoculate 250 ml LB medium containing 100 µg/ml ampicillin which was incubated at 37 °C. At an optical density (OD_{600}) of 0.4-0.6, protein expression was induced by the addition of arabinose to a final concentration of 10 µM for expression of functional enzyme and 1 mM for expression of inclusion bodies. Expression was performed over night at room temperature for functional enzyme and 30 °C for inclusion bodies at 220 rpm. Bacteria were harvested by centrifugation (4000 g, 15 min, 4 °C, Heraeus Megafuge 1.0R, rotor #2704; Heraeus Instruments GmbH, Hanau, Germany) and the pellet was either resuspended in Tris-buffer (20 mM Tris, 100 mM NaCl) for further use or stored at -80 °C.

2.7. Protein purification

All recombinantly expressed proteins are fused to a hexa histidine-tag (His-tag) used for purification or enrichment from bacterial cultures or mouse tissue homogenates by immobilized metal affinity chromatography (IMAC). Functional Cif expressed in *E. coli* is transferred to the bacterial periplasm and was isolated from there by osmotic shock prior IMAC to increase purity.

2.7.1. French Pressure Cell

Bacterial cell pellets obtained from 250 ml expression cultures were resuspended in 10 ml Tris-buffer (20 mM Tris, 100 mM NaCl). Mechanical lysis of the bacteria was performed using a French® Pressure Cell press (Slm Aminco, Thermo Fisher Scientific, Waltham, MA, USA) with a pressure of 30’000 psi. Lysis was performed slowly to avoid increase of temperature of the lysate. Bacteria and lysates were kept on ice. Inclusion bodies were separated from soluble protein by centrifugation for 20 min at 4000 g and 4 °C (Heraeus Megafuge 1.0R, rotor #2704, Heraeus Instruments GmbH, Hanau, Germany).

2.7.2. Osmotic shock

Bacterial cell pellets obtained from 250 ml expression culture were resuspended in 30 mM Tris, 20% sucrose, pH 8, for 10 min. After centrifugation (4000 g, 15 min, 4 °C, Heraeus Megafuge 1.0R, rotor #2704; Heraeus Instruments GmbH, Hanau, Germany), the pellet was resuspended in ice-cold 5 mM $MgSO_4$ and stirred slowly on ice for 10 min. During this step, the bacterial outer membrane is disrupted by osmotic forces and the periplasmic proteins are released into the buffer. The bacteria were pelleted again by centrifugation and the supernatant containing the protein of interest was collected. Mg^{2+} was removed from the protein solution by dialysis against chilled IMAC buffer A (20 mM Tris, 0.5 M NaCl, 20 mM Imidazole, pH 7.4) overnight prior purification.

2.7.3. Immobilized metal ion chromatography (IMAC)

Lysates of bacteria expressing membrane bound enzymes such as mEH were incubated with 0.5% (v/v) Genapol X-100 for 1 h on ice to release proteins from the membrane prior centrifugation for 20 min at 50'000 g (Kendro, Sorvall RC-%C, rotor SS-34; Thermo Fisher Scientific, Waltham, MA, USA) to remove insoluble cell debris. Soluble proteins such as sEH were centrifuged without Genapol X-100 treatment and Cif isolated from periplasm was used directly for purification.

Using an ÄKTA Explorer setup (GE Healthcare Life Sciences, Chalfont St Giles, UK) cleared protein samples were loaded with a flow rate of 0.5 ml/min on a 1 ml HisTrap FF column (GE Healthcare Life Sciences) primed with 100% buffer A (20 mM Tris, 0.5 M NaCl, 20 mM Imidazole, pH 7.4). The column was washed with 1 ml/min buffer A until no protein elution was detected anymore with the UV detector at 280 nm. Elution was performed with a linear gradient of 1% per 2 min of buffer B (20 mM Tris, 0.5 M NaCl, 500 mM Imidazole, pH 7.4) at a flowrate of 0.5 ml/min. The eluted protein was collected in 0.5 ml fractions which was monitored by UV. Cif was eluted with a linear two-step gradient of buffer B from 4 to 20% B in 8 min and from 20 to 100% B in 8 min and a flow rate of 0.5 ml/min. The collected fractions were analyzed by SDS-PAGE and Coomassie staining and western blot.

2.7.4. Enrichment of His-tagged protein from mouse tissue

Up to 400 mg of frozen mouse tissue were homogenized in 1 ml of ice-cold homogenization buffer (0.125 M KCl, 0.25 M sucrose, 1 mM EDTA, 0.1 M potassium phosphate, pH 7.4) supplied with 0.5% (v/v) Genapol X-100 for membrane bound enzymes, in a tissue grinder on ice. The tissue homogenate was centrifuged for 15 min at 10'000 g, 4 °C (Eppendorf Centrifuge 5430R, rotor FA-45-30-11, Eppendorf AG, Hamburg, Germany) and the cleared supernatant was loaded on a primed 1 ml HisTrap FF column using a syringe pump (Harvard Apparatus 11 Plus Syringe Pump, flow 0.5 ml/min).

The column was washed with 6 ml buffer A (20 mM Tris, 0.5 M NaCl, 20 mM Imidazole, pH 7.4) and the His-tagged protein was subsequently eluted by 3-4 ml of buffer B (20 mM Tris, 0.5 M NaCl, 500 mM Imidazole, pH 7.4) whereas the flow through was collected in 0.5-1 ml fractions and analyzed by SDS-PAGE and Coomassie staining and western blot.

2.8. Protein analysis and characterization

2.8.1. Protein quantification by Bradford assay

BSA stock solution (1 mg/ml) for the calibration curve was stirred for 1 h before use and diluted according to the following Table 11 in a 96-well plate:

Table 11: Pipetting scheme for BSA calibration curve for the Bradford assay

BSA conc. [µg/ml]	**0**	**6.67**	**13.33**	**26.67**	**40.00**	**53.33**	**66.67**
BSA stock (1 mg/ml) [µl]	0	2	4	8	12	16	20
H_2O [µl]	100	98	96	92	88	84	80

Adapted from Bettina Hew, ETH Diss. No. 25662, (Hew, 2019)

The protein sample was diluted to an expected concentration within the BSA standard curve and 100 µl were provided in a well of the 96-well plate. For the Bradford working solution, Bradford reagent (Roti®-Quant 5x concentrated Bradford Reagent K015; Carl Roth, Karlsruhe, Germany) was diluted 1:2.33 in water. 200 µl of Bradford working solution were added to each well of the standard curve or sample and the absorbance was measured in a plate reader at 595 nm (SpectraMAX GeminiXS microplate fluorescence reader; Molecular Devices, San Jose, CA, USA). The standard curve as well as the samples were determined in duplicates or triplicates.

2.8.2. Peptide quantification by Lowry assay

The performance of protein digestion was tracked by Lowry peptide assay. Solutions A (2% Na_2CO_3 in 1 M NaOH) and B (0.5% $CuSO_4$ and 1% potassium sodium tartrate ($KNaC_4H_4O_6 4H_2O$)) were prepared and mixed in a ratio 50:1 to form the Lowry solution. The BSA stock solution (1 mg/ml) for the calibration curve was stirred for 1 h before use and diluted according to the following Table 12 in 1.5 ml Eppendorf tubes:

Table 12: Pipetting scheme of the BSA standards for the Lowry assay

BSA conc. [µg/ml]	0	10	25	50	75	100
BSA stock (1mg/ml) [µl]	0	2.5	6.25	12.5	18.75	25
H_2O [µl]	250	247.5	243.75	237.5	231.25	225

The sample was diluted to an expected concentration within the BSA standards. In a 96-well plate, each well was provided with 200 µl of Lowry solution and subsequently 100 µl of the diluted protein solution or BSA standards was added and incubated at room temperature for 15 min. Subsequently, 20 µl of Folin reagent was added and incubated for 30-60 min. The absorbance was measured in a plate reader at 650 nm (SpectraMAX GeminiXS microplate fluorescence reader; Molecular Devices, San Jose, CA, USA). The standard curve as well as the samples were done in duplicates or triplicates.

2.8.3. SDS-PAGE

Protein separation was done by sodium dodecyl sulfate polyacrylamide gel electrophoresis (SDS-PAGE). The composition of the used self-casted gels is shown in Table 13. Samples were mixed with Lämmli buffer (4 x Lämmli buffer: 200 mM Tris, pH 6.8, 8% SDS, 0.4% bromophenol blue, 40% glycerol, 10% ß-mercaptoethanol) and incubated at room temperature (heat sensitive EH3) or 85 °C for 5 min. Very viscous samples were sheared trough an insulin syringe before loading. 1-60 µl of sample were loaded per pocket of the gel and run with 1 x PAA buffer (25 mM Tris, 250 mM glycine, 0.1% SDS, pH 8.3) at 80-100 V for 1-3 h (Bio-Rad PowerPac™ Basic Power Supply; Bio-Rad Laboratories, Inc., Hercules, CA, USA).

Table 13: Composition of self-casted 12.5% Tris-glycine SDS-PAGE gels.

	Stacking gel (5%) [ml]	Running gel (12.5%) [ml]
Water	20.6	24.8
Rotiphorese® Gel 30	5.0	33.3
1.5 M Tris pH 8.8	3.75	-
1 M Tris pH 6.6	-	20
10% SDS	0.3	0.8
10% APS	0.3	0.8
TEMED	0.032	0.032

The specified volumes are adequate for 7 gels of 8 x 9 cm size. Adapted from Bettina Hew, ETH Diss. No. 25662, (Hew, 2019)

2.8.4. Coomassie staining

To visualize the separated protein bands, SDS-PAGE gels were incubated with Coomassie brilliant blue solution (0.25 g Brilliant blue R250, 0.25 g G250 in 45% (v/v) methanol and 10% (v/v) acetic acid) for at least 20 min at room temperature and de-stained by incubation in de-staining solution (15% isopropanol, 10% acetic acid) for 4-18 h.

2.8.5. Western blot analysis

Western blotting was performed to detect and quantify specific proteins from tissue lysates, cultured cells or bacterial expressions. The proteins were separated by SDS-PAGE and blotted onto a PVDF membrane (Immobilion-P, Merck Millipore, Burlington, MA, USA) using the semi-dry blotting technique. A PVDF membrane was activated in methanol for 5 min and subsequently equilibrated in blotting buffer (25 mM Tris, 250 mM glycine, 0.1% SDS, pH 8.3, 20% methanol). Two filter papers were soaked in blotting buffer and placed into the transfer chamber. The membrane was placed on one filter paper and the SDS-PAGE gel put on top and both was covered with the second filter paper. Air bubbles were removed using a blot roller.

After blotting for 30 min at 25 V and 1.0 A (Bio-Rad Trans Blot Turbo Transfer System; Bio-Rad Laboratories, Inc., Hercules, CA, USA) the membrane was blocked for 1 h in blocking buffer (Odyssey Blocking Buffer (LI-COR Biosciences, Lincoln, NE, USA) for Odyssey secondary antibodies or 2.5% skimmed milk powder for alkaline phosphatase (AP) conjugated secondary antibodies). The membrane was then incubated with the primary antibody diluted 1:1000 in blocking buffer for 1 h at room temperature or overnight at 4 °C if not specified otherwise. To remove excessive antibody, the membrane was washed 3 times for 15 min in TBS (10 mM Tris, 150 mM NaCl, pH 8.0). Subsequently, the secondary antibody was added in a 1:8000 dilution in TBS and incubated for 1 h at room temperature. The membrane was washed 3 times for 15 min in TBS and scanned with the Odyssey reader (LI-COR Biosciences) or developed by AP. For AP detection, the membrane was incubated in AP-buffer (100 mM NaCl, 100 mM Tris, 5 mM MgCl, pH 9.5) for 5 min. Under exclusion of air the membrane was then incubated with a mix of 33 µl Bcip and 66 µl NBT in a plastic bag in the dark. The reaction was stopped with EDTA solution as soon as the appearing purple bands were of desired intensity.

2.9. Virus production

Production of AAV was done in collaboration with the Viral Vector Facility of the University of Zurich and protocols were kindly provided by Dr. Jean-Charles Paterna. The detailed procedure is described in the doctoral thesis of Bettina Hew (Hew, 2019). In summary, the pAM-CAG vector providing the

transgene to be packed into the virus particles was co-transfected into HEK293T cells together with a helper plasmid providing *rep* and *cap* genes and a helper plasmid providing adenovirus functions. After three days, the cells were harvested, lyzed and the viral particles was purified by iodixanol gradient ultracentrifugation. After diafiltration to reduce the sample volume and to exchange the iodixanol buffer with PBS-MK buffer (PBS pH 7.4, 1 mM $MgCl_2$, 2.5 mM KCl), the viral genome (vg) containing particles were quantified using a Qubit™ 2.0 with the Qubit™ dsDNA HS Assay Kit (Thermo Fischer Scientific, Waltham, MA, USA). The obtained virus solution was aliquoted and stored at -80 °C.

2.10. Peptide analysis by LC-MS/MS

2.10.1. In-solution digestion

Inclusion bodies separated from soluble protein by centrifugation were resuspended in 50 mM Tris, pH 8, 8 M urea, and vortexed until the sample was clear. The sample was then diluted 1:10 with 50 mM ammonium bicarbonate, pH 8, to lower the urea concentration below 1 M. Trypsin (Pierce Trypsin Protease, MS Grade; Thermo Fisher Scientific, Waltham, MA, USA) was added with a final protease to protein ratio of 1:20 to 1:50 and incubated overnight at 37 °C. SPE was used to clean up the peptide samples prior MS analysis.

2.10.2. In-gel digestion

Samples (e.g. mammalian cell culture, bacterial or mouse tissue lysates) were separated using SDS-PAGE and the gel was stained with Coomassie for protein visualization. The gel was washed twice with water and protein bands of interest were cut out and chopped into 1 mm^3 pieces. To de-stain and shrink the gel pieces, they were incubated twice with 50% ACN in 20 mM ammonium bicarbonate buffer for 30 min at 37 °C (220 rpm, Sartorius Certomat R). The buffer was removed, and the gel pieces were dried under a flow of nitrogen. In case the protein of interest did not contain a cysteine, the dried gel pieces were directly soaked with trypsin (Pierce Trypsin Protease, MS Grade; Thermo Fisher Scientific, Waltham, MA, USA) in digestion buffer (5 ng/µl in 10 mM ammonium bicarbonate, 10% ACN, 0.01% triton X-100, pH 8.0) and incubated at 37 °C overnight. Proteins with cysteine containing peptides of interest were reduced and alkylated prior digestion. The dried gel pieces were soaked with dithiotreitol (DTT) (10 mM in 25 mM NH_4HCO) for 45 min at 37 °C, washed with water and then incubated with iodoacetamide (55 mM in 25 mM NH_4HCO) for 60 min at room temperature in the dark. The gel pieces were washed, dried again and soaked with trypsin in digestion buffer and incubated at

37 °C overnight. The digested sample was sonified for 5 min, the liquid fraction was collected, and the gel pieces were sonified twice with 200 µl ACN which was collected again. The collected peptide containing fractions were dried under a flow of nitrogen and reconstituted in MS-buffer (15% ACN, 0.1% FA) prior to LC-MS/MS analysis.

2.10.3. Filter aided sample preparation (FASP) protein digestion

Protein precipitation was performed to decrease the sample volume for the following FASP digestion. 100 µl of sample (his tag enriched protein from mouse liver or brain homogenates) were provided in a 1.5 ml Eppendorf tube and 400 µl methanol and subsequently 100 µl of chloroform were added and mixed well after each addition. Following, 300 µl of water were added, vortexed, and centrifuged for 5 min at 10'000 g (Eppendorf Centrifuge 5430R, rotor FA-45-30-11; Eppendorf AG, Hamburg, Germany). The upper phase was immediately removed without disturbing the precipitated protein band at the interphase. 300 µl of methanol were added to the sample, vortexed and the protein was pelleted by centrifugation at 10'000 g for 5 min. The supernatant was completely removed and the pellet was washed with 1 ml of ice-cold acetone (-20 °C) and pelleted again at 10'000 g for 1 min. The acetone supernatant was removed and the protein pellet was air-dried for 15 min.

30 µl SDS-lysis buffer (4% (w/v) SDS, 100 mM Tris pH 8.2, 0.1 M DTT) was added to the protein pellet, mixed well and spun down briefly. After the addition of 200 µl UA buffer (8 M urea in 100 mM Tris pH 8.2) the sample was mixed well, loaded onto the filter unit (Microcon-30 kDa Centrifugal Filter Unit with Ultracel-30 membrane, MRCF0R030, Merck Millipore, Burlington, MA, USA) and centrifuged for 45 min at 14'000 g, 20 °C. Another 200 µl UA buffer were centrifuged trough the filter unit (14'000 g, 45 min, 20 °C). Subsequently 100 µl IAA solution (0.05 M Iodoacetamide in UA buffer) were loaded onto the filter unit, mixed at 600 rpm for 1 min (orbital shaker) and incubated on the bench for 5 min. The filter unit was centrifuged again for 45 min at 14'000 g, 20 °C. The flow through was discarded after all steps.

To wash the sample and remove the SDS, the filter unit was flushed 3 times with 100 µl UA buffer (14'000 g, 25 min, 20 °C) and two times with 100 µl 0.5 M NaCl (14'000 g, 25 min, 20 °C). The filter unit was then transferred to a new collection tube and 120 µl of TEAB (0.05 M triethylammonium bicarbonate in water) with trypsin (Pierce Trypsin Protease, MS Grade; Thermo Fisher Scientific, Waltham, MA, USA), in a ratio of 1:50 trypsin to protein, was added and mixed well at 600 rpm for 1 min (orbital shaker). The units were incubated in a wet chamber at room temperature overnight. The following day the units were centrifuged for 25 min at 14'000 g, 20 °C and the resulting flow through was acidified with 5% TFA solution to a final concentration of 0.5% TFA in the sample.

2.10.4. Solid phase extraction (SPE)

SPE columns (ISOLUTE C18 (EC) 100 mg/1 ml, Biotage, SWE) were used to desalt the peptide samples before LC-MS/MS analysis. The columns were primed with 2 ml ACN and subsequently washed with 2 ml of buffer A (3% ACN, 0.1% TFA). The sample was then loaded onto the column, collected and loaded for a second time. After washing the SPE column again with 2 ml of buffer A, the sample was eluted with 1 ml of buffer B (60% ACN, 0.1% TFA) and subsequently 1 ml of ACN. The eluate was collected, dried under a flow of nitrogen and resuspended in MS buffer (15% ACN, 0.1% FA).

2.10.5. LC-MS/MS analysis

2.10.5.1. LC-MS/MS analysis on the TripleTOF 6600

Peptide samples obtained from protein digestion were analyzed using LC-MS/MS. Sample separation was performed on a Kinetex C18 reversed phase column with particle size 2.6 µm, pore size 100 Å, length 30 mm and internal diameter 2.1 mm (Phenomenex, Aschaffenburg, Germany) using a Dionex UltiMate 3000 rapid separation LC system (RSLC) (Thermo Fisher Scientific, Waltham, MA, USA). The mobile phase consisted of (A) water containing 0.1% FA and (B) ACN containing 0.1% FA at a flow rate of 470 µl/min. 5-20 µl sample were injected. Starting conditions of 15% buffer B were maintained for 1 min followed by a 2-step linear gradient from 15% to 50% B within 8 min and from 50% to 90% within 1 min. An isocratic flow of 90% B was held for 1 min before the column was re-equilibrated for 1 min with 15% B. The column oven temperature was set to 40 °C and the autosampler was cooled to 7 °C.
The RSLC system was coupled to a QTOF MS instrument (TripleTOF 6600; Sciex, Concord, Ontario, Canada) with resolving power (full width at half-maximum at 400 *m/z*) set to 35'000 in MS and 30'000 in SWATH MS/MS (high-resolution mode). The Turbo V ion drive source equipped with a stainless-steel electrode (100 µm internal diameter) was operated with the following MS conditions: gas 1, nitrogen (50 psi); gas 2, nitrogen (60 psi); ion spray voltage, 5500; ion-source temperature, 450 °C; curtain gas, nitrogen (20 psi); and collision energy, 10 eV. The automated calibration device system (CDS) performed an external calibration every five samples. The MS was operated in the SWATH acquisition mode where one complete cycle consists of a survey scan and a Q1 isolation strategy. The survey scan covered a mass range of 100 to 1600 *m/z* with an accumulation time of 50 ms. The Q1 isolation strategy covered a mass range of 100-1700 *m/z* with a 123 Da SWATH window for Q1 isolation (overlap 1 Da). With every SWATH window (in total 13) collision energy was increased with approx. 7.8 eV steps from 4.1 to 97 eV with a spread of ± 15 eV. Accumulation time was 100 ms in high-resolution mode. The

total cycle time was 1.4 s. All MS parameters were controlled by AnalystTF Software 1.7 (Sciex). Data was processed with PeakView 2.2 Software (Sciex), MasterView 1.1 (Sciex), and MultiQuant 2.1 software (Sciex).

2.10.5.2. LC-MS/MS analysis on the QTrap 4000

Sample separation was performed on an Agilent Zorbax 300SB-C18 (particle size 5 µM, internal diameter 2.1 mm, length 150 mm) column with a 1 mm C18 OPTI-GUARD® pre-column (Optimize Technologies Inc., Oregon City, USA) using an Agilent 1100 liquid chromatography system. The mobile phase consisted of (A) water containing 0.1% FA and (B) ACN containing 0.1% FA at a flow rate of 170 µl/min. 5-40 µl sample were injected. Starting conditions of 2% buffer B were maintained for 5 min followed by a 3-step linear gradient from 2% to 15% B within 5 min, from 15% to 50% within 35 min and from 50% to 100% within 5 min. An isocratic flow of 100% B was held for 1 min before the column was re-equilibrated for 2 min with 0% B. The HPLC system was coupled to a 4000 QTrap hybrid quadrupole linear ion trap mass spectrometer (Applied Biosystems) equipped with a Turbo V source and electrospray (ESI) interface. Analytes were recorded using information dependent acquisition (IDA). The survey scan was performed with multiple reaction monitoring (MRM) in positive mode (+MRM) using the following source specific parameters: gas 1, nitrogen (40 psi); gas 2, nitrogen (50 psi); ion spray voltage, 4500 V; ion-source temperature, 70 °C; curtain gas, nitrogen (25 psi); and collision gas set to high. Transitions and transition specific parameters are summarized in Table 14.

Enhanced Product Ion (EPI) scan was performed as dependent scan under the following conditions: gas 1, nitrogen (40 psi); gas 2, nitrogen (50 psi); ion spray voltage, 5000 V; ion-source temperature, 450 °C; curtain gas, nitrogen (20 psi); and collision gas set to high. MRM signals with a mass tolerance of 250 mDa exceeding 200 cps triggered the EPI with rolling collision energy. After three occurrences a target ion was excluded for 20 s.

All MS parameters were controlled by AnalystTF Software 1.7 (Sciex, Concord, Ontario, Canada). Data was visualized directly in the Analyst Software and was qualitatively analyzed by hand and quantified with MultiQuant 2.1 software (Sciex). Expected parent ion and fragment masses were calculated manually or with Skyline 4.1.0.18169 software (University of Washington, USA).

Table 14: Technical details of the LC-MS/MS detection of CatNuc peptides

Peptide	Transition	DP [V]	CE [V]	CXP [V]	EP [V]
Cif CatNuc +4y5	762.400 -> 573.300	70.0	36.0	15	10
Cif CatNuc +3y14	1016.500 -> 1673.963	70.0	52.9	15	10
Cif CatNuc +4y21	762.627 -> 1236.952	70.0	39.1	15	10
EH3 CatNuc +4y	780.445 -> 700.600	81.0	33.0	15	10
EH3 CatNuc +4y9	779.900 -> 1139.610	88.0	31.3	15	10
EH3 CatNuc +4	781.000 -> 350.700	80.0	35.0	15	10
EH3 CatNuc +3	1040.900 -> 175.300	120.0	85.0	15	10
EH4 CatNuc +4y8	1022.492 -> 1057.600	61.0	39.0	15	10
EH4 CatNuc +4b24	766.900 -> 930.200	100.0	15.0	15	10
Mest CatNuc +3a1	745.219 -> 86.202	56.0	95.0	15	10
Mest CatNuc +2a1	1117.211 -> 86.202	146.0	129.0	15	10
Mest CatNuc +3y2	745.600 -> 338.200	68.0	24.0	15	10
sEH CatNuc +2y15	1628.810 -> 1832.886	149.9	88.6	15	10
sEH CatNuc +4y5	815.500 -> 711.800	100.0	35.0	15	10
sEH CatNuc +3y15	1086.210 -> 1832.886	110.3	40.8	15	10
mEH CatNuc +4y9	849.669 -> 978.573	93.1	33.4	15	10
mEH CatNuc +3y12	1132.556 -> 1324.704	113.7	42.2	15	10
mEH CatNuc +2y16	1698.331 -> 1797.935	154.9	92.5	15	10
mEH CatNuc +3y5	1133.700 -> 567.600	100.0	65.0	15	10
mEH CatNuc +3y22	1133.700 -> 1200.000	100.0	45.0	15	10
mEH CatNuc +3y12	1133.700 -> 1325.500	100.0	60.0	15	10

CE, collision energy; CXP, collision exit potential; EP, entrance potential; DP, declustering potential

2.11. Fluorometric assay for the analysis of trypsin performance

To exclude unspecific cleavage or inactivity of the used trypsin, a Foerster resonance energy transfer (FRET)-based assay, which was established in our group, was performed. FRET can detect protein-protein interaction in the range of 1-10 nm. A FRET-pair consists of a donor and an acceptor fluorophore. The FRET-donor is excited at its specific excitation wavelength and its emission wavelength is the excitation wavelength of the acceptor fluorophore, which gets excited by means of non-radiative energy transfer. The used assay consisted of two different fusion proteins of the FRET-pair Cerulean (donor) and Ruby (acceptor) separated by a short linker. In one protein construct the linker carried an ideal trypsin restriction site (RK), which was well presented on the 10 amino acids long linker. In the second fusion protein Cerulean and Ruby were separated by a linker missing the trypsin restriction site, thus impeding trypsin restriction. FRET can only occur when the donor and the acceptor

fluorophore are in close proximity (1-10 nm), this means that the energy transfer from Cerulean to Ruby is not possible anymore upon cleavage of the linker by trypsin.

2 µg of the respective fusion protein were premixed in 200 µl of Tris-buffer (20 mM Tris, 100 mM NaCl, pH 7.5) in a 96-well plate. After the initial reading 1 µl of trypsin solution (0.2 mg/ml) was added and mixed well by shaking. The digests were immediately monitored by measuring the total emission spectrum from 470 to 700 nm at an excitation wavelength of 435 nm every minute for 20 min with a fluorescence reader (Tecan Infinite 200 Pro, gain set to 90; Tecan Group, ZH, Switzerland).

2.12. *In vitro* trapping experiments

2.12.1. EET trapping with EHs expressed in *E. coli*

Purified enzymes were incubated with 5 µM of the respective EETs (11,12-EET for mEH, 14,15-EET for sEH) for 20 min at 37 °C. As negative control, the same amount of trapping EH was incubated for 20 min at 37 °C without EET. Subsequently, the proteins were in-gel digested with trypsin and analyzed using SWATH on the TripleTOF 6600 MS. The SWATH data of the mEH trapping approach was filtered for 835.91519 *m/z*, the CatNuc peptide LGFQEFYIQGGDWGSLICTNMAQLVPSHVK (monoisotopic mass containing one ^{13}C and carbamidomethyl C) and 929.97942 *m/z* corresponding to the 11,12-EET modified CatNuc peptide. In the sEH trapping experiment SWATH windows were filtered for 815.1596 *m/z* which corresponds to the sEH CatNuc peptide LGLSQAVFIGHDWGGMLVWYMALFYPER, z = 4 (monoisotopic mass containing one ^{13}C) and 895.2184 *m/z* corresponding to the mass of the CatNuc peptide plus the mass of 14,15-EET.

2.12.2. EET trapping in HEK293T cells

A 10 cm dish of HEK293T cells was transiently transfected with trapping EH (mEH HQ or sEH HQ) or the WT variant. Transgene expression was allowed for 24 h, subsequently fresh cell culture medium containing 5 µM 11,12-EET (mEH) or 14,15-EET (sEH) was added to the cell culture. After 24 h incubation with the substrate, additional 5 µM of the respective EET was added to the cell culture medium. The cells were harvested 3 h later, homogenized and the proteins were in-gel digested with trypsin and analyzed using SWATH on the TripleTOF 6600 MS. The SWATH data was filtered for the same *m/z* as in 2.12.1.

2.13. Animal experiments

Two different mouse strains were used, C57BL/6J WT originally purchased from The Jackson Laboratory (Bar Harbor, ME, USA) and C57BL/6J mEH KO mice (Miyata *et al.*, 1999) kindly provided by Dr. F. J. Gonzalez, NH Bethesda, MD, USA. Colonies were maintained by the Laboratory Animal Service Center (LASC) of the University of Zurich. Animals were kept in a 12 h light/ dark cycle and had access to food and water *ad libitum*. All animal experiments were approved by the Swiss cantonal veterinary office (Zurich, license number 005/2016).

2.13.1. *In vivo* trapping

100 µl virus suspension (1-4 x 10^{12} vg/ml) was injected into the tail vein of 6-11 week old female mice and animals were sacrificed 14 days later if not indicated otherwise. Brain, liver, heart, kidneys, lung, stomach and a piece of hamstring muscle was excised and frozen at -80 °C for analysis. Mice used for IHC staining of tissue sections were deeply anesthetized and transcardially perfused with PBS (pH 7.4) and post-fixed for 2 h with 4% paraformaldehyde (PFA) on ice and subsequently incubated in PBS containing 30% sucrose overnight at 4 °C for cryoprotection.

2.13.2. GFP fluorescence in tissue sections

Cryoprotected tissue was sectioned with a Hyrax S30 sliding microtome (Zeiss, Oberkochen, Germany) at 40 µm. After washing with PBS 274 mM NaCl three times for 10 min, the sections were mounted on Superfrost Plus glass slides (Thermo Fisher Scientific, Waltham, MA, USA). Tile scans of fluorescent images were acquired on a Zeiss Apotome.2 microscope. Free-floating sections were stored in antifreeze solution (50 mM PB, 30% glucose (m/v), 30% ethylene glycol (v/v), 6.7 mM sodium azide, pH 7.4) at -20 °C.

2.13.3. IHC staining of liver and brain sections

Cryoprotected tissue was sectioned with a Hyrax S30 sliding microtome at 40 µm. Free-floating sections were washed three times for 10 min with 50% ethanol, twice with PBS with 274 mM NaCl and were then incubated in 0.3% Triton X-100, 10% normal donkey serum (NDS) in PBS with 274 mM NaCl for 1 h. Sections were incubated overnight at 4 °C with the primary antibody (anti-His-tag or anti-human mEH, 1:3000) in NDS blocking buffer. The next day, sections were extensively rinsed with PBS and incubated with the secondary antibody cyanine 3 (Cy3) (1:700) and DAPI (1:10'000) in 0.3% Triton X-100, 10% NDS in PBS with 274 mM NaCl for 45 min at room temperature. After washing with PBS

274 mM NaCl three times for 10 min the sections were mounted on Superfrost Plus glass slides (Thermo Fisher Scientific, Waltham, MA, USA). Tile scans of fluorescent images were acquired on a Zeiss Apotome.2 microscope. Free-floating sections were stored in antifreeze solution (50 mM PB, 30% glucose (m/v), 30% ethylene glycol (v/v), 6.7 mM sodium azide, pH 7.4) at -20 °C.

2.13.4. Behavioral experiments

Animals were placed onto a rotarod setup (IITC, Woodland Hills, CA) and the speed was linearly accelerated from 4 to 40 rpm over a time period of 300 s. Two training sessions were performed before the latency to fall was measured in 5-6 test sessions per mouse. An interval of at least 10 min during which the mouse was placed back into its home cage was allowed between consecutive test sessions.

2.14. Enzyme assay

EETs, 17,18-EpETE, 19,20-EpDPA, leukotoxin and isoleukotoxin were obtained from Cayman Chemical (Ann Arbor, MI, USA) and hepoxilin A3 and B3 from Biomol (Hamburg, Germany). ESA was synthesized as described in (Muller *et al.*, 1997). Typically, 100 ng purified enzyme was incubated with different substrate concentrations in 20 mM Tris 0.1 M NaCl for 10 min at 37 °C in a final volume of 20 µl. The reaction was stopped by the addition of 30 µl acetonitrile and thorough vortexing. To reduce the percentage of organic solvent interfering with the chromatography, 50 µl water was added.

Product formation was quantified by LC-MS/MS. Sample separation was performed on a Gemini XS-C18 reversed phase column (2.1 µm x 150 mm, 5 µm pore size, Phenomenex, USA) with a corresponding 1 mm C18 OPTI-GUARD® pre-column (Optimize Technologies Inc., Oregon City, USA) using an Agilent 1100 liquid chromatography system. Mobile phases consisted of (A) water containing 0.0125% NH4OH and (B) 95% acetonitrile 5% methanol containing 0.0125% NH4OH. Analytes were eluted with a three-step linear gradient from 16% B to 26% B in 2 min, 26% B to 36% B in 5 min and 36% B to 95% B in 0.7 min, at a flow rate of 350 µl/min. Hepoxilin A3 and B3 were analyzed under the same conditions except the second linear gradient from 26% B to 36% B which was in 16 min instead of 5 min.

The HPLC system was coupled to a 4000 QTRAP hybrid quadrupole linear ion trap mass spectrometer (AB Sciex) equipped with a TurboV source and electrospray (ESI) interface. Analytes were recorded using multiple reaction monitoring (MRM) in negative mode (-MRM) using the following source specific parameters: gas 1, nitrogen (50 psi); gas 2, nitrogen (50 psi); ion spray voltage, -3800 V; ion-source temperature, 550 °C; curtain gas, nitrogen (30 psi); and collision gas set to medium. The transition and the respective parameters are summarized in Table 16. Quantification was done using MultiQuant software (Sciex) and comparison to synthetic standards.

Table 15: Technical details of the LC-MS/MS detection of epoxides and corresponding diols

Compound	Transition	DP [V]	CE [V]	CXP [V]	EP [V]
8,9-EET	319.171 -> 68.900	-70	-30	-1	-10
11,12-EET	319.200 -> 167.100	-65	-18	-13	-10
14,15-EET	319.186 -> 218.800	-70	-16	-13	-10
8,9-DHET	337.209 -> 126.800	-70	-28	-7	-10
11,12-DHET	337.198 -> 166.800	-70	-26	-11	-10
14,15-DHET	337.193 -> 206.900	-70	-26	-15	-10
Hepoxilin A3	335.156 -> 273.300	-80	-20	-9	-10
Trioxilin A3	353.159 -> 126.900	-55	-30	-7	-10
Hepoxilin B3	335.156 -> 317.200	-80	-18	-3	-10
Trioxilin B3	353.191 -> 194.900	-55	-24	-13	-10
Leukotoxin	295.200 -> 171.100	-55	-17	-10	-10
Leukotoxin-diol	313.200 -> 201.100	-60	-23	-10	-10
Isoleukotoxin	295.200 -> 195.100	-55	-17	-10	-10
Isoleukotoxin-diol	313.200 -> 183.100	-60	-23	-10	-10
Epoxystearic acid	297.208 -> 279.200	-80	-28	-11	-10
Epoxystearic acid 2	297.208 -> 171.000	-100	-28	-47	-10
Epoxystearic acid diol	315.083 -> 140.800	-85	-38	-11	-10

CE, collision energy; CXP, collision exit potential; EP, entrance potential; DP, declustering potential

3. RESULTS

3.1. Deciphering the (patho)physiologic role of epoxide hydrolases by *ex vivo* cartography of their substrate landscape

3.1.1. Strategy

The goal of this project was to identify physiologically relevant substrates of EHs. With the trapping mutant approach, we expressed point-mutated versions of EHs *in vivo* in mice which can bind but not hydrolyze their substrates. These enzymes trap their preferred *in vivo* substrate and were extracted and analyzed by mass spectrometry. For this, the enriched proteins were digested with trypsin and the peptides containing the catalytic nucleophile (CatNuc) with the bound substrates were analyzed. An increase in mass of the peptide reflects the mass of the substrate, which can be used to identify it. High transgene expression *in vivo* and a good analytical method are crucial for success. Figure 15 summarizes our strategy to express the trapping EHs in the tissues of interest and to identify bound substrates using LC-MS/MS, which is explained in the following:

The first step (left row of Figure 15) was the production of enough protein of interest to create methods on our in-house QTrap LC-MS/MS. The pRSET vector was used which allowed high transgene expression upon arabinose induction in *E. coli* BL21-AI. Since we did not require correctly folded enzymes to establish the methods, transgene expression was highly induced leading to the formation of inclusion bodies which could be separated from the soluble fraction by centrifugation. The solubilized and digested inclusion bodies were used to create and optimize the QTrap LC-MS/MS methods for the unmodified CatNuc peptides.

Because the pRSET is small, this plasmid was also used for site-directed mutagenesis PCR to obtain the trapping mutants (top left of Figure 15). We created three different mutants for every EH. In the trapping mutant HQ, the catalytic His (H) was replaced by Gln (Q) which is of similar size. In case of expression problems due to this mutation, we also created the HA trapping mutant, replacing the His (H) with Ala (A) which possesses the simplest side chain. In the third mutant, DA, we replaced the CatNuc Asp (D) with Ala (A) leading to an enzyme unable to covalently bind the substrate, serving as negative control.

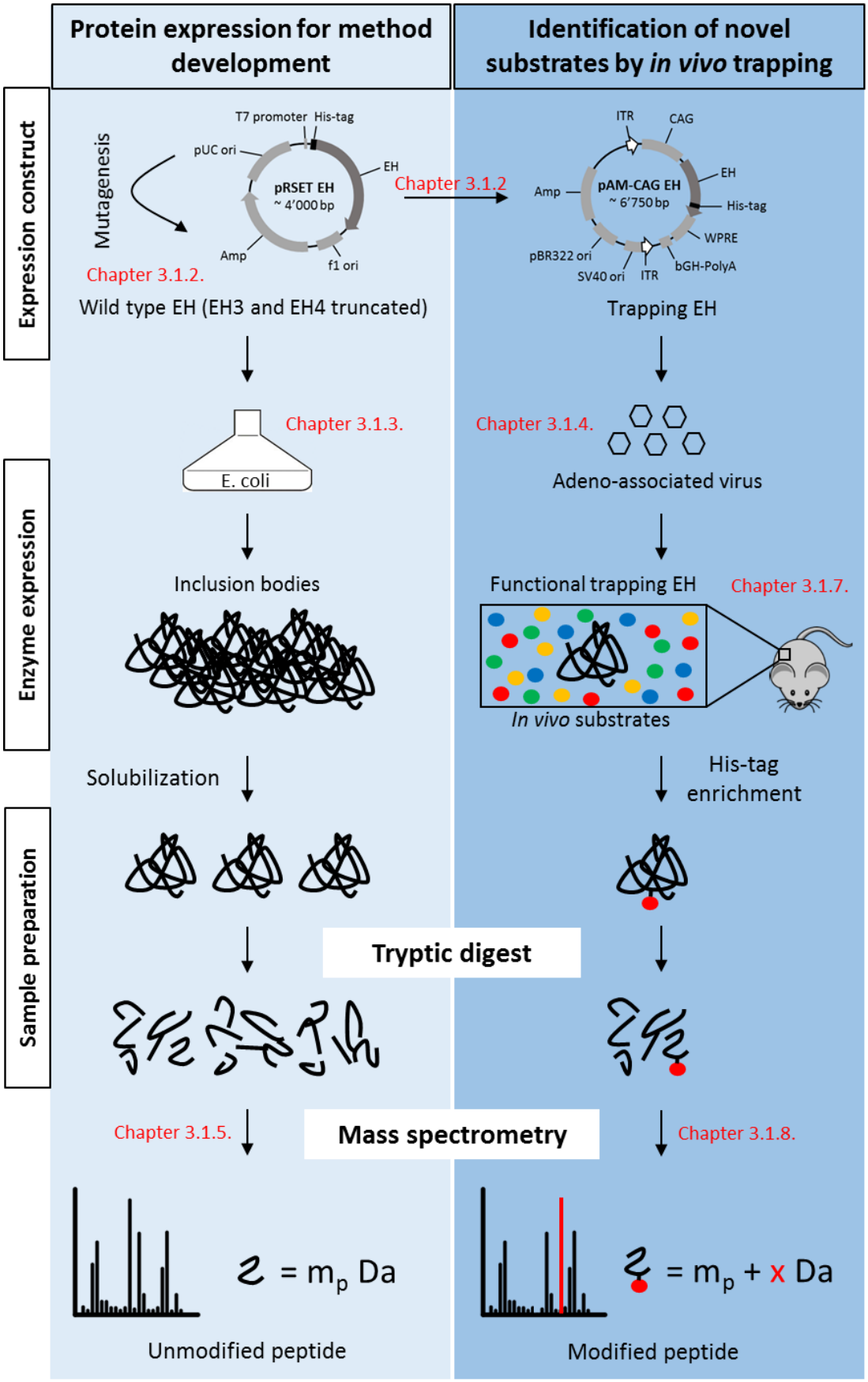

Figure 15: Initial strategy to trap and analyze substrates *in vivo* with EH trapping enzymes. Detailed description in the text. The red numbers indicate the respective chapters in the results section.

For the main experiment, the trapping and identification of *in vivo* substrates in mice (right row of Figure 15), high transgene expression in the target organs was required. We chose AAV as a viral vector for transgene delivery due to its long-lasting high transgene expression, non-pathogenicity, low immunogenicity, and the ability to transduce dividing and non-dividing cells (Kaplitt *et al.*, 1994; Lo *et al.*, 1999; Mastakov *et al.*, 2002).

To produce AAVs, the transgenes were cloned into the pAM-CAG vector. To increase transgene translation efficacy, the Kozak consensus sequence (GCCGCC) was added upstream of the start codon of the transgene. This sequence is present in eukaryotic mRNA and is important for the initiation of translation (Kozak, 1984). A scaffold attachment region (SAR), which was shown to increase retroviral transgene expression in primary human lymphocytes, was included in the pAM-CAG vector and the effect on transgene expression was tested. The virus serotype determines the infectivity of the virus towards different tissues and cell types. Our goal was to achieve high expression in various tissues after tail vein injection of the viral solution with highest priority for liver, brain, lung, kidney and heart. The brain, being the most difficult organ to reach after i.v. injection, could also be targeted by direct injection through the skull. The most suitable serotype was elected in preliminarily tests.

After expression in mice, the trapping enzymes were enriched using His-tag purification, digested with trypsin and analyzed for modifications of the CatNuc peptide with a substrate. By measuring the exact mass of the bound substrate with high resolution mass spectrometry, the chemical formula can be derived. If not yet determinable from the chemical formula, the final structure of these substrates can be obtained by release of the substrate from the protein and further analysis.

3.1.2. Cloning

Six pRSET constructs containing the wild type EHs of interest were generated using the primers described in Table 2 and the indicated restriction sites. Sanger sequencing confirmed correct insertion of the genes in frame with the N-terminal His-tag. Two additional pRSET constructs were generated which contain N-terminally truncated EH3 and EH4 to improve the otherwise difficult expression of these two enzymes in *E. coli* (Decker *et al.*, 2012). The two different trapping mutants and the negative control were generated by site-directed mutagenesis PCR of the pRSET constructs using the primers listed in Table 3. If possible, an additional silent mutation creating or removing an endonuclease restriction site was inserted to test successful mutagenesis. Sequences were confirmed by Sanger sequencing.

The pAM-CAG constructs of the wild type and the three mutants of every EH were generated using the primers listed in Table 4. The respective forward primers were used to insert the Kozak consensus

sequence GCCGCC before the start codon. Sanger sequencing confirmed the correct sequences in frame with the C-terminal His-tag.

3.1.3. Protein expression

To obtain inclusion bodies of the six EHs for MS method development, the enzymes were expressed in *E. coli* BL21-AI using the pRSET vector constructs. Expression was induced with 1 µM arabinose and performed over night at 30 °C. After lysis of the bacteria with French press, the sample was centrifuged (4000 g, 15 min, 4 °C) to separate inclusion bodies from the soluble protein and analyzed by SDS-PAGE (Figure 16).

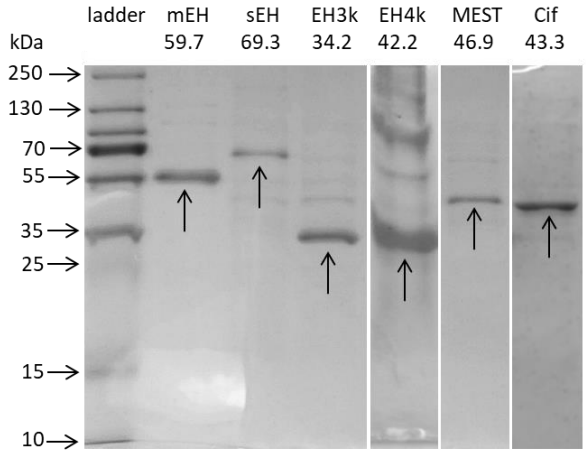

Figure 16: SDS-PAGE analysis of inclusion bodies of the six different EHs expressed in *E. coli*. Inclusion bodies were separated from soluble protein by centrifugation and an equivalent of 600 µl bacterial culture was analyzed with SDS-PAGE and stained with Coomassie. Protein size was compared to the molecular weight standard, indicated with arrows. For EH3 and EH4, the truncated proteins missing the N-terminal membrane anchor were expressed.

Proteins with the correct size (arrows) were obtained in adequate purity. Only the analysis of EH4k inclusion bodies showed another prominent protein of 70-100 kDa size which is most likely an EH4k dimer generated during sample preparation. For EH3 and EH4, the truncated proteins EH3k and EH4k which still contain the relevant sequence parts for MS analysis were expressed to increase protein expression yield.

3.1.4. Virus production

AAV were used to mediate long-lasting and high transgene expression in mice after virus injection into the tail vein. To maximize transgene expression in the target organs liver, brain, kidney, heart, stomach, and lung, transcription and translation were optimized, and different serotype were tested which is described in detail in the doctoral thesis of Bettina Hew (Hew, 2019). The results are summarized in

the following section. Viruses were produced ourselves (description of the method available in the doctoral thesis of Bettina Hew (Hew, 2019)) or by the Viral Vector Facility of the University of Zurich. An SAR element, which was reported to increase retroviral transgene expression in primary human lymphocytes (Agarwal *et al.*, 1998), was included in the pAM-CAG vector but did not increase transgene expression when transfected into cultured cells and was therefore omitted. It was futher shown that an 11 bp deletion in the 3'-ITR of the pAM-CAG constructs did not lower the titer of the produced virus nor impair the infectivity of the viral paricles towards U87 glioma cells in cell culture.

Depending on the serotype, a virus can infect different cells and tissues. To match the native expression pattern of the different EHs, the two serotypes rh10 and PHP.B were tested with a reporter virus mediating GFP expression. With serotype rh10, western blot analysis showed highest GFP expression in liver, followed by the heart, stomach and kidneys but no expression in the brain. Serotype PHP.B resulted highest GFP expression in liver and bain. Detectable transgene expression in the muscle and lung was not achieved with either of the two serotypes. The experiments showed furhtermore that first detectable transgene expression occured after three days in the liver and after seven days in the brain and that highest transgene expression was achieved 14 days post-infection. Analysis of native GFP fluorescence in brain (serotype PHP.B) and liver (serotype rh10) sections showed wide expression throughout these organs. Judged from the shape of the labelled cells, predominantely neurones were targeted in the brain with a extraordonary high expression in the CA2 region of the hippocampus which is in line with the reported expression pattern (Deverman *et al.*, 2016). In the liver, the virus mediated GFP expression in hepatocytes.

3.1.5. LC-MS/MS method development

The development of a QTrap LC-MS/MS method for a peptide modified with an unknown substrate is challenging because the mass as well as the retention time are unknown. The modified peptide needs to be identified solely by its MS/MS fragments which are predictable from the peptide sequence. The properties of our peptides of interest are summarized in Table 16.

Table 16: Properties of the six CatNuc peptides.

Name	Sequence	Sum formula	Mass [Da]	*m/z* [Da]
mEH	LGFQEFYIQGG**D**WGSLIC[CAM]TNMAQLVPSHVK	$C_{154}H_{231}N_{39}O_{44}S_2$	3396.655	850.172
sEH	LGLSQAVFIGH**D**WGGMLVWYMALFYPER	$C_{156}H_{222}N_{36}O_{37}S_2$	3257.611	815.411
EH3	C[CAM]ILVAH**D**WGALLAWHFSIYYPSLVER	$C_{149}H_{214}N_{36}O_{36}S_1$	3116.578	780.152
EH4	C[CAM]VLIGH**D**WGGMIAWLIAIC[CAM]YPEMVMK	$C_{140}H_{215}N_{33}O_{34}S_5$	3064.478	767.127
Cif	QFSPDRPFDLVAH**D**IGIWNTYPMVVK	$C_{142}H_{209}N_{35}O_{38}S_1$	3045.525	762.389
MEST	INLLSH**D**YGDIVAQELLYR	$C_{101}H_{158}N_{26}O_{31}$	2232.162	745.062

D, CatNuc and site of modification; Mass, mass of the most abundant isotope, z = 4 except MEST z = 3

MRM EPI methods were developed on the in-house QTrap 4000 for the unmodified CatNuc peptides for which both parent mass and fragment masses are known. Recombinantly expressed inclusion bodies were solubilized with 8 M urea, in-solution digested with trypsin or chymotrypsin and cleaned up by SPE. MS method development was done by direct peptide infusion (15 µl/min). To ensure that the correct parent mass and typical fragment masses were used for optimization, tuning was done manually. Methods could be developed for the Cif CatNuc peptide digested with trypsin or chymotrypsin (peptide concentration 66 ng/µl) and the MEST CatNuc peptide digested with trypsin (peptide concentration 2.5 ng/µl). Figure 17 shows representative chromatograms of the Cif CatNuc which eluted with a retention time of 40.74 min (Figure 17A) and produced typical Cif CatNuc peptide fragments (Figure 17B).

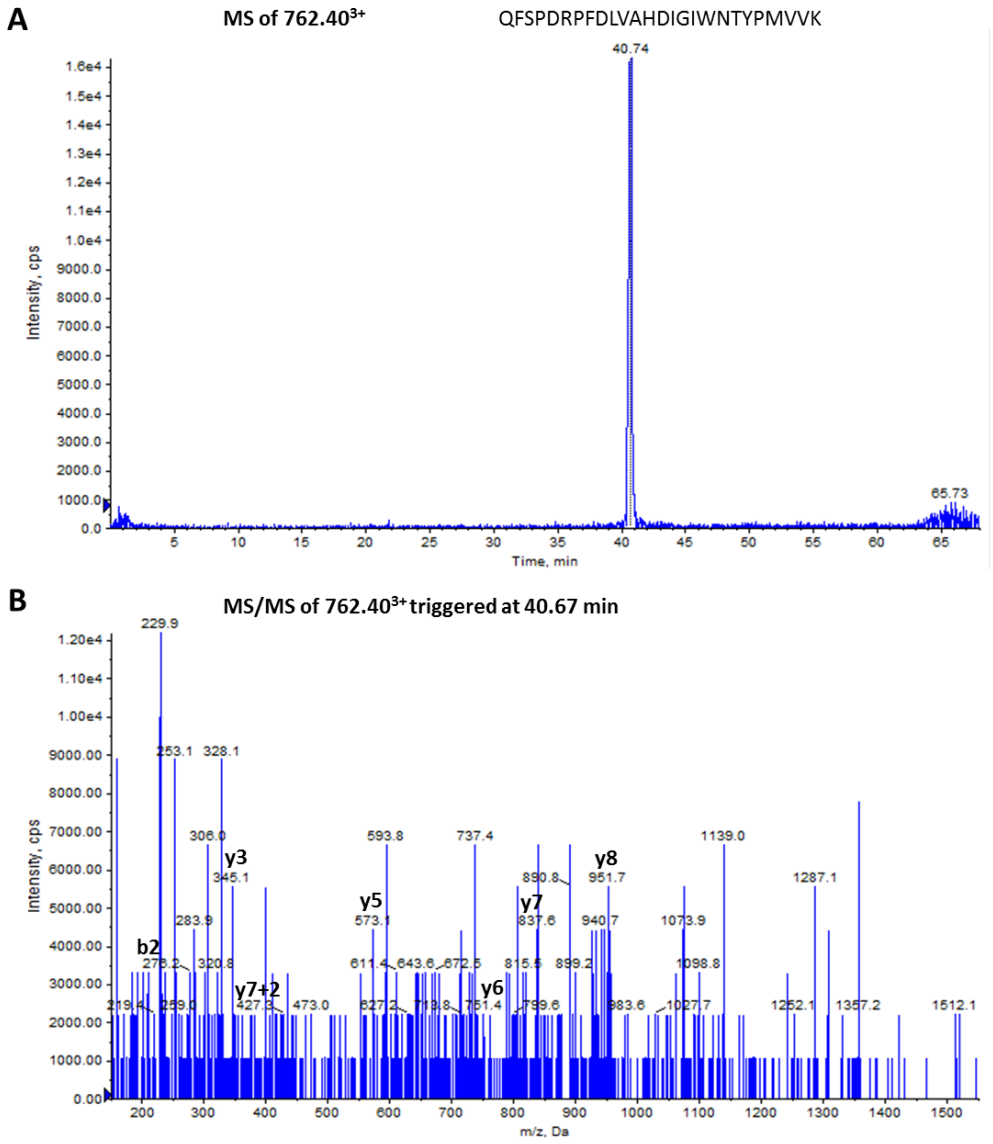

Figure 17: MS spectrum (A) and MS/MS spectrum (B) of Cif CatNuc peptide. Cif inclusion bodies were digested with trypsin and analyzed on a QTrap 4000 with MRM EPI data acquisition. The parent ion with 762.40^{3+} *m/z* eluted with a retention time of 40.74 min and the MS/MS spectrum showed seven typical Cif CatNuc peptide fragments.

The method development for the CatNuc peptides of the other enzymes was not successful. No parent ion with the correct mass could be detected. Furthermore, protein digestion with the proteases GluC or chymotrypsin, which cleave the peptide bond after Glu and Asp or aromatic amino acids, respectively, was not successful.

To verify that the peptides were not lost during sample clean-up using SPE, we determined the protein concentration after every step of sample preparation using the Lowry protein assay. EH3k and Cif inclusion bodies were digested with trypsin and protein concentrations were measured before the addition of trypsin, after the digestion, after the elution from the SPE column and after solvent evaporation and reconstitution of the sample. Furthermore, the flow-through during sample loading on the SPE column and during washing was analyzed (Figure 18).

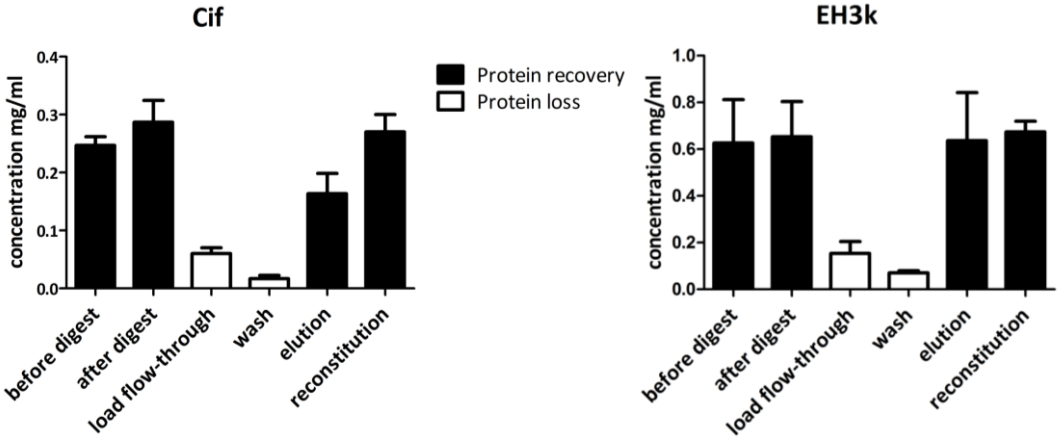

Figure 18: Peptide recovery during sample preparation with in-solution digestion and SPE. Protein concentration was determined in triplicates after every step of sample preparation of Cif and EH3k inclusion bodies using Lowry protein assay. Calibration curves were determined with matching buffer compositions. The error bars show the standard deviation of three separate determinations.

For both Cif and EH3k, the concentrations before digestion and after reconstitution were comparable, indicating good general recovery of the peptides during SPE. The collected fractions during loading and washing resulted in signals summing up to 25% of the initial sample. This indicates a moderate loss of peptides during these steps. However, the signal might also be caused by other substances present in the sample which interfere with the Lowry assay. Taken together, peptide recovery is high, yet we cannot exclude that we lose individual peptides during SPE.

So far, we have only focused on the analysis of the CatNuc peptides which are not present in the publicly available trypsin peptide libraries (except for MEST and mEH) indicating that they are difficult to detect. Other peptides that are generated by tryptic digestion of EHs and may possess better properties can be included in the LC-MS/MS method to confirm the presence of the protein. With methods created *in silico* using the Skyline Software, we were able to detect other peptides of mEH, sEH, EH3k, and Cif that were obtained when inclusion bodies were digested with trypsin. Figure 19 shows an example chromatogram of EH3k digested with trypsin.

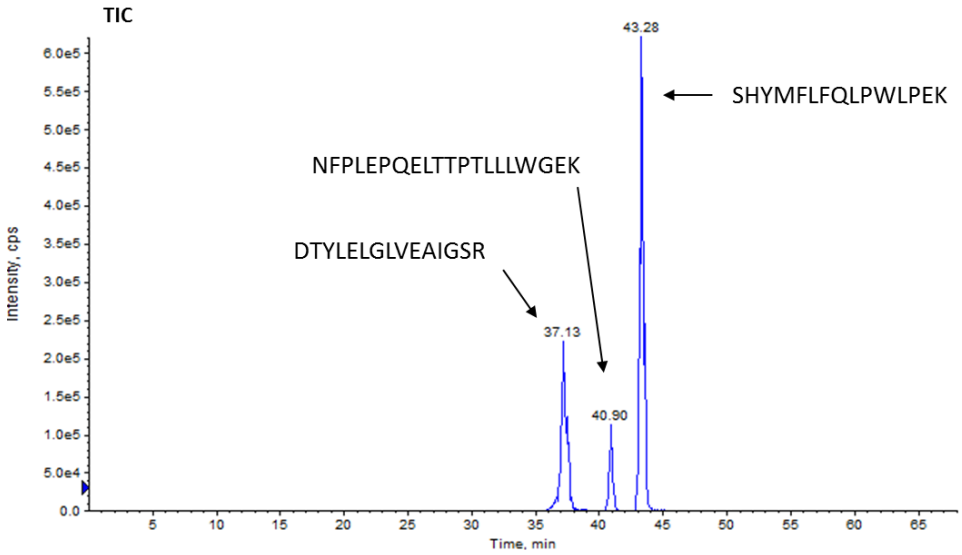

Figure 19: Total ion chromatogram of EH3k digested with trypsin. Three peptides of EH3k were detected whereas the CatNuc peptide was not found.

In contrast to the successfully detected Cif and MEST CatNuc peptides, the mEH, EH3 and EH4 CatNuc peptides contain one or more cysteines. Cysteines can form disulfide bridges which can affect the mass of the respective peptides or the digestion. To detect these peptides, the cysteine residues were reduced and alkylated with dithiothreitol and iodoacetamide (Sechi & Chait, 1998). The resulting carbamidomethyl cysteine gives a mass increase of 57.0215 Da (H_3C_2NO). With the new digestion protocol, we were able to detect the CatNuc peptide of EH3. At the same time, the intensity of the peptide SHYMFLFQLPWLPEK was reduced (Figure 20).

To develop methods for mEH, sEH and EH4 CatNuc peptides, pure synthetic peptides were ordered from JPT Technologies (Berlin, Germany). With the synthetic peptides, MRM EPI methods for the missing CatNuc peptides were developed and the existing methods were optimized.

In order to detect substrate modified CatNuc peptides from mouse tissue, we needed a method where the detection was triggered based on a fragment alone and not based on an MRM transition because the parent ion mass was unknown. In the first approach, approximately 100 MRM transitions were added to the method with the identical fragment ion but increasing parent ion masses. Like this, peptides with higher parent masses that produce the same specific fragment trigger EPI acquisition. We chose to increase the parent mass by steps of 0.3 Da. As all peptides except MEST are charged with z = 4, every step represents an increase of 1.2 Da and a range of approximately 100 Da could be covered per run. The second approach was the use of the precursor ion scan mode where the Q3 quadrupole is fixed at a specific *m/z* and the Q1 scans a mass range. In our case, the Q3 mass was fixed to a typical CatNuc peptide fragment which was known and the Q1 scan identified all masses of molecules that produced the specified fragment.

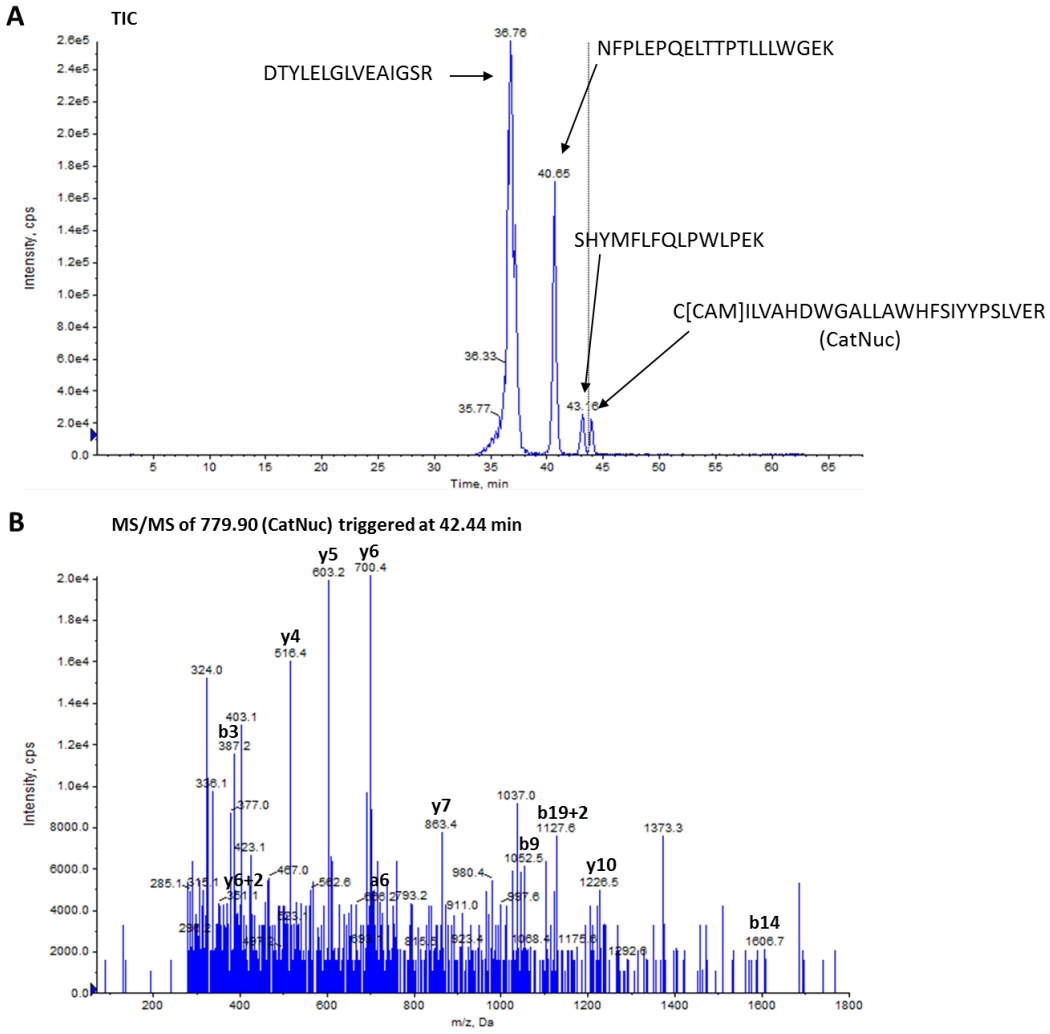

Figure 20: Detection of the CatNuc peptide and other peptides of EH3k reduced and alkylated prior to trypsin digestion and analyzed with MRM EPI data acquisition. (**A**) shows the total ion chromatogram (TIC) of four precursor ions including the CatNuc peptide of EH3k. The identity of the CatNuc peptide was confirmed with (**B**) the MS/MS spectrum triggered at retention time = 42.44 min which shows a series of expected y- and b-fragments.

With the new methods to identify substrate modified peptides we analyzed in-gel digested liver tissue from AAV-PHP.B sEH HQ infected mice. The presence of sEH in the sample was confirmed by the detection of other specific sEH peptides, while the unmodified CatNuc peptide was not detected. In the adduct mass range of 240-375 Da, which contains the typical known sEH substrates, we identified five peptide-substrate complex masses which triggered EPI acquisition. The hit with the best fragment spectrum is shown in Figure 21. The peptide eluted at 63.71 min and produced three typical sEH CatNuc peptide fragment ions in the MS/MS. However, the same molecule was also found in the negative control, indicating that the result was a false positive. This was also the case for the other identified parent masses. In all cases, the acquisition was triggered by the y5 fragment 711.800 *m/z*, which was most intense in the analysis of the unmodified sEH CatNuc peptide. However, this fragment was not present in the obtained fragment spectrum, indicating that the triggering signal was low. To

reduce false positive results, the threshold for the signal that triggers acquisition could be increased with the risk of missing peptide-substrate amounts below the threshold. Another approach is to use high resolution mass spectrometry, what we finally did.

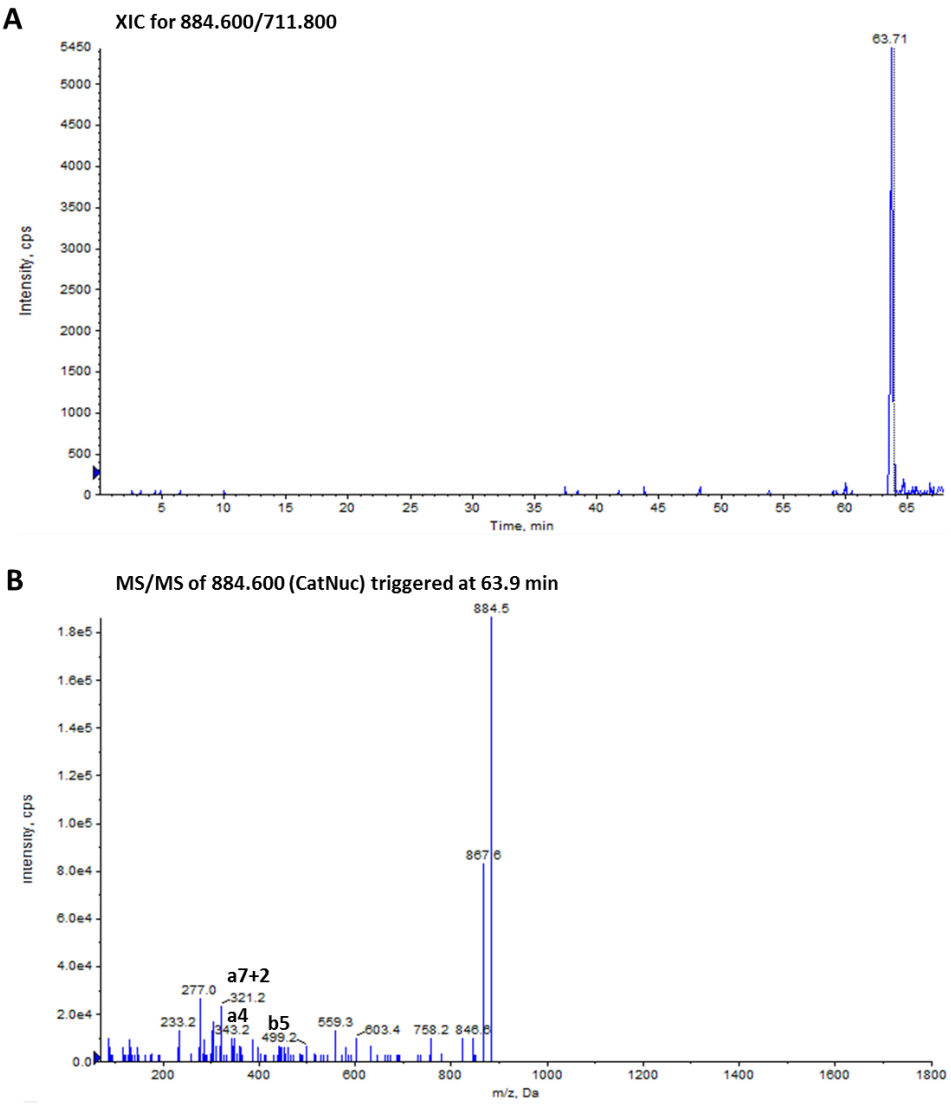

Figure 21: Best hit for a substrate modified CatNuc peptide of sEH HQ expressed in mouse liver. sEH HQ was in-gel digested with trypsin and analyzed with MRM EPI. (**A**) The extracted ion chromatogram (XIC) shows the identified parent mass of 884.600 *m/z* putatively representing a peptide-substrate complex which eluted at 63.71 min and (**B**) produced three typical sEH CatNuc peptide fragment ions in the MS/MS spectrum triggered at 63.9 min.

Via our collaborators at the Institute of Forensic Medicine (IRM Zurich) we could get access to a TripleTOF 6600. This MS offers high resolution and can be coupled to SWATH technology. High resolution MS offers the advantage that the isotope pattern of multiply charged analytes can be resolved and allows conclusions on the molecular formula. SWATH is suited for our problem because parent and fragment masses are measured all the time, recording data for every molecule that is

present above the detection limit. Data acquired with SWATH contain information about all molecules with all possible charge and isotope variants and can be analyzed multiple times, for example when more information about the peptide or the substrate has been gained, without repeating the measurement. The drawback of the SWATH technology is lower sensitivity compared to a targeted approach. However, direct comparison of dilution series of the synthetic peptides analyzed with the TripleTOF 6600 and the QTrap 4000 showed similar or even better performance with the TripleTOF 6600. Especially, the fragmentation patterns obtained on the TripleTOF were better in the way that a higher number and more exact fragments of our peptides were detected, except for Cif. Additionally, the TripleTOF measurements showed less background. Taking these advantages into account, we decided to measure the *in vivo* trapping tissue samples with the TripleTOF 6600 system at the IRM Zurich. The SWATH method used consisted of 123 Da windows covering a precursor ion mass range from 100-1700 Da.

3.1.6. TripleTOF method characterization

In this project we aim to identify the mass of a bound substrate but exact quantification is not required. Therefore, the precision, linearity and limit of detection of the method were characterized but no further validation was required.

The TripleTOF 6600 method was tested with 100 ng of each synthetic peptide. The six peptides could be chromatographically separated from each other and all were eluted in the second third of the LC-program (Figure 22). This centered and rather narrow elution profile is suitable for the trapping experiments because binding of a substrate might change the retention time of the peptide in either direction in an unpredictable manner.

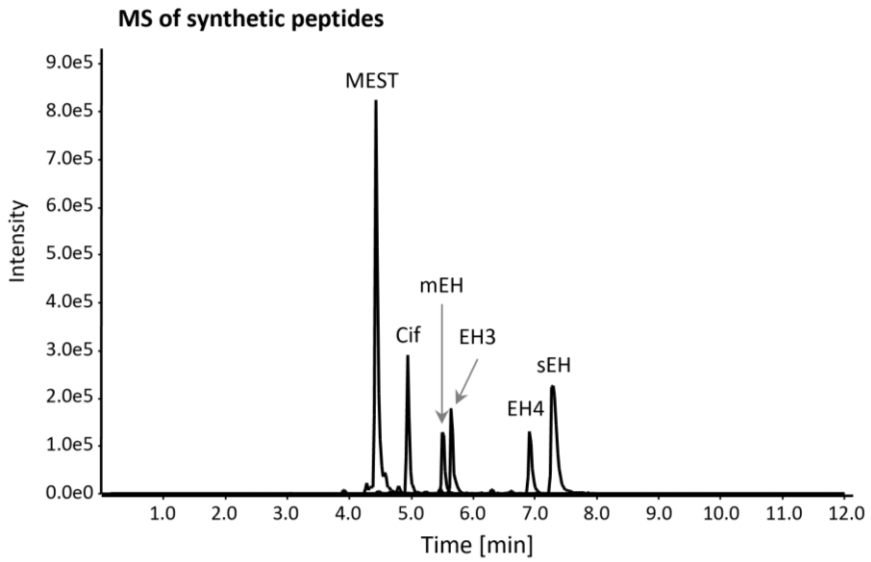

Figure 22: MS spectra of the six synthetic peptides of interest. 100 ng of each peptide were injected and analyzed on the TripleTOF 6600 using SWATH. Data extraction was done with PeakView 2.2 software.

The MEST peptide resulted in the highest peak intensity which was expected as it has optimal length and it was present in peptide libraries (PeptideAtlas) indicating good properties for LC-MS/MS detection. Figure 23 shows the MS and MS/MS spectra of each synthetic peptide. In the MS/MS spectra, sEH and MEST peptides showed a series of y- and/or b-fragments with high intensities whereas for mEH, EH3 and EH4 less typical fragments were detected. Cif resulted in only one predicted fragment, the y5-fragment. When Cif was analyzed on the QTrap 4000, more fragments were detected (Figure 17) probably due to peptide specific parameter optimization. However, one specific Cif fragment was enough to identify the modified peptide and further analysis could be performed on the QTrap 4000. The MS spectra in Figure 23 show multiple peaks for sEH, EH3 and Cif that are not present in Figure 22. The graphs were obtained from different experiments but the additional peaks are most likely due to differences in the data analysis procedure. If the precursor mass is known as was the case here, the MS spectrum is filtered with the PeakView 2.2 software for a certain mass of interest. The filter specificity can be increased by decreasing the tolerated error which can eliminate additional peaks.

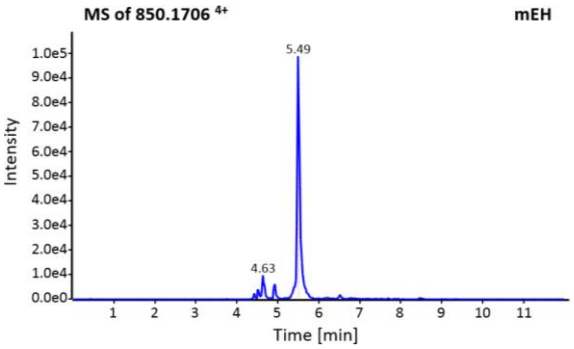
MS of 850.1706 4+
mEH
Intensity
Time [min]
5.49
4.63

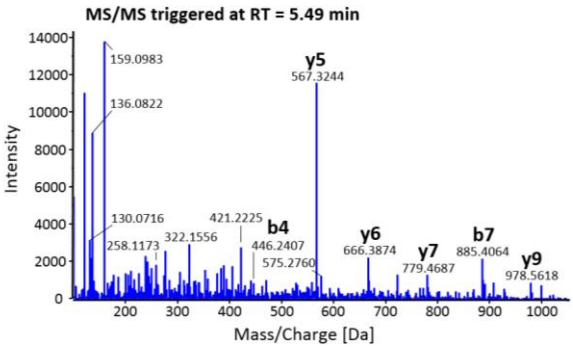
MS/MS triggered at RT = 5.49 min
Intensity
Mass/Charge [Da]
159.0983
y5
567.3244
136.0822
130.0716
421.2225
b4
258.1173
322.1556
446.2407
575.2760
y6
666.3874
y7
779.4687
b7
885.4064
y9
978.5618

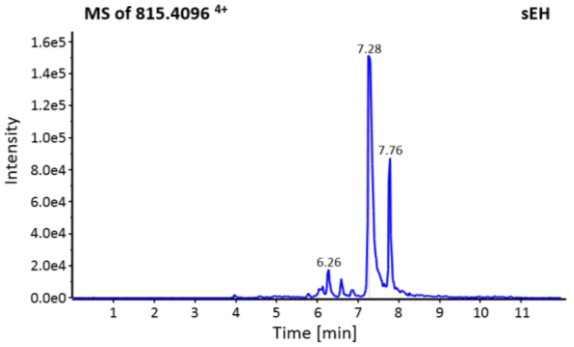
MS of 815.4096 4+
sEH
Intensity
Time [min]
7.28
7.76
6.26

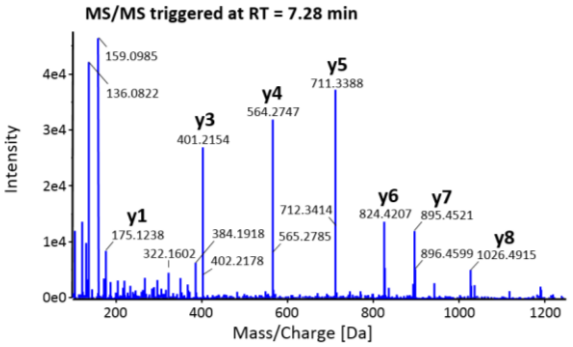
MS/MS triggered at RT = 7.28 min
Intensity
Mass/Charge [Da]
159.0985
136.0822
y5
711.3388
y4
564.2747
y3
401.2154
y1
175.1238
322.1602
384.1918
402.2178
712.3414
565.2785
y6
824.4207
y7
895.4521
y8
896.4599
1026.4915

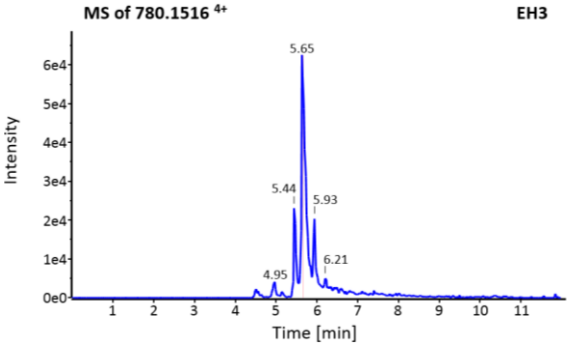
MS of 780.1516 4+
EH3
Intensity
Time [min]
5.65
5.44
5.93
4.95
6.21

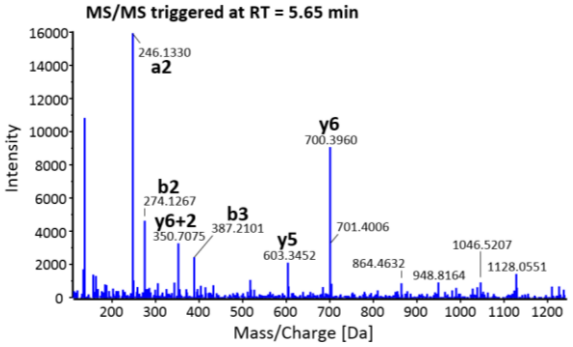
MS/MS triggered at RT = 5.65 min
Intensity
Mass/Charge [Da]
246.1330
a2
y6
700.3960
b2
274.1267
y6+2
350.7075
b3
387.2101
y5
603.3452
701.4006
1046.5207
864.4632
948.8164
1128.0551

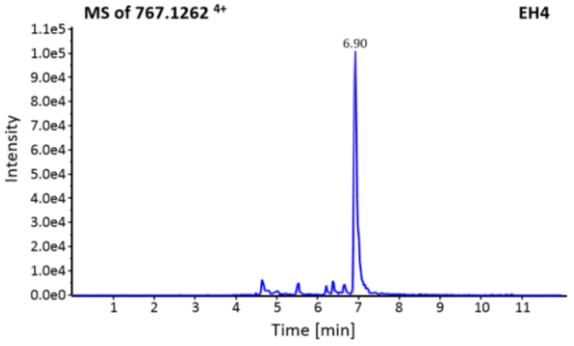
MS of 767.1262 4+
EH4
Intensity
Time [min]
6.90

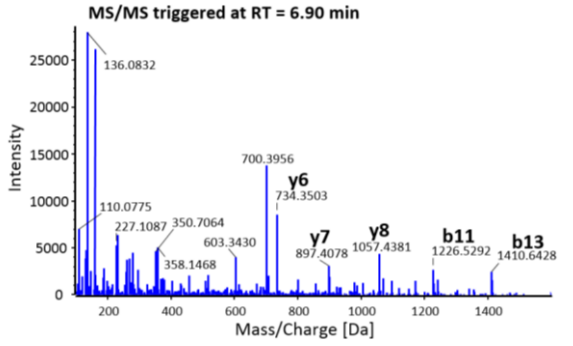
MS/MS triggered at RT = 6.90 min
Intensity
Mass/Charge [Da]
136.0832
700.3956
y6
734.3503
110.0775
227.1087
350.7064
603.3430
358.1468
y7
897.4078
y8
1057.4381
b11
1226.5292
b13
1410.6428

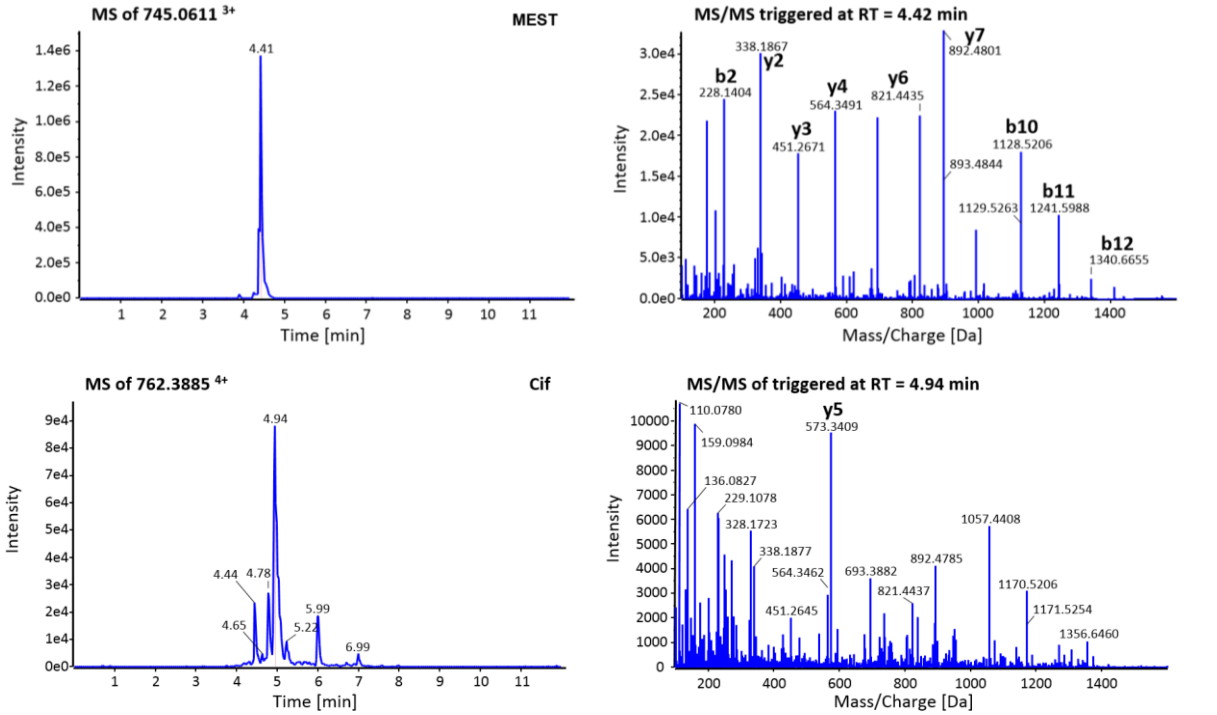

Figure 23: MS and MS/MS spectra for the synthetic CatNuc peptides. 100 ng of each peptide were injected and analyzed on the TripleTOF 6600 using SWATH. Data extraction was done with PeakView 2.2 software.

The precision of the method was determined by repetitive measurements of the identical sample containing 10 ng/µl of each synthetic peptide. The coefficients of variation (CV) are given in Table 17, calculated from six injections of the same sample.

Table 17: Average AUC, standard deviation and coefficients of variation of indicated peptides.

	Average AUC	SD	CV [%]
MEST	113900	2408	2.11
sEH	24411	3049	12.49
Cif	9207	739	8.03
mEH	5916	236	3.99
EH3	13925	1758	12.62
EH4	13918	499	3.59

The limit of detection and linearity of the method were tested with a 1:3 dilution series of the synthetic peptide mix. The relation between area under the curve (AUC) and the amount of injected peptide was plotted (Figure 24). While the graphs of mEH, EH3 and MEST displayed good linearity, sEH, EH4 and Cif did not. The limit of detection was 11 ng for all CatNuc peptides except for MEST, which had a limit of detection of 3 ng.

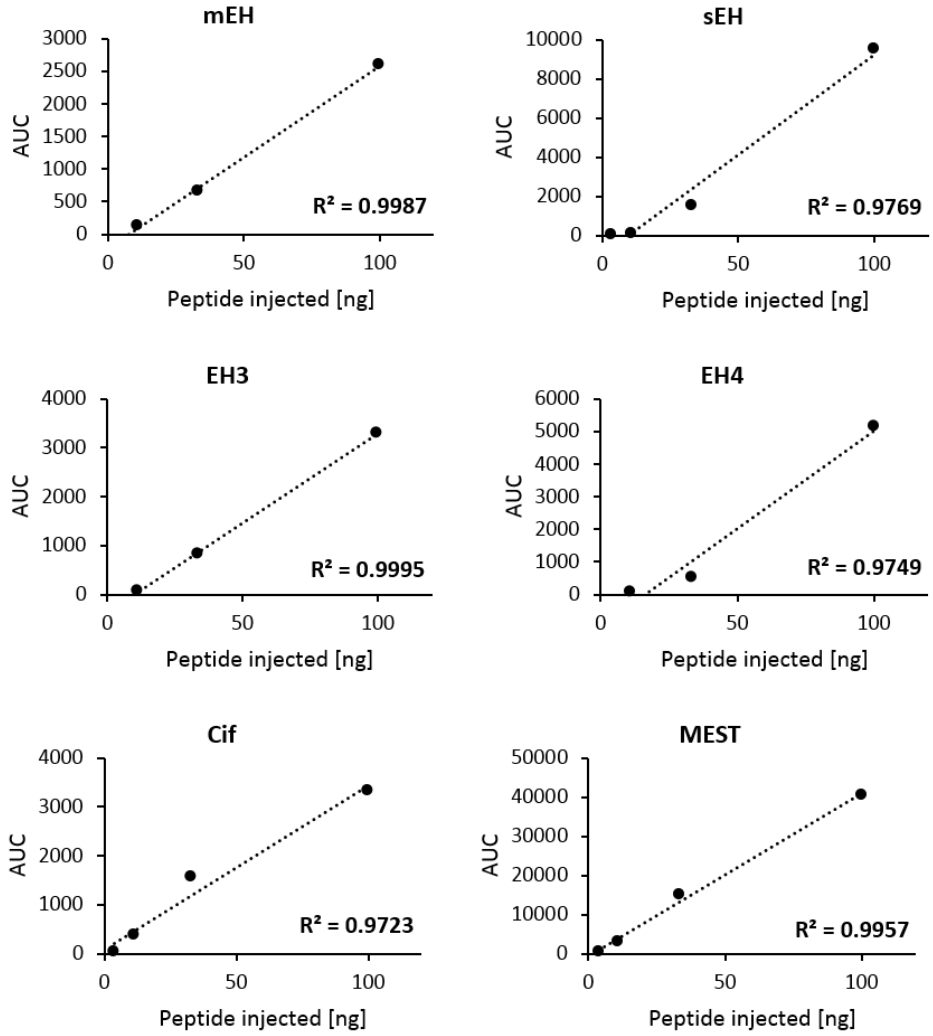

Figure 24: Linear regression of a dilution series of the synthetic CatNuc peptides. A 1:3 dilution series of a synthetic peptide mix (100 ng/µl of each synthetic peptide) was measured with the TripleTOF 6600 using SWATH. Data extraction and quantification was done with the PeakView 2.2 software.

3.1.7. Viral expression of trapping EHs in mice

For mEH, sEH, EH4 and MEST which are naturally expressed in the brain and in peripheral organs, viruses with both serotypes, PHP.B targeting the brain and rh10 targeting peripheral organs, were used. For Cif and EH3 expression, only the serotype rh10 was required as the target organs are the lung for Cif and the stomach for EH3. The performed virus injections are summarized in Table 18. 100 µl virus solution corresponding to 1-4 x 10^{12} vg/ml were injected into the tail vein of the animals. After 14 days, the mice were euthanized, and the tissues of interest were snap frozen and stored at -80 °C. For IHC analysis, animals were perfused. Unexpectedly, mice injected with the virus AAV-PHP.B mEH HQ developed a phenotype described in chapter 3.1.10 and had to be euthanized 2-3 days earlier than planned. To study this phenotype, more mice including mEH KO mice were injected and a second virus preparation as well as a virus which mediates the expression of wild type mEH were used.

Table 18: Virus injections in female C57BL/6J WT and C57BL/6J mEH KO mice.

Virus	Number of mice
AAV-PHP.B sEH HQ	7 WT
AAV-rh10 sEH HQ	4 WT
AAV-PHP.B mEH HQ*	7 WT + 2 mEH KO
AAV-rh10 mEH HQ	2 WT
AAV-PHP.B mEH WT	1 WT + 2 mEH KO
AAV-rh10 EH3 HQ	5 WT
AAV-PHP.B EH4 HQ	6 WT
AAV-PHP.B MEST HQ	6 WT
AAV-rh10 Cif HQ	2 WT

* Two different AAV-PHP.B mEH HQ virus preparations were uses for these injections.

The analysis of the mouse tissue by WB and IHC is described in detail in the doctoral thesis of Bettina Hew (Hew, 2019). The following section summarizes the results relevant for further LC-MS/MS analysis.

The preliminary virus expression experiments with the GFP reporter viruses showed highest transgene expression in the brain and in the liver (Hew, 2019), therefore analysis was focused on these two organs even though they were not of primary interest for Cif and EH3.

Manual IMAC using 1 ml HiTrap FF columns was performed to enrich the virally expressed trapping EHs from liver and brain tissue. Western blot analysis of the obtained protein solutions confirmed the presence of mEH, sEH, EH4, MEST and Cif in the liver, and mEH, sEH, and EH4 in the brain (Figure 25).

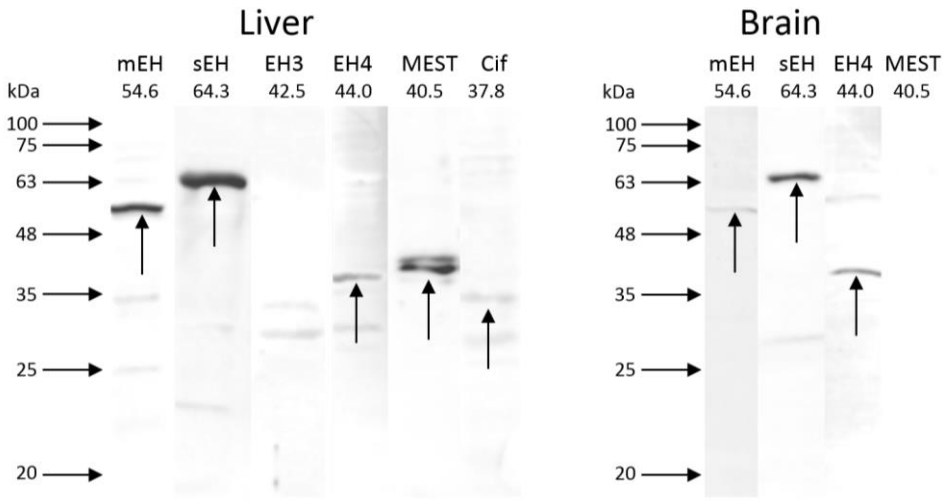

Figure 25: Western blot of trapping EHs enriched from liver and brain tissue by manual IMAC. Enriched protein from an equivalent of 5 mg tissue was analyzed. Arrows indicate the proteins of expected size. No signal was detected for EH3 in the liver and MEST in the brain. Adapted from Bettina Hew, ETH Diss. No. 25662, (Hew, 2019).

The amounts of protein virally expressed in the mouse tissue were estimated to 100-200 ng/mg tissue sEH HQ, 50-100 ng/mg tissue mEH HQ, 1-5 ng/mg liver tissue MEST HQ and 0.1-0.5 ng/mg tissue EH4 HQ and Cif HQ.

Transgene expression was further characterized by IHC which is discussed in detail in the doctoral thesis of Bettina Hew. Judging from the shape of the labelled cells, AAV mediated mEH HQ expression primarily in hepatocytes in the liver and neurons in the brain (Hew, 2019).

3.1.8. Mass spectrometric analysis of trapped substrates

For mass spectrometric analysis, the expressed trapping EHs were enriched with IMAC of 200 mg liver or brain tissue and digested using FASP. This resulted in the digestion of approximately 30 µg sEH HQ and 15 µg mEH HQ and injection of 250 ng sEH HQ CatNuc peptide and 125 ng mEH HQ CatNuc peptide into the MS, assuming efficient sample preparation (1/6 of the digest was injected and the CatNuc peptide is approximately 1/20 of the protein). With a detection limit of 11 ng, these amounts should be detectable even if some sample is lost during preparation. For the EH4, Cif and MEST trapping mutants that showed low tissue expression (Figure 25), amounts of approximately 0.5 ng EH4 HQ and Cif HQ CatNuc peptide and 10 ng MEST HQ CatNuc peptide could be injected into the MS, which suggests that the only peptide above the detection limit is the MEST CatNuc but not the CatNuc peptides of EH4 and Cif.

The first step of data analysis was to confirm the presence of the EHs in the sample by the identification of other peptides that were specific for the respective trapping EH. Presence was confirmed with two to six peptides of the trapping mEH, sEH, MEST and Cif in the liver and trapping mEH and sEH in the brain sample. EH3 and EH4 could not be detected in the mouse tissue. EH sequences showing all peptides separated by dots are listed below. The detected peptides are highlighted in bold and underlined. The CatNuc is marked with a star.

Sequence of trapping sEH

MTLR.AAVFDLDGVLALPAVFGVLGR.**TEEALALPR**.**GLLNDAFQK**.GGPEGATTR.LMK.GEITLSQWIPLMEENCR.K.CSETAK.VCLPK.NFSIK.EIFDK.AISAR.K.INRPMLQAALMLR.K.K.GFTTAILTNTWLDDR.AER.DGLAQLMCELK.MHFDFLIESCQVGMVKPEPQIYK.FLLDTLK.**ASPSEVVFLDDIGANLKPAR**.**DLGMVTILVQDTDTALK**.ELEK.VTGIQLLNTPAPLPTSCNPSDMSHGYVTVKPR.VR.LHFVELGSGPAVCLCHGFPESWYSWR.**YQIPALAQAGYR**.VLAMDMKGYGESSAPPEIEEYCMEVLCKEMVTFLDK.LGLSQAVFIGH**D***WGGMLVWYMALFYPER.VR.AVASLNTPFIPANPNMSPLESIK.ANPVFDYQLYFQEPGVAEAELEQNLSR.TFK.SLFR.ASDESVLSMHK.VCEAGGLFVNSPEEPSLSR.MVTEEEIQFYVQQFK.K.SGFR.**GPLNWYR**.NMERNWK.WACK.SLGR.K.ILIPALMVTAEK.DFVLVPQMSQHMEDWIPHLK.R.GHIEDCGQWTQMDKPTEVNQILIK.WLDSDAR.NPPVVSK.MASNR.EHHHHHHR.E

Sequence of trapping mEH

MWLEILLTSVLGFAIYWFISR.DK.EETLPLEDGWWGPGTR.SAAR.EDDSIRPFK.VETSDEEIHDLHQR.IDK.FR.FTP
PLEDSCFHYGFNSNYLK.K.VISYWR.NEFDWK.K.QVEILNR.YPHFK.TK.IEGLDIHFIHVKPPQLPAGHTPKPLLMVH
GWPGSFYEFYK.**IIPLLTDPK**.NHGLSDEHVFEVICPSIPGYGFSEASSK.K.GFNSVATAR.IFYKLMLR.**LGFQEFYIQG
GD*WGSLICTNMAQLVPSHVK**.GLHLNMALVLSNFSTLTLLLGQR.FGR.FLGLTER.**DVELLYPVK**.EK.VFYSLMR.**E
SGYMHIQCTKPDTVGSALNDSPVGLAAYILEK**.**FSTWTNTEFR**.**YLEDGGLER**.K.**FSLDDLLTNVMLYWTTGTIISS
QR**.FYK.ENLGQGWMTQK.HER.MK.**VYVPTGFSAFPFELLHTPEK**.WVR.FK.YPK.LISYSYMVR.GGQFAAFEEPEL
LAQDIR.K.FLSVLER.QASNR.EHHHHHHR.E

Sequence of trapping MEST

MVR.R.DR.LR.R.MR.EWWVQVGLLAVPLLAAYLHIPPPQLSPALHSWK.SSGK.FFTYK.GLR.IFYQDSVGVVGSPEI
VVLLHGFPTSSYDWYK.IWEGLTLR.FHR.VIALDFLGFGFSDKPRPHHYSIFEQASIVEALLR.HLGLQNR.R.**INLLSHD
*YGDIVAQELLYR**.YK.QNR.SGR.LTIK.SLCLSNGGIFPETHRPLLLQK.LLK.DGGVLSPILTR.LMNFFVFSR.GLTPVF
GPYTRPSESELWDMWAGIR.**NNDGNLVIDSLLQYINQR**.K.K.FR.R.R.WVGALASVTIPIHFIYGPLDPVNPYPEFLEL
YR.K.TLPR.STVSILDDHISQYPQLEDPMGFLNAYMGFINSFASNR.EHHHHHHR.E

Sequence of trapping Cif

MVLDR.LCR.GLLAGIALTFSLGGFAAEEFPVPNGFESAYR.EVDGVK.LHYVK.GGQGPLVMLVHGFGQTWYEWHQ
LMPELAK.R.**FTVIAPDLPGLGQSEPPK**.TGYSGEQVAVYLHK.LAR.QFSPDRPF**D***LVAHDIGIWNTYPMVVK.NQ
ADIAR.**LVYMEAPIPDAR**.IYR.FPAFTAQGESLVWHFSFFAADDR.LAETLIAGK.ER.FFLEHFIK.SHSSNTEVFSER.LL
DLYAR.SYAKPHSLNASFEYYR.ALNESVR.QNAELAK.TR.LQMPTMTLAGGGHGGMGTFQLEQMK.AYADDVEG
HVLPGCGQWLPEECAAPMNR.LVIDFLSR.GR.GGDLASNR.EHHHHHHR.E

The next step was to search for the substrate modified CatNuc peptides. For this, the MS/MS spectra were filtered for typical fragments of the CatNuc peptides using the Analyst Software. For mEH HQ a promising MS/MS spectrum could be identified. The MS/MS spectra of the single SWATH windows were filtered for the mEH CatNuc peptide fragments y5 or y6 with 567.3249 *m/z* and 666.3933 *m/z*, respectively. In the SWATH window from 960.5 to 1084.6 Da, a spectrum with three characteristic fragments was identified at a retention time of 1.34 min (Figure 26A and B). The highest peak in the fragment spectrum is 975.5593 *m/z* which is most likely the precursor ion. Indeed, when the data was filtered for this precursor *m/z*, a peak was identified with a retention time of 1.34 min (Figure 26A) which resulted in the same fragment spectrum which was identified before (Figure 26B). Besides the fragment spectrum, also the precursor spectrum at the time of peptide elution was analyzed to check the isotope pattern of the found peptide. The CatNuc mEH HQ peptide is expected to have a charge

state of 4+, thus the isotope pattern of the precursor should reveal intervals of 0.25 Da, which is not the case for the identified parent mass (Figure 26C), eliminating it as a candidate for the substrate modified CatNuc peptide.

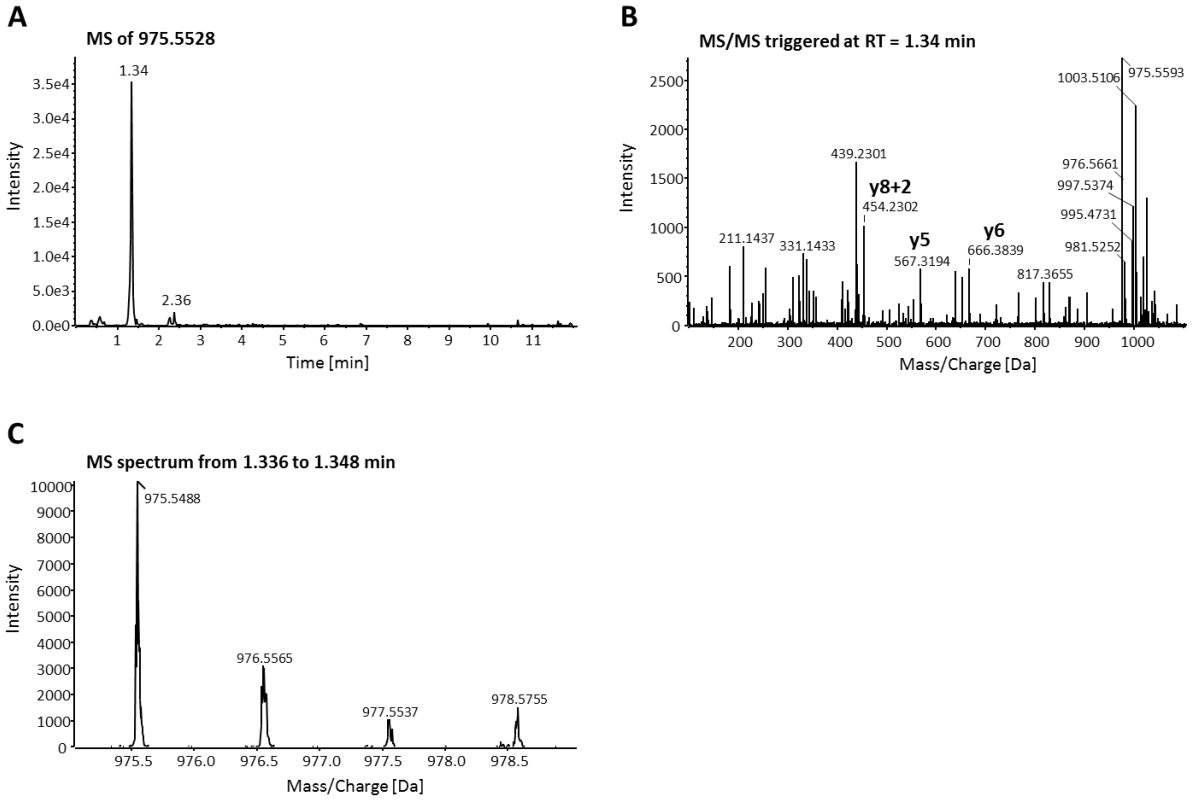

Figure 26: Detection of a peptide with three expected y-fragments but incorrect isotope pattern. Trapping mEH enriched from 500 mg mouse liver infected with AAV-PHP.B mEH HQ was digested with trypsin and analyzed with SWATH. The MS/MS spectra were filtered for typical mEH CatNuc peptide y-fragments. (**A**) shows the MS spectrum of the best hit, the precursor ion with 775.5528 *m/z*. (**B**) shows the corresponding fragment spectrum where three typical fragments of the mEH CatNuc peptide, y8+2, y5 and y6, were detected. (**C**) is the MS spectrum at the retention time = 1.336–1.348 showing the isotope pattern of the precursor ion.

No other spectra showed typical fragments except some spectra from MEST HQ from the liver and mEH HQ from liver and brain. However, these spectra were obtained from the unmodified peptide. Detecting unmodified peptides indicates that substrate trapping failed for mEH and MEST or that the substrate was lost during sample preparation.

sEH HQ expression *in vivo* was higher than expression of all other trapping EH. Failing to detect the sEH CatNuc peptide with analyzed amounts 20-times above the detection limit was unexpected. Trouble shooting, which was done in parallel to the tissue analysis, is summarized in the following chapter 3.1.9.

3.1.9. Trouble shooting

Trapping and analysis of substrates *in vivo* was difficult and not successful. Especially in the case of trapping sEH, where amounts 20 times above the determined detection limit of the MS method were analyzed, failing to detect the CatNuc peptide was unexpected. Possible explanations for this are substantial peptide loss during sample preparation or trapping of many different substrates reducing the signal of every substrate-peptide adduct below detection limit. In the case of mEH and MEST, the unmodified CatNuc peptide was detected but it remains unclear whether the enzymes are partially unmodified or whether the trapping failed completely.

To test and improve the sample preparation, the procedure was analyzed step by step to ensure efficient production and recovery of peptides of interest. This was done in parallel to the analysis of the mouse tissue and is described in the following subchapters. To avoid wasting mouse tissue for the optimization and to obtain sufficient protein amounts, trapping EHs were recombinantly expressed in HEK293T cells and *E. coli* as described in doctoral thesis of Bettina Hew (Hew, 2019). As a final measure, *in vitro* trapping experiments with recombinantly expressed trapping enzyme and known substrates were performed. This was done for mEH, sEH and Cif because the WT forms of these enzymes can be expressed actively in *E. coli* and their substrates are known and available.

3.1.9.1. Optimization of tissue sample preparation

The sample preparation for proteomic analysis consists of multiple steps. Figure 27 shows a scheme of different combinations of methods that were used for the tissue sample preparation before SWATH acquisition on the TripleTOF 6600.

The first step in sample preparation is denaturation/dissolution of the protein. Protein obtained either directly from cell culture or animal tissue or after His-tag enrichment was denatured with SDS either prior to SDS-PAGE with Lämmli buffer or during FASP with SDS-lysis buffer. The second step, the digestion with trypsin, was performed overnight either in-gel or on a filter (FASP). Before injection into the MS, the sample was cleaned up either by SPE or solvent evaporation and reconstitution.

First, the performance of trypsin was analyzed (3.1.9.1.1) and the peptide yield was compared between in-gel and filter-assisted digestion (3.1.9.1.2). To rule out that the peptides of interest are lost during clean-up, every step was analyzed individually with a mix of the synthetic peptides (3.1.9.1.3).

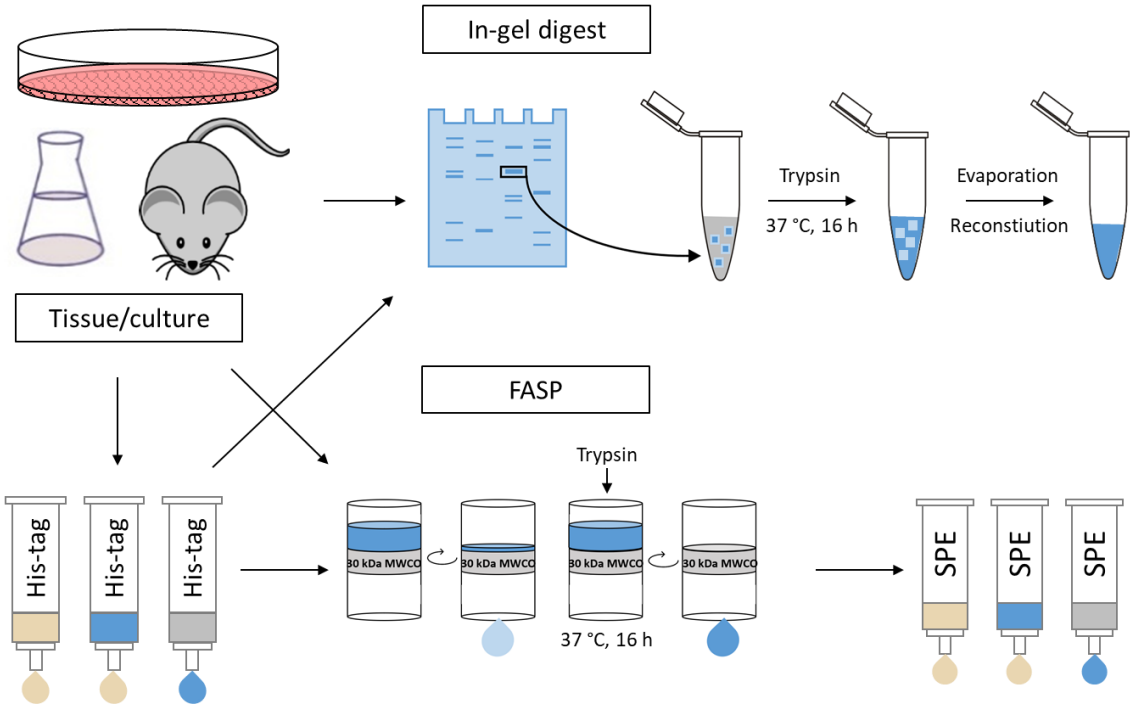

Figure 27: Scheme of sample preparation prior to TripleTOF LC-MS/MS analysis. Protein samples can be digested using in-gel digestion or FASP (filter assisted sample preparation). In-gel digest includes sample solubilization with SDS prior to separation by SDS-PAGE. Proteins are visualized using Coomassie and excised. The gel pieces are washed to remove SDS and digestion takes place directly within the gel piece. The peptides are extracted from the gel piece with ultrasound. FASP includes protein solubilization with SDS prior to loading of the proteins on the filter. SDS, impurities and proteins smaller than the filter cutoff are washed away before digestion. The peptides obtained after digestion are small enough to pass the filter and are eluted by centrifugation. FASP is usually combined with SPE to remove triethylammonium bicarbonate present in the elution buffer. Both digestion protocols can be used for homogenized tissue/cultures directly or after protein enrichment using IMAC.

3.1.9.1.1. Functionality and specificity of the trypsin digestion

To exclude unspecific cleavage or inactivity of the used trypsin, a Foerster resonance energy transfer (FRET)-based assay with the FRET-pair Cerulean-Ruby, which was established in our group, was performed. The FRET-signal of the construct with a linker including trypsin restriction sites is gradually and completely lost over the 20 min trypsin digest, seen by the reduction of the Ruby emission peak at 590 nm (Figure 28A). At the same time, the Cerulean emission peak at 480 nm is gradually increasing due to the lost energy transfer (de-quenching). This suggests efficient digestion of the linker by trypsin. The same experiment done with the FRET-construct lacking the trypsin restriction sites showed constant FRET-signal over time (Figure 28B) indicating that no unspecific digestion occurs. The small reduction of both peaks in parallel is probably due to partial digestion of the fluorophores. Taken together, these data indicate that trypsin digests exposed protein structures available in denatured protein efficiently and no unspecific cleavage occurs.

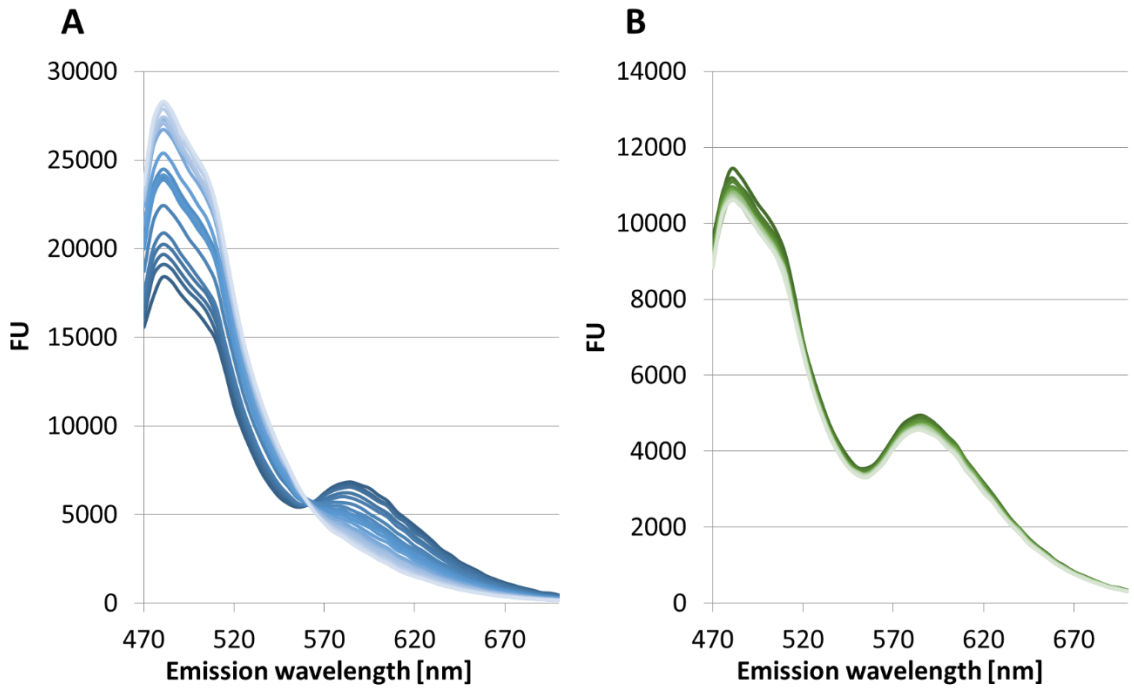

Figure 28: FRET analysis of the trypsin digest of the two different Cerulean-Ruby fusion proteins. 2 µg of the respective fusion protein (**A**) containing or (**B**) lacking trypsin specific restrictions site within the linker, was incubated with 0.2 µg trypsin at 30 °C and excited at the excitation wavelength of Cerulean, 435 nm. The digest was monitored every minute for 20 min by measuring the emission spectrum from 470 nm to 700 nm. The color shift from dark to bright indicates the different measurements over time. The Ruby emission peak at 590 nm shows FRET between the two fluorophores which is gradually lost with the fusion protein containing a trypsin specific restriction site.

3.1.9.1.2. Comparison of FASP and in-gel digestion

Tissue samples from the *in vivo* trapping experiments were initially processed using in-gel digestion. With this method the proteins are first separated by SDS-PAGE, thus proteins are efficiently solubilized by SDS, many impurities are removed, and the protein of interest is enriched in the excised gel-plug. However, the gel matrix might prevent peptide recovery. FASP, which has recently become the gold standard in proteomics, combines the use of strong detergents for universal solubilization with efficient clean-up before digestion to obtain purified peptides while avoiding the disadvantages of the gel format (Manza *et al.*, 2005; Wisniewski *et al.*, 2009). With the help of the Functional Genomics Center Zurich (FGCZ, Irchel Campus, Zurich) we compared these two methods measuring a liver MEST trapping sample. The MEST trapping mutant expressed in mouse liver (145 mg liver) was manually enriched by IMAC and the subsequent sample preparation for MS-detection was done either by in-gel digestion or FASP followed by SPE.

Table 19: Intensities and AUC of liver MEST trapping samples prepared via FASP or in-gel digestion measured with SWATH.

	Intensity MEST CatNuc 3+ 745.06113 *m/z*	**AUC MEST CatNuc 3+** 745.06113 *m/z*
FASP	31958	1856
In-gel digest	22875	1125

The MEST CatNuc peptide was detected in both samples with correct fragmentation pattern. The FASP technique provided slightly better results with higher peak areas, intensities and fragmentation patterns (Table 19). Because of these results, FASP became the favored technique for the time being for mouse tissue sample preparation.

3.1.9.1.3. Selective peptide loss during FASP sample preparation

FASP has been used for efficient detection of hydrophobic membrane proteins (Wisniewski *et al.*, 2009). However, this study, like most proteomics studies, did not require the detection of one specific peptide but any peptide can be used for protein identification. To rule out whether we lose the CatNuc peptides specificly during sample preparation, the synthetic peptide mix (100 ng/µl of each peptide) was processed like a protein sample using a combination of FASP and SPE and quantified on the TripleTOF 6600 after every step (Figure 29).

Surprisingly, the peptide recovery was strikingly different for the six different synthetic CatNuc peptides. Cif and MEST were recovered in high amounts but the other peptides were almost completely lost. The addition of trypsin alone already caused mEH to lose about 80% of its signal intensity. Evaporation of the solvent and subsequent reconstitution of the synthetic peptides in MS-buffer was causative for the substantial loss of the mEH, sEH, EH3 and EH4 CatNuc peptides. With every further processing step (FASP, SPE), the recovery of the synthetic peptides decreased. With our current protocol which combines FASP digestion followed by SPE and evaporation, only approximately 60% of MEST and Cif CatNuc peptides could be recovered, the other peptides were almost completely lost.

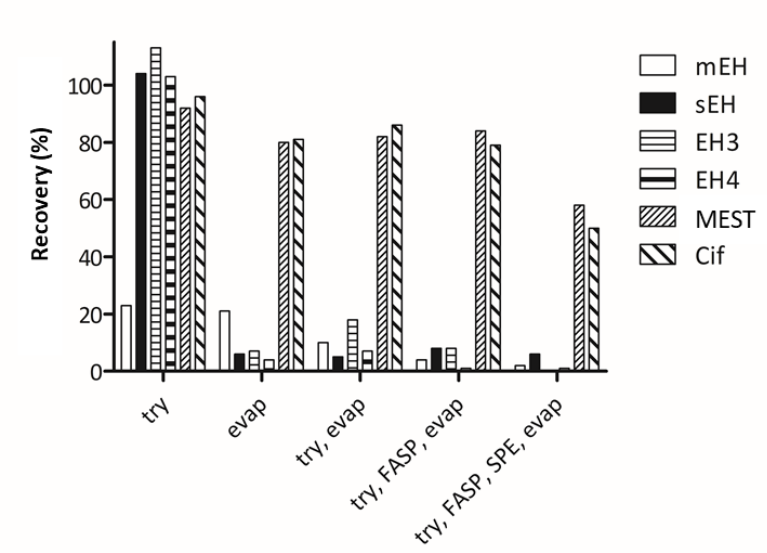

Figure 29: mEH, sEH, EH3 and EH4 CatNuc peptides were selectively lost during sample preparation. A mix of 100 ng/µl of each synthetic peptide was processed like a protein sample and the peptide content was quantified using LC-MS/MS after every step. Amounts are expressed in % signal of the unprocessed synthetic peptide mix. Try = trypsin was added to the synthetic peptide, evap = the sample was dried under a stream of nitrogen and reconstituted in MS-buffer, FASP = the sample was digested on a filter and spun through, SPE = the sample was purified using SPE.

The same phenomenon was also observed when the synthetic peptide mix was processed in a liver tissue matrix (Figure 30). Furthermore, the peptides of MEST and Cif, which were highly recovered before, have a higher loss when liver matrix was present.

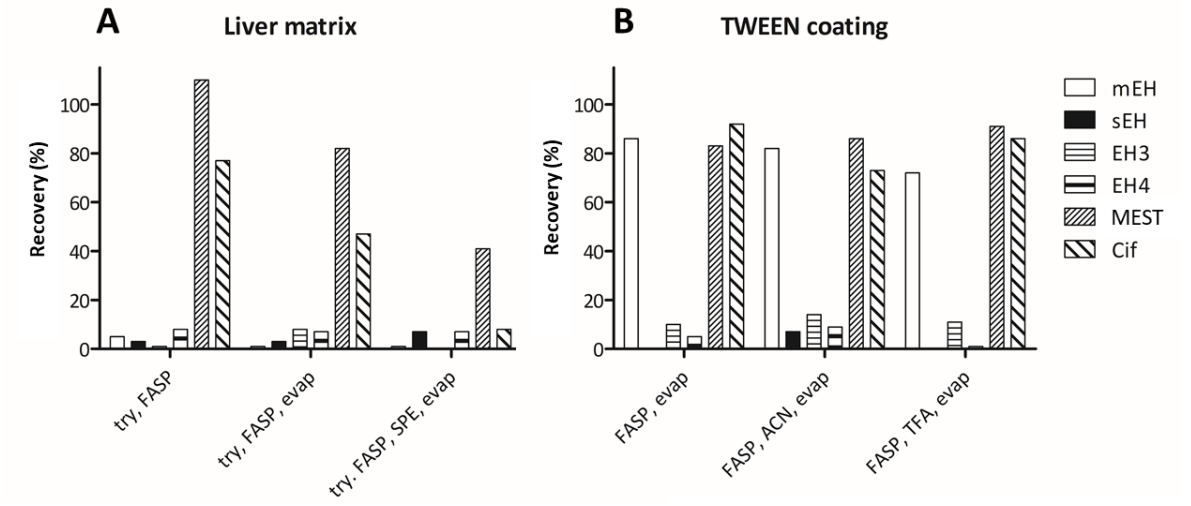

Figure 30: Peptide recovery with a liver matrix was lower but TWEEN coating increased mEH CatNuc peptide recovery. A mix of 100 ng/µl of each synthetic peptide was processed like a protein sample and the peptide content was quantified after every step in % signal of the unprocessed synthetic peptide mix. (**A**) the sample preparation was done in a liver tissue matrix. (**B**) all filters and tubes were coated with 5% TWEEN to reduce peptide adsorption and elution was performed under normal conditions, with pure ACN or after acidification with a final concentration of 0.5% TFA. Try = trypsin was added to the synthetic peptide, evap = the sample was dried under a stream of nitrogen and reconstituted in MS-buffer, FASP = the sample was digested on a filter and spun through, SPE = the sample was purified using SPE, ACN = acetonitrile, TFA = trifluoroacetic acid.

To reduce peptide loss after FASP and evaporation we coated FASP filters and used vials with 5% TWEEN, which is known to reduce protein adsorption to surfaces (Erde *et al.*, 2014). With this the recovery of mEH was highly increased. Elution of the FASP filters under acidic conditions with 0.5% TFA or with pure ACN did not increase recovery of the peptides (Figure 30).

Based on these results, we decided to use in-gel digestion combined with His-tag enrichment for all future samples of the *in vivo* trapping experiment and to treat plastic wear with TWEEN for preparation of mEH samples.

3.1.9.2. *In vitro* trapping

Recombinant trapping mEH and sEH were incubated with their known preferred substrates, 11,12-EET for mEH and 14,15-EET for sEH, in-gel digested with trypsin and analyzed for CatNuc peptide-EET adducts. The trapping experiment was done with purified trapping enzymes recombinantly expressed in *E. coli,* as well as with HEK293T cells (Hew, 2019) expressing these trapping mutants to have a more complex and eukaryotic *in vitro* system. The samples were analyzed by LC-TripleTOF 6600 using SWATH. As the substrate mass is known (EET, 320.235 Da) the parent masses of the substrate modified CatNuc peptides could be calculated. Thus, the SWATH data could be filtered for the known *m/z* of the modified and unmodified CatNuc peptides and the percentage of substrate modified vs. unmodified CatNuc peptide was determined. SWATH data was analyzed using the PeakView 2.2 software (AB Sciex).

Figure 31 shows representative spectra of sEH expressed in HEK293T cells. The unmodified sEH CatNuc peptide eluted at 7.28 min (Figure 31A) with the same retention time as the synthetic standard. The MS/MS spectrum derived at this time contains the typical y-fragments also obtained with the synthetic peptide (Figure 31B). A molecule with the *m/z* of 895.2177 corresponding to the mass of the peptide modified with EET eluted at 9.03 min and resulted in the same MS/MS pattern as the unmodified peptide (Figure 31C and D) indicating that it is indeed the substrate modified peptide. In the trapping sEH sample derived from HEK293T cells, two thirds of the peptide were substrate modified and one third was unmodified. The modified peptide was also found with the purified recombinant sEH HQ, however, the percentage of the modified peptide was much lower, between 2 and 8% and could not be quantified reliably. The modified peptide was also found when the data was filtered for MS/MS fragments without the information about the modification. This confirms that data filtering works as expected. As control, the same experiment was performed with sEH WT where no modified peptide was detected as expected.

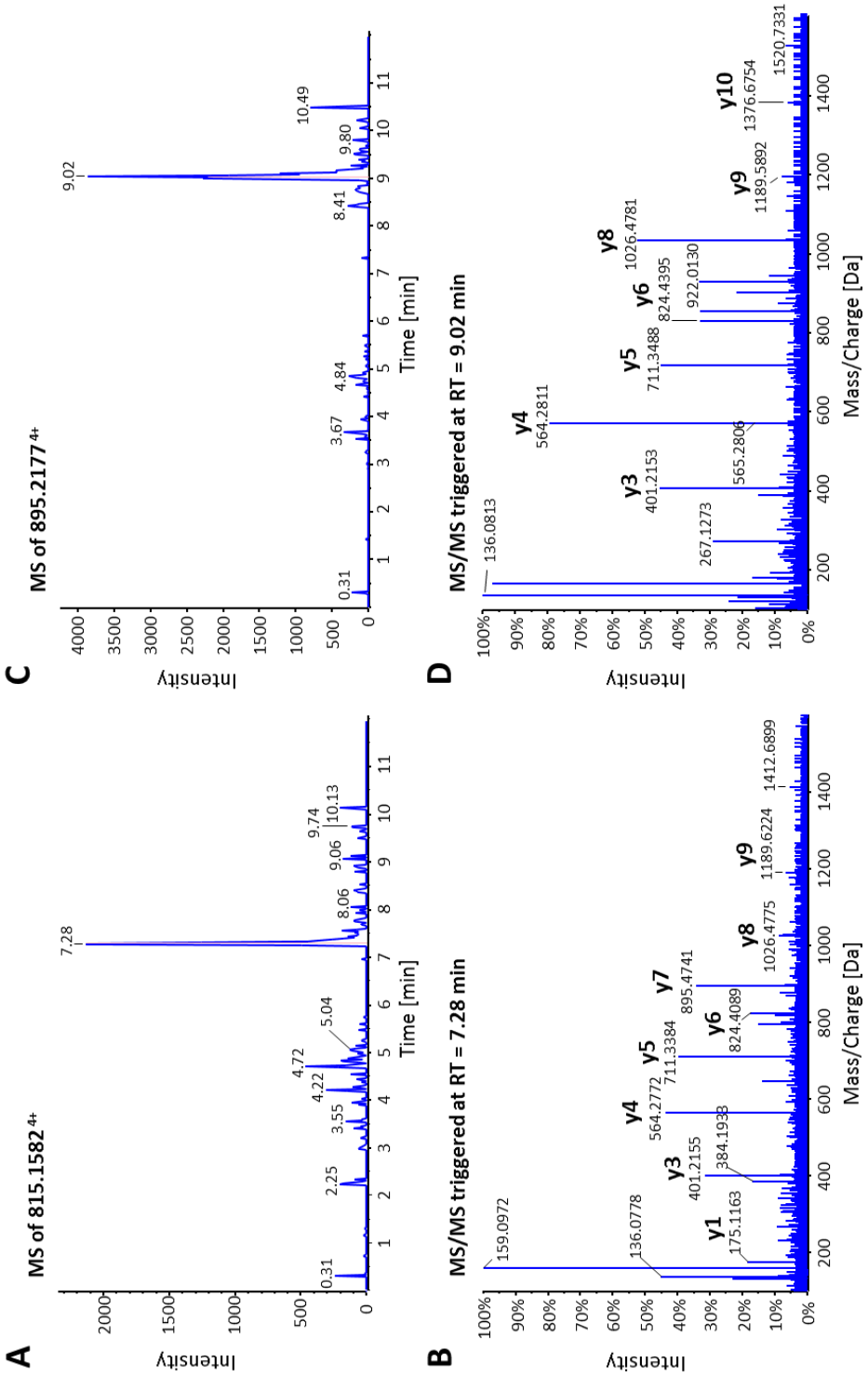

Figure 31: Detection of the sEH HQ CatNuc peptide modified with EET. Representative spectra from the analysis of sEH HQ expressed in HEK293T cells incubated with 1 µM 14,15-EET. (**A**) shows the MS spectrum of the precursor ion 815.1582^{4+} corresponding to the unmodified sEH CatNuc peptide. The identity of the peptide is confirmed with the fragment ion spectrum in (**B**) which shows a series of y-fragments as well as with its retention time of 7.28 min which is identical to the synthetic peptide. (**C**) shows the MS spectrum of the precursor ion 895.2177^{4+} corresponding to the sEH CatNuc peptide modified with EET. The retention time of this peptide is shifted to 9.03 min due to the modification. The identity of the peptide is confirmed with the fragment ion spectrum in (**D**) which shows a series of y-fragments similar to the unmodified peptide.

The SWATH analysis of the trapping mEH (bacterially expressed and in HEK293T) revealed that mEH HQ did not bind its substrate 11,12-EET (data not shown). No substrate modified peptide was found and the signal for the unmodified peptide was comparable in both mEH trapping sample and mEH WT sample. This is in line with the results from the *in vivo* trapping and indicates, that trapping mEH is non-functional and is not able to bind the substrate at all.

An *in vitro* trapping experiment with Cif HQ was planned but recombinant expression in bacteria failed. Trapping Cif expression in *E. coli* with the pET construct led to inclusion body formation and no functional Cif HQ could be purified (data not shown).

3.1.10. Mice infected with AAV-PHP.B mEH HQ developed a trembling phenotype

The in total seven wild type mice that were successfully injected with the virus AAV-PHP.B mEH HQ (see Table 18) developed a phenotype with the first signs 8 days post-infection. At the beginning, the animals showed slight trembling of the whole body which increased over time. Around 10 days post-infection, mice showed obvious shaking during movement and during rest which was combined with insecure walk. Shaking of the head was more intense than of the rest of the body. No signs of pain were observed, and grip strength observed while handling the animals was comparable to non-infected animals. The mice were euthanized 11 or 12 days post-infection as food and water intake was not guaranteed anymore.

The animals infected with AAV-rh10 mEH HQ, the virus serotype that does not lead to transgene expression in the brain, or animals infected with any other virus did not show any sign of trembling. To exclude that the phenotype was due to a contamination of the virus preparation, a second virus was produced which was used to inject three of the total seven animals. The phenotype developed after virus injection was not different between the two virus preparations.

In contrast to the trapping enzyme, the virus AAV-PHP.B mEH WT mediating wild type mEH expression did not elicit any phenotype. Furthermore, the virus AAV-PHP.B mEH HQ was tested in two mEH KO mice. The mEH KO mice developed the same phenotype seen with wild type mice but with a later onset around 11-12 days after injection and slower progression. No preterm euthanasia was required. Expression of wild type mEH in mEH KO mice did not lead to any phenotype as expected from the results with the wild type mice.

The rotarod test, a behavioral test to assess motor function and coordination (Hamm *et al.*, 1994), was used to get a quantitative measure of the trembling phenotype (Figure 32). However, due to the obvious phenotype, the investigator was not blinded during the experiment, and the number of animals was low as behavioral experiments were initially not planned. Mice infected with AAV-PHP.B

mEH HQ performed worse than control mice but no difference was seen between mice infected with AAV-PHP.B mEH WT and control mice. This result should be confirmed with higher animal numbers and assessment at different time points after virus injection.

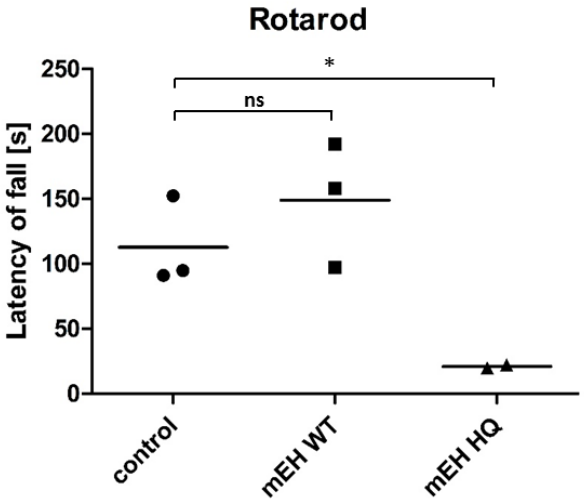

Figure 32: Mice expressing mEH HQ but not mice expressing mEH WT in the brain performed worse in the rotarod than non-infected control mice. Female mice infected with AAV-PHP.B mEH HQ or AAV-PHP.B mEH WT and uninfected control animals were tested 14 days post-injection after two training sessions on the day before and in the morning of the experiment. The plotted values represent means of five repeated measurements per animal and horizontal lines represent means of the group. Unpaired 2-tailed t-tests revealed no significant difference between mEH WT to control (p=0.3471) but significant difference between mEH HQ and control (p=0.0372). The investigator was not blinded during the study. Mean ± SEM of control: 112.8±19.8 s, n=3; mEH WT: 149.1±27.78 s, n=3; mEH HQ: 21.00±1.2 s, n=2. (ns = non-significant, * = significant, $p<0.05$)

Absence of a phenotype in animals infected with the virus AAV-rh10 mEH HQ suggests that the phenotype is caused by trapping mEH expressed in the brain. A possible cause is the loss of dopaminergic neurons in the substantia nigra (SN), the pathologic feature of Parkinson's disease (Kalia & Lang, 2015). IHC staining of brain sections obtained from mEH KO mice infected with AAV-PHP.B mEH HQ and AAV-PHP.B mEH WT confirmed expression in the SN and striatum (St), the brain regions involved in Parkinson's disease pathology (Hew, 2019). Both mEH WT and mEH HQ were expressed throughout the whole brain including SN and St which is in line with the reported tropism of the AAV-PHP.B serotype (Deverman *et al.*, 2016). Based on these results, loss of dopaminergic neurons in the SN is a possible scenario but co-staining with specific markers for dopaminergic neurons (e.g. tyrosine hydroxylase) and cell death are required.

3.2. Kinetic analysis of Cif

3.2.1. Cif expression and purification

The plasmid pGEF Cif was available in the group (Dengler, 2012). Cif cDNA was initially obtained from the DNASU Plasmid Repository (CloneID PaCD00007278, The Biodesign Institute, Arizona State University, USA). The sequence contained a point mutation, H297Y, which was reversed using site-directed mutagenesis before the gene was inserted into the pGEF expression vector to obtain a C-terminally His-tagged fusion protein.

The construct was transformed into *E. coli* BL21-AI for recombinant expression with 5 µM arabinose overnight at room temperature. The *E. coli* periplasm was isolated using osmotic shock and used for the purification of His-tagged Cif by IMAC. The purified protein was diluted with 50% glycerin to a concentration of 100 µg/ml and was stored at -80 °C until further use. The recombinant protein was purified to apparent homogeneity, as judged by the absence of impurities on Coomassie stained SDS-PAGE of 1 µg protein.

3.2.2. Cif can hydrolyze endogenous epoxides

It was shown that Cif is able to hydrolyze endogenous fatty acid epoxides (Flitter *et al.*, 2016; Hvorecny *et al.*, 2017). With a substrate screening, where Cif expressing *E. coli* lysates were incubated with 3-5 µM of different substrates, we confirm these recent findings. Additionally to the reported substrates EpETEs, EpDPAs, and 14,15-EET, we found hydrolysis of isoleukotoxin and to a low extent 11,12-EET and hepoxilin B3 (Figure 33). With mock-transfected *E. coli*, enzymatic activity was absent. The best substrates in our screening were 17,18-EpETE and 19,20-EpDPA which is in line with previous studies.

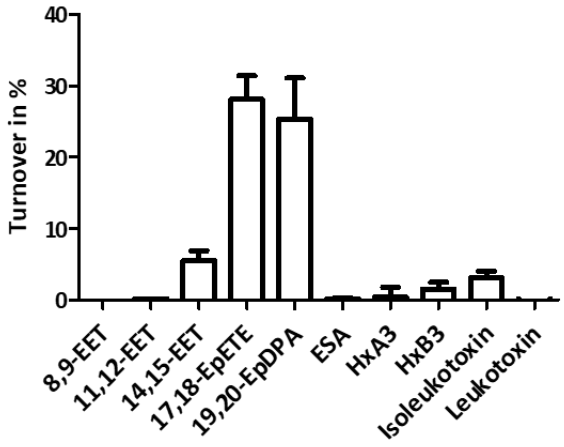

Figure 33: Fatty acid epoxide substrate screening with Cif expressing *E. coli* lysate. *E. coli* lysate was incubated with different substrates individually and turnover was quantified with LC-MS/MS. Data represent turnover in duplicates with three independent Cif expressions. The error bars show the standard deviation of the separate determinations.

3.2.3. Enzyme kinetics with endogenous epoxides

To get a better idea of the potential physiologic relevance of the 17,18-EpETE, 19,20-EpDPA and 14,15-EET turnover by Cif, we determined the respective kinetic parameters. 100 ng purified Cif was incubated with different substrate concentrations ranging from 0.05 to 30 µM in a volume of 20 µl. Linear correlation of product formation with incubation time and enzyme amount was confirmed in a preliminary test (data not shown). With increasing substrate concentrations, a linear increase of the reaction rate was determined, and saturation of the enzyme was not achieved with substrate concentrations up to 30 µM (Figure 34). Higher substrate concentrations were not tested to avoid micelle formation and due to lack of physiological relevance. In the absence of enzyme saturation, it is not possible to determine the two central kinetic parameters, i.e. maximum reaction rate v_{max} and the Michaelis constant K_m, but the catalytic efficiency k_{cat}/K_m can be determined (Figure 34).

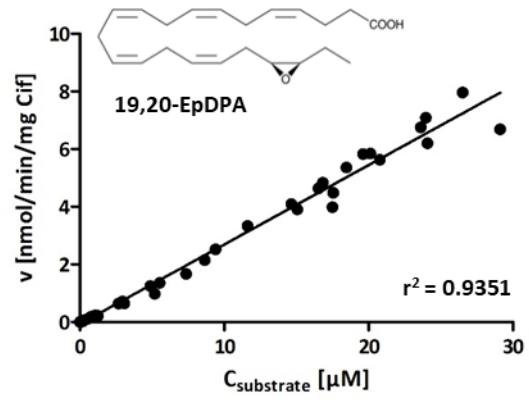

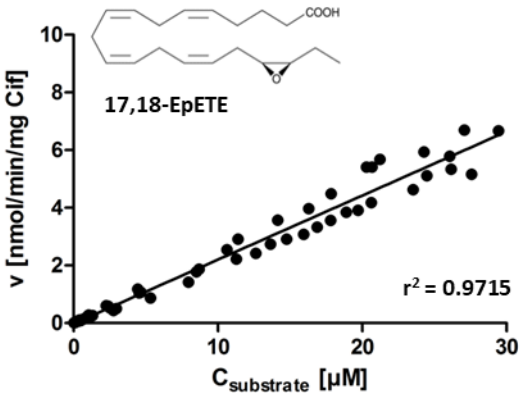

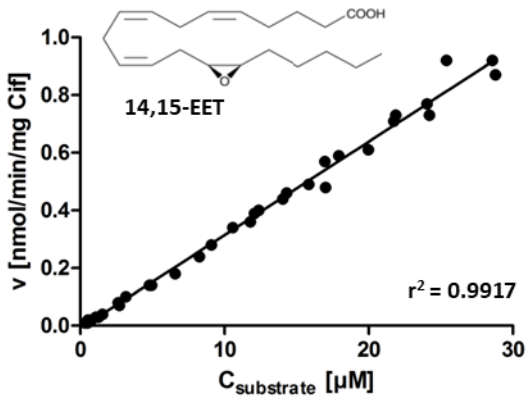

	k_{cat}/K_m [s^{-1} x M^{-1}]	95% conf. interval
19,20-EpDPA	1.54 x 10^2	1.50 - 1.59 x 10^2
17,18-EpETE	1.45 x 10^2	1.43 - 1.47 x 10^2
14,15-EET	1.48 x 10^1	1.37 - 1.60 x 10^1

Figure 34: Kinetic analysis of Cif catalyzed 19,20-EpDPA, 17,18-EpETE and 14,15-EET turnover. 100 ng purified Cif was incubated with substrate for 10 minutes using substrate concentrations ranging from 0.05 to 30 µM in a volume of 20 µl. Michaelis-Menten kinetics (solid line) was linear over the entire concentration range tested. No enzyme saturation occurred with substrate concentrations up to 30 µM. The Lineweaver-Burk plot was used to determine the catalytic efficiency k_{cat}/K_m. The individual symbols represent single determinations from 3-5 individual experiments.

Although Cif hydrolyzes 17,18-EpETE and 19,12-EpDPA with similar turnover rates when tested in individual reactions, Hvorecny et. al found no 17,18-EpETE hydrolysis when tested in a mixed-substrate assay. They incubated a mixture of 14 epoxy-fatty acids (each at a final concentration of 1 µM) with purified Cif. In this competing substrate format, Cif was only able to hydrolyze epoxides from the EpDPA family and 14,15-EET, but not from the EpETE family. We performed a mixed approach only including the best substrate of each family, 17,18-EpETE, 19,12-EpDPA and 14,15-EET (Figure 35). In the substrate concentration range tested, Cif hydrolyzed all three substrates to the same extent as predicted from the individual turnovers.

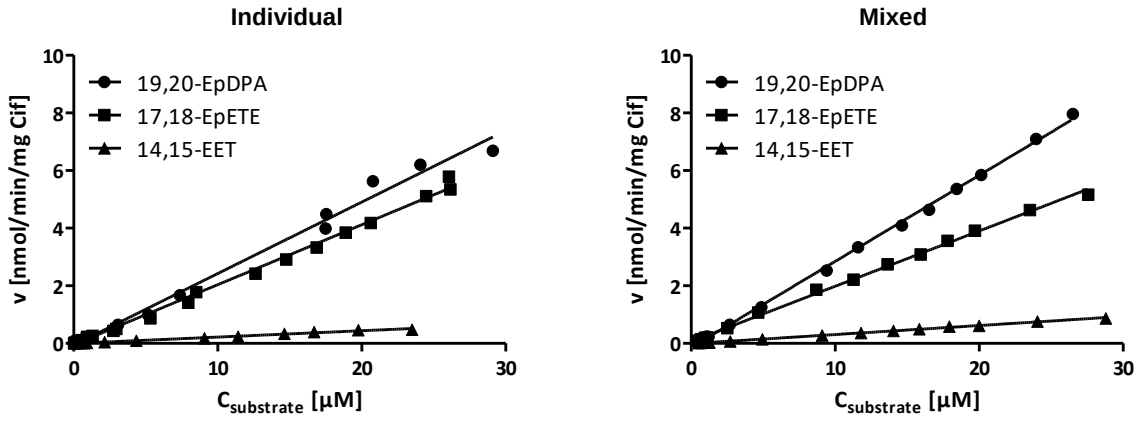

Figure 35: Kinetic analysis of Cif catalyzed 17,18-EpETE, 19,20-EpDPA and 14,15-EET turnover in an individual format (left) compared to a competing format (right). 100 ng purified Cif was incubated with each substrate individually or with a mix of all substrates. Linear regression (solid line) is comparable in both, individual and competing format.

4. DISCUSSION

4.1. Deciphering the (patho)physiologic role of epoxide hydrolases by *ex vivo* cartography of their substrate landscape

Of the five mammalian EHs that belong to the α/β hydrolase fold enzyme family, mEH and sEH have a well described substrate spectrum and some substrates are known for EH3 but no substrate has been identified for MEST and EH4. Substrate identification for the orphan enzymes EH4 and MEST would bring new insight into their role, but also for mEH, sEH and EH3, which share overlapping substrate specificities, e.g. for EETs, more information is required to resolve their function especially in metabolism of endogenous signaling epoxides. For the bacterial EH Cif, some substrates have been described but an epoxide that links the EH activity of Cif to its effect on CFTR has not been identified yet.

With the substrate trapping approach, we developed an unbiased strategy to identify the preferred substrates of EHs *in vivo*. This brings an advantage over classical approaches like substrate screening with recombinantly expressed enzymes and kinetic studies because: 1) The offered substrates do not depend on the researcher's choice and are not limited to epoxides that are known and available, 2) the substrate is captured under physiologic conditions, keeping for example subcellular organization intact, and 3) no recombinant enzyme synthesis in bacteria is required.

We have not succeeded in trapping and detecting substrates *in vivo*. The reasons for lack of success and potential measures to improve the *in vivo* trapping are discussed in the following subchapters. In chapter 4.3., current hypotheses and open questions regarding the role of the different EHs is discussed which the trapping approach could help to answer.

4.1.1. LC-MS/MS detection of CatNuc peptides

The LC-MS/MS based analysis of the *in vivo* substrate trapping was a major challenge, as our LC-MS/MS approach differed from a classical proteomics approach. We needed to detect one specific peptide of a protein and not just a subset of well detectable peptides of this protein. Furthermore, this peptide was modified with an unknown mass resulting in an unknown precursor mass which required identification by its fragment pattern.

A potential problem for LC-MS/MS method development and sample analysis were modifications of the CatNuc peptides (other than the bound substrate), either introduced by the expressing organism as post-translational modifications or artefacts from sample preparation. Post-translational modifications by bacteria were only an issue during method development with inclusion bodies but are of no concern for the analysis of proteins expressed in mice. Modifications that can be introduced during sample preparation include carbamylation, oxidation, deamination and intermolecular ester formation between Ser and Asp. For example, it was shown that urea used for inclusion body solubilization might lead to carbamylation of N-termini, Lys or Arg (Kollipara & Zahedi, 2013). To reduce this, urea buffer was freshly prepared before use and exposure to heat combined with urea concentrations above 1 M was avoided. With pure synthetic peptides we could circumvent the problem of modifications during method development. During tissue sample analysis there was no indication of protein modifications. The mEH and MEST CatNuc peptides were detected in the liver samples and the sEH and Cif CatNuc peptides did not show any modification (other than the substrate) when expressed in HEK cells (Hew, 2019). For the EH3 and EH4 trapping mutant CatNuc peptides, modifications cannot be excluded but the main issue here was most likely low protein concentration in the target tissues. Due to the unbiased recording of all peptides with SWATH, modifications that do not affect the main fragments of the CatNuc peptides would be detected in the same way as the modification with the substrate.

The sensitivity for the MEST CatNuc peptide was higher than for all the other CatNuc peptides (Figure 22), probably due to its smaller size of 19 compared to 26-30 amino acids. Guidelines for targeted proteomic assays suggest selection of peptides of 7-20 amino acid length, which only the MEST CatNuc peptide fulfilled (Hoofnagle *et al.*, 2016). Moreover, of the peptides of interest, only the MEST and mEH CatNuc peptides are present in trypsin-based peptide data bases (PeptideAtlas), indicating that the other peptides are difficult to detect or are lost during routine sample preparation. We addressed the problem of peptide size by using the alternative protease chymotrypsin, which cleaves after aromatic amino acids. The Cif CatNuc peptide, which was 8 amino acids long, could be detected but the peptides of the other enzymes were not detected, probably due to their length of only 4-5 amino acids. With the alternative protease GluC, digestion would lead to adequate peptide sizes, but this enzyme cleaves the peptide bond after Asp or Glu including the CatNuc, which might be impaired if it is modified with a substrate. Based on this, we decided to focus on trypsin generated peptides. Another strategy to reduce the peptide size would be to introduce another trypsin restriction site (Lys or Arg) into the amino acid sequences of the trapping mutants by site-directed mutagenesis PCR. However, this would likely interfere with the substrate interaction, and potential induction of undesired artifacts (from altered substrate selectivity to non-reactivity) prohibits such an approach.

4.1.2. *In vitro* substrate trapping

Trapping mutants of the rat mEH and sEH have been used before to trap radioactively labelled substrates *in vitro* (Arand *et al.*, 1996; Arand *et al.*, 1999a) to elucidate the reaction mechanism. Furthermore, successful detection of the substrate-peptide complex with LC-MS/MS was shown in a preliminary *in vitro* experiment performed in our group. However, these experiments were performed with the rat enzymes. In the *in vitro* trapping experiment performed in this project in parallel with the *in vivo* trapping, human trapping mEH and sEH were used.

Of the trapping sEH expressed in HEK293T cells, two thirds were modified with the provided substrate, 14,15-EET, confirming the functionality of the substrate trapping and detection method. Possible reasons for the occurrence of unmodified peptide are hydrolysis during sample preparation, residual hydrolytic activity of the trapping mutant or lack of ability to bind the substrate due to misfolding. However, the occurrence of unmodified peptide was low and of minor relevance for the trapping experiment.

In contrast to the rat trapping mEH used by others, the human trapping mEH used here did not bind the offered substrate in the *in vitro* trapping experiment. As no residual hydrolytic activity could be detected with the recombinantly expressed mEH HQ in a turnover assay (data not shown) and no substantial hydrolysis during sample preparation is expected, the most likely explanation is that human mEH HQ is not functional. This difference between human and mouse trapping mEH was unexpected but demonstrates that the use of trapping EHs from a different species might be useful to overcome enzyme folding problems.

In vitro trapping with recombinant Cif HQ failed due to misfolding of the protein which was confirmed by others during the course of this project (Flitter *et al.*, 2016).

4.1.3. *In vivo* substrate trapping

In the *in vivo* trapping experiment, viral expression of mEH, sEH, MEST and Cif *in situ* was high enough to detect the protein by LC-MS/MS. However, no substrate modified CatNuc peptide could be detected from mouse tissue.

Possible explanations for this outcome can be categorized in three main groups: 1) the peptide is absent, 2) the peptide is not modified or 3) the (modified) peptide was missed in the analysis. Absence of the peptide can occur if 1.1) the protein or peptide is lost during sample preparation or when 1.2) the expression of the enzyme in the tissue fails or is too low. Reasons that could explain why the peptide is not modified are that 2.1) the trapping enzyme is not functional and thus not able to perform the first catalytic step including binding of the substrate or that 2.2) the substrate-peptide ester bond is hydrolyzed during sample preparation. It is also possible that 2.3) the trapping enzyme did not meet

its substrate due to wrong expression site or that 2.4) the enzyme has residual activity leading to the hydrolysis and release of the product. The peptide can be missed in the analysis if 3.1) it carries a modification (besides the substrate modification) which changes the fragment fingerprint substantially. Also, if 3.2) the enzyme traps many different substrates the amount of every single peptide-substrate complex can be lowered below the detection limit of the LC-MS/MS. Another possibility is that 3.3) the data analysis failed and positive spectra were missed.

In the case of sEH HQ, we assume that it is a combination of two reasons, peptide loss during sample preparation (1.1) and trapping of different substrates which lowers the amount of every peptide-substrate complex below the detection limit (3.2). The unmodified peptide was not found, excluding problems that lead to unmodified peptides. In the *in vitro* trapping experiment, sEH CatNuc-EET intermediates were successfully detected (Figure 31) confirming that the trapping mutant is functional and that the peptide analysis works. However, analysis of the sample preparation showed selective and substantial loss of the sEH CatNuc peptide. EH3, EH4 and mEH CatNuc peptides were also lost to a major extend. Solvent evaporation or centrifugation through the filter used for FASP was enough to lose >80% of these peptides. In contrast, the recovery of Cif and MEST peptides was around 60% even after the combination of FASP, evaporation, and SPE (Figure 29). Judging from the LC-elution profile, sEH is the most hydrophobic peptide and Cif and MEST the most hydrophilic. It is well recognized that hydrophobic peptides can be lost during sample preparation and analysis due to nonspecific adsorption to vials, tips and parts of the HPLC (Hoofnagle *et al.*, 2016). This effect is more prominent at low concentrations. Different approaches are proposed to reduce nonspecific adsorption including organic solvent, detergents, peptide mixtures or addition of BSA. The strategy must be compatible with the chromatography and the MS-analysis. For example, addition of peptides might lead to ion suppression and organic solvent or detergents might interfere with the chromatography. Success depends on the peptide and needs to be evaluated individually (Kovalchuk *et al.*, 2015; Hoofnagle *et al.*, 2016). We addressed this problem with substantial effort, including use of low binding plastic ware, pre-treating filters and vials with TWEEN, peptide elution under acidic conditions or elution with organic solvent. The initially very poor mEH CatNuc peptide recovery could be increased to >80% with use of TWEEN treated plastic ware. However, for sEH, EH3 and EH4, no improvement was achieved (Figure 30).

The mEH HQ CatNuc peptide was due to the comparably high expression a promising candidate and the CatNuc peptide could be detected in liver and brain tissue, however, unmodified. The same result was obtained in the mEH HQ *in vitro* trapping. Residual activity in terms of diol formation of the recombinant trapping mEH expressed in bacteria was not observed (2.4) (data not shown), indicating that the trapping mEH is not capable of covalent substrate binding (2.1) or that the substrate is cleaved

off the enzyme/peptide during sample preparation (2.2). In the trapping mutants the His of the charge relay system was replaced by Gln. His is the only amino acid that can switch between the protonated and unprotonated form at physiologic pH, which potentially interferes with protein folding when absent. However, functionality of the Gln mutant was shown for rat sEH HQ and reported for rat mEH HQ (Arand *et al.*, 1999b) which led to the decision to use the Gln mutant. As discussed later in this section, also Cif and MEST trapping mutants seem to be non-functional. Alternative trapping mutants like the HA mutant, enzymes in which the acidic residue of the catalytic triad is replaced, or trapping EHs from a different species, need to be evaluated *in vitro*. This is not possible for EH4 and MEST as no substrates are known.

The CatNuc peptides of EH3 HQ and EH4 HQ were not detected at all. The poor viral expression of these enzymes in the mouse tissue is a major factor to explain this outcome (1.2). This was further aggravated by peptide loss during sample preparation (2.2). Low EH4 HQ expression was shown by western blot and the EH4 CatNuc peptide could not be detected with LC-MS/MS, which is in line with the estimated injected CatNuc peptide amount of 0.1-0.5 ng which is far below the detection limit of 11 ng. Both enzymes are suggested to be membrane bound which poses a challenge for recombinant expression. EH3 was reported to cause problems in different expression systems (Decker *et al.*, 2012) and we encountered problems with both enzymes in our bacterial expression system (Hew, 2019) where expression was only successful after removal of the membrane anchor. However, the cells of living mice should provide everything required for the expression of these enzymes as they naturally express EH3 and EH4 homologues. The lower tissue concentrations of EH3 and EH4 trapping mutants compared to the other enzymes is likely due to shorter half-lives of the EH3 and EH4 proteins and possibly mRNA.

The MEST trapping mutant was a very promising candidate as the CatNuc peptide showed the best detection properties (Figure 22). Its expression in liver tissue and peptide recovery during sample preparation was high enough to detect the CatNuc peptide and other peptides from infected liver tissue by LC-MS/MS. However, the CatNuc peptide was only detected without a bound substrate. Possible reasons are: the mutant was unable to bind the substrate (2.1), the ester bond between substrate and peptide was hydrolyzed during sample preparation (2.2) or because of residual hydrolytic activity (2.4), or the substrate was not present at the expression site (2.3). The functionality of trapping MEST and the stability of the peptide-substrate complex cannot be analyzed as no MEST substrate is known. However, a misfolded trapping mutant not able to perform the first substrate binding step is a likely scenario considering the non-functionality of mEH and Cif (see below) trapping mutants. Absence of the substrate at the expression site, in our case the liver, is unlikely as MEST is widely expressed throughout the body.

The expression of Cif HQ could be detected by LC-MS/MS but *in vitro* data indicated that the trapping mutant HQ is unable to bind its substrate (2.1). Furthermore, Cif is present in the lung after *P. aeruginosa* infection but transgene expression in the lung was not detected after AAV infection (Hew, 2019). During the course of this project a functional Cif E153Q trapping mutant was reported (Flitter *et al.*, 2016), thus substrate trapping could possibly be performed with this trapping mutant as recombinant, purified enzyme by adding it to a lung homogenate. This approach would not be suitable for mEH or sEH as we are interested in the substrate trapped in a subcellular context but in the case of Cif, unknown substrates might be revealed. However, the advantage of continuous production of metabolites in a living system is lost when using a lung homogenate which reduces substrate availability. For example, reliable Cif detection required approx. 5 µg Cif which translates to 130 pmol enzyme. Assuming efficient trapping, a minimum of 130 pmol substrate need to be available in the lung homogenate to load the trapping Cif. If one lung (approximately 200 mg tissue translating to 200 µl homogenate) was used, an overall substrate concentration of 0.65 µM would be required which we do not expect for epoxides, in particular because they might only be produced in a particular cell type constituting only a moderate fraction of the overall tissue (there are more than 30 individual cell types in the lung). However, in the absence of better alternatives, either the use of high lung tissue amounts or, possibly more promising, the expression of trapping Cif in a CFTR expressing cell line (e.g. lung cell line) are a worthwhile approach to find substrates for Cif.

4.1.4. AAV-PHP.B mEH HQ trembling phenotype

Mice injected with AAV-PHP.B mEH HQ developed a striking phenotype with severe shaking during movement and in rest, combined with insecure walk. In wild type mice, first signs developed 8 days after injection of the virus with fast progression. In contrast, mEH KO mice injected with AAV-PHP.B mEH HQ showed a later onset 11-12 days after the virus application and a slower progression.

The well-studied AAVs are safe and elicit low immunogenicity (Salganik *et al.*, 2015) and the absence of any phenotype after the application of AAV-PHP.B sEH HQ, AAV-PHP.B EH4 HQ, and AAV-PHP.B MEST HQ indicate that the phenotype is driven by trapping mEH expression and not the virus itself. Furthermore, no phenotype was observed when trapping mEH was expressed in the periphery using AAV serotype rh10, indicating that expression in the brain is causal for the phenotype.

The hypothesis that the trapping mEH exhibits residual hydrolytic activity and is virally expressed in cells that lack natural mEH expression, leading to dysregulation of mEH substrates, was excluded as the viral expression of wild type mEH with the same virus did not lead to a phenotype.

A possible explanation is that trapping mEH is misfolded due to the point mutation forming protein aggregates which lead to neurotoxicity and perhaps neurodegeneration eliciting a Parkinson's disease-

like pathogenesis. In Parkinson's disease, loss of dopaminergic neurons in the substantia nigra pars compacta (SNpc) causes in humans the typical motor symptoms: resting tremor, bradykinesia and rigidity (Kalia & Lang, 2015). The dopaminergic neurons in the SNpc project to the basal ganglia and synapse in the striatum. Loss of these neurons leads to dopamine deficiency in the striatum responsible for the motor symptoms of Parkinson's disease (Blesa & Przedborski, 2014). The observed trembling phenotype resembles one of the typical hallmarks of Parkinson's disease. Furthermore, the trapping mEH was not able to trap a substrate *in vitro* and *in vivo* likely due to misfolding, supporting the hypothesis of aggregate formation.

The hypothesis was addressed in a preliminary experiment by other members of the group with mEH and tyrosine hydroxylase (TH) co-staining of brain sections obtained from mEH KO mice infected with AAV-PHP.B mEH HQ. TH is the rate limiting enzyme in the synthesis of dopamine and a marker for dopaminergic neurons. AAV-PHP.B mEH HQ injected mice showed substantially reduced TH-immunoreactivity in the SNpc compared to control mice, suggesting loss of dopaminergic neurons.

Interestingly, mEH KO mice infected with the same virus which led to the same mEH HQ expression pattern in the brain showed a later onset and slower progression of the phenotype. mEH KO mice show no overt phenotype (Miyata *et al.*, 1999) but when treated with the neurotoxin MPTP, they show significant lower TH-positive cell loss compared to wild type mice (Liu *et al.*, 2008). MPTP, which commonly used to create a mouse model for Parkinson's disease, exerts selective toxicity towards dopaminergic neurons and causes gradual loss of these neurons in the SNpc (Tieu, 2011). The results of Liu et al. suggest increased resistance of dopaminergic neurons in mEH KO mice which could explain the milder phenotype after injection of AAV-PHP.B mEH HQ. The increased resistance could be driven by increased EET levels in mEH KO mice, as EETs exert neuroprotective effects via various pathways (Wang *et al.*, 2018).

Another, very speculative hypothesis to explain the trembling phenotype is that mEH functions as a receptor which is activated upon substrate binding and inactivated upon hydrolysis of the product. This would result in cell signal transduction as long as the enzyme-substrate complex persists. Under natural conditions, this complex would only exist for a short time during the first catalytic step but in case of the mEH trapping mutant, the complex would be stable, probably resulting in constant signal transduction, which could appear as trembling due to overstimulation of the brain motor system. This theory of mEH being a receptor would solve another mystery: mEH which contains Asp instead of Glu as acidic residue in the catalytic triad (E404D) shows 20-40 faster turnover than the by nature preferred wild type mEH (Arand *et al.*, 1999a). The mutation causes faster hydrolysis and release of the product which would decrease the time the enzyme-substrate complex persists and cell signaling occurs. This

reduction in signaling would explain why the catalytically slower enzyme is avoided by nature. (Comprehensive discussion of mEH E404D in chapter 4.3.1.)

Further experiments are required to draw conclusions on the cause of the phenotype. It would be very interesting whether application of L-dopa reduces the symptoms indicating that a lack of dopamine is responsible for the phenotype. Furthermore, application of mEH inhibitors could potentially be used to investigate whether the phenotype is due to a receptor function of mEH.

4.2. Kinetic analysis of Cif

In a substrate screening the additional Cif substrates isoleukotoxin, hepoxilin B3 and 11,12-EET were identified. However, the turnover rates under the used screening-conditions were below the turnover rates of the already reported substrates 17,18-EpETE, 19,20-EpDPA and 14,15-EET, indicating that these new substrates are less relevant. The best substrate in the screening, 19,20-EpDPE, was poorly hydrolyzed with a catalytic efficiency of k_{cat}/K_m = 1.54 x 10^2 s^{-1} x M^{-1} and K_m >> 30 µM. In comparison, sEH, the main enzyme involved in epoxy-fatty acid turnover in mammals, hydrolyzes 14,15-EET with k_{cat}/K_m = 0.5 x 10^6 s^{-1} x M^{-1} and a K_m = 15 µM (Decker *et al.*, 2012), thus with several orders of magnitude higher efficiency. Furthermore, other microbial EHs, such as an EH from *Aspergillus niger* or the limonene-1,2-EH from *Rhodococcus erythropolis*, possess even higher turnover rates of their substrates up to 100 µmol/mg/min (van der Werf *et al.*, 1998; Arand *et al.*, 1999b). Taken together we believe that 17,18-EpETE and also the other substrates tested are not relevant Cif substrates *in vivo*.

The EH activity was shown to be crucial for the effect of Cif on CFTR (Bahl *et al.*, 2015). The current model proposes that Cif blocks deubiquitination by stabilizing the inhibitory effect G3BP1 on USP10 (Bomberger *et al.*, 2011). Whether this stabilization is direct or indirect needs to be revealed. We hypothesize that an endogenous Cif substrate supports (or its hydrolysis product blocks) CFTR recycling potentially by increasing the inhibitory effect of G3PB1 on USP10. Whether the fatty acid epoxide substrates identified in this and previous work are involved in CFTR recycling needs to be analyzed but the low hydrolysis efficiency by Cif indicates that they are likely not the relevant *in vivo* targets.

Cif was shown to hydrolyze EpETEs and EpDPAs with rates that decrease from the n-3 to the n-6 position when tested individually. Turnover rate of the two best substrates, the n-3 epoxides 17,18-EpETE and 19,20-EpDPA was in the same range when tested individually. However, in a mixed substrate approach of EETs, EpETEs and EpDPAs, only EpDPAs and 14,15-EETs were hydrolyzed (Hvorecny *et al.*, 2017). This is in contrast with our present results. We compared the turnover of the best substrate of every substrate series, 14,15-EET, 17,18-EpETE and 19,20-EpDPA in a competing or individual format. In both formats, turnover was very similar with concentrations up to 30 µM of each substrate, which is also in line with the fact that we do not see any indication of substrate saturation in these assays.

Flitter *et al.* recently reported 14,15-EET turnover by Cif and connected it to a new, additional effect of Cif on neutrophilic inflammation in the lung. They propose that 14,15-EET produced by airway epithelial cells acts as a transcellular signal for neutrophils to generate the pro-resolving mediator 15-epi LXA4. By the hydrolysis of 14,15-EET, Cif reduces the production of 15-epi LXA4. This contributes to a robust, damaging neutrophilic inflammation which is typical for *P. aeruginosa* infection in cystic fibrosis (Flitter *et al.*, 2016). Our kinetic analysis showed a $k_{cat}/K_m = 1.29 \times 10^1\ s^{-1} \times M^{-1}$ for the turnover of 14,15-EET which is 40'000 times less efficient than sEH for the same substrate (Decker *et al.*, 2012). A significant additional effect of Cif on the 14,15-EET levels therefore seems unlikely in the presence of sEH, which was shown to be present in Calu-3 cells, freshly isolated human PMNs (granulocytes) and normal human bronchial epithelial cells (NHBE) (Planagumà *et al.*, 2010).

Despite the unknown mechanism, Cif seems to be a promising target for antibiotic treatment of *P. aeruginosa* lung infections, which is a major problem in patients with cystic fibrosis and other airway diseases. Due to antibiotic resistance and biofilm formation of *P. aeruginosa*, treatment is very difficult (Parkins *et al.*, 2018). Drugs targeting Cif might compromise the colonization of the lung by *P. aeruginosa* and reduce infections.

4.3. The physiologic functions of EHs

4.3.1. Three enzymes for the turnover of one substrate

EETs, which have many beneficial effects, can be hydrolyzed by three different enzymes, sEH, mEH and EH3 but only sEH is generally regarded as responsible enzyme for EET metabolism by many researchers, due to its kinetic properties. Under same conditions, sEH is orders of magnitudes more efficient in hydrolyzing EETs than mEH. EH3 hydrolyzes EETs faster than sEH but at the same time shows a higher K_m, resulting in a similar catalytic efficiency (k_{cat}/K_m) (Decker *et al.*, 2012). However, EH3 is mainly expressed in skin, upper gastro-intestinal tract and lung but not in the liver (Marowsky *et al.*, 2017) and its contribution to EETs turnover is unknown.

Multiple studies indicate that mEH plays a role in EETs turnover despite its kinetic disadvantage. When cells isolated from hippocampi of either mEH KO or sEH KO mice were incubated with AA, mEH accounted for 25% of the 11,12-EET, 20% of the 8,9- and 5% of the 14,15-EET turnover (Marowsky *et al.*, 2009a). Furthermore, in plasma of mEH KO mice, 8,9-EET levels were lower compared to plasma from wild type animals (Marowsky *et al.*, 2017). Beside the difference in subcellular localization and expression in different cell types, for example in the brain where mEH is expressed in neurons and sEH mainly present in astrocytes, there is another finding that points towards a distinct role of mEH in signaling molecule metabolism: An mEH variant with faster hydrolysis rate is avoided by nature. mEH

is the only EH found so far in vertebrate species that possesses a Glu instead of Asp as charge-relay acid in the catalytic triad. All other described EHs have a conserved Asp. Replacing the catalytic Glu with Asp (mEH E404D) increased the enzyme activity 20-24-fold for different substrates (Arand *et al.*, 1999a; Marowsky *et al.*, 2016). But why would evolution favor an inefficient enzyme?

For detoxification, the slower enzyme variant comes at a high cost: high mEH concentrations are required to ensure efficient detoxification. mEH expression in the liver is in the µM range (Oesch *et al.*, 2000) leading to the unusual situation that the substrate is similar or less concentrated than mEH and no enzyme saturation occurs. Below enzyme saturation, the first catalytic step determines the detoxification capacity which is similar for wild type mEH and mEH E404D. However, under saturating conditions, mEH E404D is 20-40 time faster than the wild type mEH (Arand *et al.*, 1999a) and lower enzyme expression could provide similar or more efficient detoxification. But nature prefers to express a slower enzyme version in higher amounts to ensure efficient detoxification. One explanation for this could be that the slower enzyme is an advantage in the metabolism of xenobiotic compounds like B[*a*]p where mEH contributes to the production of a carcinogenic metabolite. High amounts of the slow wild type mEH have similar detoxification capacity than low amounts of mEH E404D but the release of the toxic product is slower by the wild type mEH. However, only a subset of xenobiotics is activated to more toxic compounds by mEH. It seems more likely that the slower wild type mEH brings an advantage in physiology.

A current hypothesis is that mEH and sEH are both required to fine tune the level of EETs, for example in the brain. EETs were suggested to attenuate epileptic seizures in mice (Inceoglu *et al.*, 2013) and specifically 11,12-EET was shown to reduced excitation in CA1 pyramidal cells by inhibiting the release of glutamate and opening a G protein-coupled inward rectifier potassium (GIRK) channel (Mule *et al.*, 2017). mEH is present in neurons and with its proximity to CYPs and high affinity but slow turnover of EETs, hydrolyzes low amounts of EETs efficiently, keeping the ratio of EETs and DHETs constant. Upon a stimulus that leads to increased EET production, the slow wild type mEH is possibly saturated and EETs can accumulate resulting in paracrine EET signaling which is terminated by sEH present in astrocytes. The fast mEH E404D would quickly hydrolyze most of the EETs produced upon a stimulus abolishing paracrine signaling.

Surprisingly, in a study of Hung *et al*., pharmacological inhibition of sEH reduced spontaneous motor seizures in the pilocarpine-induced status epilepticus mouse model but sEH KO mice were more susceptible to seizures than WT mice (Hung *et al.*, 2015). One could speculate that in sEH KO mice mEH expression in the brain is upregulated (which is the case in the liver of sEH KO mice (Marowsky *et al.*, 2017)) leading to a dysregulation of EETs and higher susceptibility to seizures in sEH KO mice. Another observation that supports the theory that mEH activity is connected to epilepsy is, that the anti-

epileptic drugs valpromide and valproic acid inhibit mEH which might contribute to their pharmacologic effect (Kerr *et al.*, 1989).

More studies are required to understand the role of mEH in the turnover of signaling epoxides and to determine, whether mEH is a potential drug target, too.

4.3.2. Potential function of EH3 in skin barrier formation

EH3 can efficiently hydrolyze EETs but the role of this enzyme remains unknown. However, genetic disruption of the EPHX3 gene in mice showed no significant effects on the metabolism of EETs *in vivo* and no other overt phenotype (Hoopes *et al.*, 2017). A study which predicted a role of EH3 in ichthyosis in humans (Ala *et al.*, 2008) and its expression pattern led to the hypothesis that EH3 is important for barrier formation in the skin. This hypothesis is supported by the very recent finding that EH3 hydrolyzes an epoxy alcohol (9*R*,10*R*-*trans*-epoxy-13*R*-hydroxy-octadeca-11*E*-enoic acid, Figure 36) to a triol which is postulated to be involved in skin barrier formation (Yamanashi *et al.*, 2018). The authors hypothesize that linoleic acid that is present in the linoleate ceramide ester is oxidized by 12R-LOX and eLOX3 resulting in the respective epoxy alcohol that is esterified to the ceramide. Hydrolyzed to the triol, this compound has a disruptive effect on the lipid environment, facilitating cleavage of the ceramide for covalent coupling to protein required for barrier formation (Chiba *et al.*, 2016; Yamanashi *et al.*, 2018).

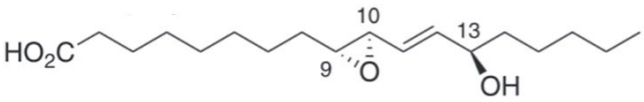

Figure 36: Free epoxy alcohol (9*R*,10*R*-*trans*-epoxy-13*R*-hydroxy-octadeca-11*E*-enoic acid) postulated to be involved in barrier formation.

Kinetic analysis revealed that EH3 hydrolyzed this epoxy alcohol 31-fold more efficient than 14,15-EET. However, the study was done with the free epoxy alcohol and in the proposed model, the epoxy alcohol is coupled to ceramide which might affect the turnover by EH3. sEH was also capable of hydrolyzing the epoxy alcohol, but at a slower rate, which could explain the lack of a skin phenotype in the single knock-outs of sEH and EH3 (Yamanashi *et al.*, 2018). A double-KO of sEH and EH3 could give more insight in the role of EHs in skin barrier formation.

4.3.3. Potential function of MEST in adipose tissue expansion

Besides the growth retardation and behavioral phenotype of MEST KO mice, MEST was also associated with adipose tissue expansion. In mice fed with a high energy diet, expression of MEST in adipose tissue

is induced and the expression levels correlated with expansion of fat mass (Nikonova *et al.*, 2008). Additionally, when MEST is depleted in adipose tissue or globally, fat mass accumulation with high fat diet is reduced compared to WT animals (Anunciado-Koza *et al.*, 2017). The correlation between a catalytic activity of MEST and adipose tissue expansion is unknown. A possible scenario could be that MEST modulates fatty-acid epoxides which are thought to be endogenous mediators of PPARs. Further studies are required to elucidate the physiologic function of MEST in development, maternal behavior and adipose tissue.

4.3.4. Understanding Cif could reveal new drug targets

Cif was shown to reduce Cl^- secretion of airway epithelial cells by interfering with CFTR trafficking. It was proposed that Cif directly or indirectly stabilizes an inhibitory interaction between USP10 and G3BP1, preventing deubiquitination of incorporated CFTR. This leads to reduced apical membrane abundance of CFTR and reduced Cl^- secretion (Bomberger *et al.*, 2011). Cif inhibitors are a promising tool for the treatment of *P. aeruginosa* infections which would be especially beneficial for patients with CF where *P. aeruginosa* infections are the leading cause for mortality (Parkins *et al.*, 2018). Additionally, increased understanding of CFTR trafficking could contribute to the development of CFTR correctors for CFTR modulator therapy of CF (Grasemann, 2017). CF is caused by many different mutations, leading to different CFTR functional defects. The most frequent mutation accounting for up to two thirds of all mutations is a deletion of Phe508 leading to defective CFTR protein traffic. The Phe508 mutated CFTR is retained at the ER from where it is rapidly sent for degradation by the ubiquitin-proteasome pathway (Amaral & Farinha, 2013). Small molecules which act as CFTR correctors to increase the abundance of CFTR on the apical plasma membrane have been developed and approved for treatment, but their mechanism of action is poorly understood. Identification of the target of Cif which we hypothesize to be an epoxide or a diol product that is involved in the ubiquitin-proteasome pathway, could shed light on CFTR protein trafficking and could boost the development of CFTR correctors.

Besides CFTR, also other members of the ABC transporter family were shown to be affected by Cif via the same mechanism. Cif enhanced the ubiquitination and degradation of the transporter associated with antigen processing-1 (TAP1) (Bomberger *et al.*, 2014). In antigen processing, TAP1 is required for translocation of peptides into the ER where they bind MHC class I molecules for antigen presentation at the plasma membrane. $CD8^+$ T cells recognize foreign peptides presented on MHC I which activates cytotoxic actions required to kill the infected cell. The downregulation of TAP1 by Cif might help *P. aeruginosa* to evade T cell response. However, further studies are needed to elucidate whether the interference of Cif with antigen presentation promotes *P. aeruginosa* infections.

Another ABC transporter that was shown to be affected by Cif is P-glycoprotein (P-gp), an efflux pump that excretes foreign substances out of cells. Cif was shown to reduce the apical membrane abundance of P-gp in kidney, airway, and intestinal epithelial cells (Ye *et al.*, 2008). P-gp is often overexpressed in cancer cells and pumps chemotherapeutic agents out of the cell, contributing to multi drug resistance in cancer. Elucidation of the mechanism of Cif on P-gp trafficking or in general ABC transporter trafficking could reveal drug targets to inhibit P-gp expression. The downregulation of P-gp could be used to increase sensitivity of tumors to chemotherapeutic drugs, improving the bioavailability of P-glycoprotein transport substrates.

5. OUTLOOK

sEH is the most promising EH to continue the project, as the trapping mutant was functional. The first step would be to increase the CatNuc peptide recovery in the sample preparation for example by the addition of BSA to the peptide mixture eluted from the gel piece, or in the FASP protocol, the evaporation step after elution could be omitted.

For mEH, EH3 and Cif, the next step is to produce functional trapping mutants which should be confirmed *in vitro*. Human mEH could be replaced by the rat enzyme, which had been used successfully. For Cif, exchange of the catalytic Glu by Gln was reported to be successful. This exchange is also promising for the other EHs. With *in vitro* trapping experiments, the sample preparation can be further optimized to reduce hydrolysis of the peptide-substrate complex. The functionality of EH4 and MEST trapping mutants cannot be tested due to the lack of known substrates, but with the experience gained with the other enzymes, the most promising mutants can be tested.

For Cif and EH3, the relevant tissues need to be addressed. In a first step, trapping could be performed in a lung cell line with Cif and in barrier-forming keratinocytes with EH3. To target these tissues *in vivo*, other AAV serotypes or direct lung instillation should be considered.

As soon as the substrate trapping is established, trapping could be expanded to other organs such as kidney and heart for sEH or adipose tissue for MEST. It is, however, important to take differences in the site of expression of the native enzyme and the virally expressed trapping enzyme into account when evaluating the results. Different promoters could be used to restrict the viral expression to cell types of interest. In a different set of experiments, animals could be challenged with xenobiotic precursors of sEH and mEH substrates to identify the extent to which these enzymes are occupied with detoxification in a concentration-dependent manner.

To investigate the mechanism of the trembling phenotype developed by mice injected with AAV-PHP.B mEH HQ, comprehensive brain tissue analysis at different time points including quantification of TH-positive dopaminergic neurons in the SN is required. Immunostaining with synaptic markers or other neuronal markers could reveal loss of synapses, dendrites or axons associated with neurodegeneration (Yamaguchi & Shen, 2013). Furthermore, the locomotive activity of the animals and the response to the administration of L-dopa should be analyzed (Tieu, 2011). If the trembling is indeed caused by loss of dopaminergic neurons, these mice could potentially be used as Parkinson's disease model. Advantages over currently used neurotoxic animal models would be robust reproducibility, apparent behavioral phenotype, and easier handling compared to neurotoxins like MPTP.

REFERENCES

Agarwal M., Austin T.W., Morel F., Chen J., Bohnlein E. & Plavec I. (1998) Scaffold attachment region-mediated enhancement of retroviral vector expression in primary T cells. *Journal of Virology* **72**, 3720-3728.

Ala U., Piro R.M., Grassi E., Damasco C., Silengo L., Oti M., Provero P. & Di Cunto F. (2008) Prediction of human disease genes by human-mouse conserved coexpression analysis. *PLoS Computational Biology* **4**, e1000043.

Amaral M.D. & Farinha C.M. (2013) Rescuing mutant CFTR: a multi-task approach to a better outcome in treating cystic fibrosis. *Current Pharmaceutical Design* **19**, 3497-3508.

Anunciado-Koza R.P., Manuel J., Mynatt R.L., Zhang J., Kozak L.P. & Koza R.A. (2017) Diet-induced adipose tissue expansion is mitigated in mice with a targeted inactivation of mesoderm specific transcript (Mest). *PloS One* **12**, e0179879.

Arand M., Cronin A., Adamska M. & Oesch F. (2005) Epoxide hydrolases: structure, function, mechanism, and assay. *Methods in Enzymology* **400**, 569-588.

Arand M., Cronin A., Oesch F., Mowbray S.L. & Jones T.A. (2003c) The telltale structures of epoxide hydrolases. *Drug Metabolism Reviews* **35**, 365-383.

Arand M., Grant D.F., Beetham J.K., Friedberg T., Oesch F. & Hammock B.D. (1994) Sequence similarity of mammalian epoxide hydrolases to the bacterial haloalkane dehalogenase and other related proteins. Implication for the potential catalytic mechanism of enzymatic epoxide hydrolysis. *FEBS Letters* **338**, 251-256.

Arand M., Hemmer H., Durk H., Baratti J., Archelas A., Furstoss R. & Oesch F. (1999b) Cloning and molecular characterization of a soluble epoxide hydrolase from Aspergillus niger that is related to mammalian microsomal epoxide hydrolase. *Biochemical Journal* **344 Pt 1**, 273-280.

Arand M., Knehr M., Thomas H., Zeller H.D. & Oesch F. (1991) An impaired peroxisomal targeting sequence leading to an unusual bicompartmental distribution of cytosolic epoxide hydrolase. *FEBS Letters* **294**, 19-22.

Arand M., Müller F., Mecky A., Hinz W., Urban P., Pompon D., Kellner R. & Oesch F. (1999a) Catalytic triad of microsomal epoxide hydrolase: replacement of Glu404 with Asp leads to a strongly increased turnover rate. *Biochemical Journal* **337**, 37-43.

Arand M., Wagner H. & Oesch F. (1996) Asp333, Asp495, and His523 form the catalytic triad of rat soluble epoxide hydrolase. *The Journal of Biological Chemistry* **271**, 4223-4229.

Argiriadi M.A., Morisseau C., Hammock B.D. & Christianson D.W. (1999) Detoxification of environmental mutagens and carcinogens: structure, mechanism, and evolution of liver epoxide hydrolase. *Proceedings of the National Academy of Sciences* **96**, 10637-10642.

Bahl C.D., Hvorecny K.L., Bomberger J.M., Stanton B.A., Hammock B.D., Morisseau C. & Madden D.R. (2015) Inhibiting an Epoxide Hydrolase Virulence Factor from Pseudomonas aeruginosa Protects CFTR. *Angewandte Chemie. International Ed. In English* **54**, 9881-9885.

Bahl C.D., Hvorecny K.L., Morisseau C., Gerber S.A. & Madden D.R. (2016) Visualizing the Mechanism of Epoxide Hydrolysis by the Bacterial Virulence Enzyme Cif. *Biochemistry* **55**, 788-797.

Bahl C.D., Morisseau C., Bomberger J.M., Stanton B.A., Hammock B.D., O'Toole G.A. & Madden D.R. (2010) Crystal structure of the cystic fibrosis transmembrane conductance regulator inhibitory factor Cif reveals novel active-site features of an epoxide hydrolase virulence factor. *Journal of Bacteriology* **192**, 1785-1795.

Bellucci G., Berti G., Chiappe C., Lippi A. & Marioni F. (1987) The metabolism of carbamazepine in humans: steric course of the enzymatic hydrolysis of the 10,11-epoxide. *Journal of Medicinal Chemistry* **30**, 768-773.

Blesa J. & Przedborski S. (2014) Parkinson's disease: animal models and dopaminergic cell vulnerability. *Frontiers in Neuroanatomy* **8**, 155.

Bomberger J.M., Ely K.H., Bangia N., Ye S., Green K.A., Green W.R., Enelow R.I. & Stanton B.A. (2014) Pseudomonas aeruginosa Cif protein enhances the ubiquitination and proteasomal degradation of the transporter associated with antigen processing (TAP) and reduces major histocompatibility complex (MHC) class I antigen presentation. *Journal of Biological Chemistry* **289**, 152-162.

Bomberger J.M., Ye S., Maceachran D.P., Koeppen K., Barnaby R.L., O'Toole G.A. & Stanton B.A. (2011) A Pseudomonas aeruginosa toxin that hijacks the host ubiquitin proteolytic system. *PLoS Pathogens* **7**, e1001325.

Brogger J., Steen V.M., Eiken H.G., Gulsvik A. & Bakke P. (2006) Genetic association between COPD and polymorphisms in TNF, ADRB2 and EPHX1. *European Respiratory Journal* **27**, 682-688.

Campbell W.B., Imig J.D., Schmitz J.M. & Falck J.R. (2017) Orally Active Epoxyeicosatrienoic Acid Analogs. *Journal of Cardiovascular Pharmacology* **70**, 211-224.

Carratt S.A., Morin D., Buckpitt A.R., Edwards P.C. & Van Winkle L.S. (2016) Naphthalene cytotoxicity in microsomal epoxide hydrolase deficient mice. *Toxicology Letters* **246**, 35-41.

Cearley C.N., Vandenberghe L.H., Parente M.K., Carnish E.R., Wilson J.M. & Wolfe J.H. (2008) Expanded repertoire of AAV vector serotypes mediate unique patterns of transduction in mouse brain. *Molecular Therapy* **16**, 1710-1718.

Chen D., Whitcomb R., MacIntyre E., Tran V., Do Z.N., Sabry J., Patel D.V., Anandan S.K., Gless R. & Webb H.K. (2012) Pharmacokinetics and pharmacodynamics of AR9281, an inhibitor of soluble epoxide hydrolase, in single- and multiple-dose studies in healthy human subjects. *Journal of Clinical Pharmacology* **52**, 319-328.

Chiba T., Thomas C.P., Calcutt M.W., Boeglin W.E., O'Donnell V.B. & Brash A.R. (2016) The Precise Structures and Stereochemistry of Trihydroxy-linoleates Esterified in Human and Porcine Epidermis and Their Significance in Skin Barrier Function IMPLICATION OF AN EPOXIDE HYDROLASE IN THE TRANSFORMATIONS OF LINOLEATE. *Journal of Biological Chemistry* **291**, 14540-14554.

Chownk M., Sharma A., Singh K. & Kaur J. (2017) mesT, a unique epoxide hydrolase, is essential for optimal growth of Mycobacterium tuberculosis in the presence of styrene oxide. *Future Microbiology* **12**, 527-546.

Coller J.K., Fritz P., Zanger U.M., Siegle I., Eichelbaum M., Kroemer H.K. & Mürdter T.E. (2001) Distribution of microsomal epoxide hydrolase in humans: an immunohistochemical study in normal tissues, and benign and malignant tumours. *The Histochemical Journal* **33**, 329-336.

Cronin A., Decker M. & Arand M. (2011) Mammalian soluble epoxide hydrolase is identical to liver hepoxilin hydrolase. *Journal of Lipid Research* **52**, 712-719.

Cronin A., Mowbray S., Durk H., Homburg S., Fleming I., Fisslthaler B., Oesch F. & Arand M. (2003) The N-terminal domain of mammalian soluble epoxide hydrolase is a phosphatase. *Proceedings of the National Academy of Sciences of the United States of America* **100**, 1552-1557.

Dahlhoff M., Frohlich T., Arnold G.J., Muller U., Leonhardt H., Zouboulis C.C. & Schneider M.R. (2015) Characterization of the sebocyte lipid droplet proteome reveals novel potential regulators of sebaceous lipogenesis. *Experimental Cell Research* **332**, 146-155.

de Medina P., Paillasse M.R., Segala G., Poirot M. & Silvente-Poirot S. (2010) Identification and pharmacological characterization of cholesterol-5,6-epoxide hydrolase as a target for tamoxifen and AEBS ligands. *Proceedings of the National Academy of Sciences of the United States of America* **107**, 13520-13525.

Decker M., Adamska M., Cronin A., Di Giallonardo F., Burgener J., Marowsky A., Falck J.R., Morisseau C., Hammock B.D., Gruzdev A., Zeldin D.C. & Arand M. (2012) EH3 (ABHD9): the first member of a new epoxide hydrolase family with high activity for fatty acid epoxides. *Journal of Lipid Research* **53**, 2038-2045.

Decker M., Arand M. & Cronin A. (2009) Mammalian epoxide hydrolases in xenobiotic metabolism and signalling. *Archives of Toxicology* **83**, 297-318.

Dengler M. (2012) Expression and Analysis of the Substrate Specificity of the CFTR Inhibitory Factor Cif. *Master Thesis*. pp. 1-66. ETH, Zurich.

Deverman B.E., Pravdo P.L., Simpson B.P., Kumar S.R., Chan K.Y., Banerjee A., Wu W.L., Yang B., Huber N., Pasca S.P. & Gradinaru V. (2016) Cre-dependent selection yields AAV variants for widespread gene transfer to the adult brain. *Nature Biotechnology* **34**, 204-209.

Domon B. & Aebersold R. (2006) Mass spectrometry and protein analysis. *Science* **312**, 212-217.

Enayetallah A.E., French R.A., Barber M. & Grant D.F. (2006) Cell-specific subcellular localization of soluble epoxide hydrolase in human tissues. *Journal of Histochemistry and Cytochemistry* **54**, 329-335.

Enayetallah A.E., French R.A., Thibodeau M.S. & Grant D.F. (2004) Distribution of soluble epoxide hydrolase and of cytochrome P450 2C8, 2C9, and 2J2 in human tissues. *Journal of Histochemistry and Cytochemistry* **52**, 447-454.

EnayetAllah A.E., Luria A., Luo B., Tsai H.J., Sura P., Hammock B.D. & Grant D.F. (2008) Opposite regulation of cholesterol levels by the phosphatase and hydrolase domains of soluble epoxide hydrolase. *Journal of Biological Chemistry* **283**, 36592-36598.

Erde J., Loo R.R. & Loo J.A. (2014) Enhanced FASP (eFASP) to increase proteome coverage and sample recovery for quantitative proteomic experiments. *Journal of Proteome Research* **13**, 1885-1895.

Fenn J.B., Mann M., Meng C.K., Wong S.F. & Whitehouse C.M. (1989) Electrospray ionization for mass spectrometry of large biomolecules. *Science* **246**, 64-71.

Flitter B.A., Hvorecny K.L., Ono E., Eddens T., Yang J., Kwak D.H., Bahl C.D., Hampton T.H., Morisseau C., Hammock B.D., Liu X., Lee J.S., Kolls J.K., Levy B.D., Madden D.R. & Bomberger J.M. (2016) Pseudomonas aeruginosa sabotages the generation of host proresolving lipid mediators. *Proceedings of the National Academy of Sciences of the United States of America*.

Fornage M., Boerwinkle E., Doris P.A., Jacobs D., Liu K. & Wong N.D. (2004) Polymorphism of the soluble epoxide hydrolase is associated with coronary artery calcification in African-American subjects: The Coronary Artery Risk Development in Young Adults (CARDIA) study. *Circulation* **109**, 335-339.

Friedberg T., Löllmann B., Becker R., Holler R. & Oesch F. (1994) The microsomal epoxide hydrolase has a single membrane signal anchor sequence which is dispensable for the catalytic activity of this protein. *Biochemical Journal* **303**, 967-972.

Gao K., Wang J.Z., Rao C.M. & Wu X.B. (2003) [Quality control of recombinant adeno-associated virus type 2/human blood coagulation factor IX]. *Yao Xue Xue Bao. Acta Pharmaceutica Sinica* **38**, 684-689.

Gillet L.C., Leitner A. & Aebersold R. (2016) Mass spectrometry applied to bottom-up proteomics: entering the high-throughput era for hypothesis testing. *Annual Review of Analytical Chemistry* **9**, 449-472.

Gillet L.C., Navarro P., Tate S., Röst H., Selevsek N., Reiter L., Bonner R. & Aebersold R. (2012) Targeted data extraction of the MS/MS spectra generated by data-independent acquisition: a new concept for consistent and accurate proteome analysis. *Molecular & Cellular Proteomics* **11**, O111. 016717.

Gomez G.A., Morisseau C., Hammock B.D. & Christianson D.W. (2004) Structure of human epoxide hydrolase reveals mechanistic inferences on bifunctional catalysis in epoxide and phosphate ester hydrolysis. *Biochemistry* **43**, 4716-4723.

Grasemann H. (2017) CFTR Modulator Therapy for Cystic Fibrosis. *New England Journal of Medicine* **377**, 2085-2088.

Groten T., Schleussner E., Lehmann T., Reister F., Holzer B., Danso K. & Zeillinger R. (2014) eNOSI4 and EPHX1 polymorphisms affect maternal susceptibility to preeclampsia: analysis of five polymorphisms predisposing to cardiovascular disease in 279 Caucasian and 241 African women. *Archives of Gynecology and Obstetrics* **289**, 581-593.

Gschwendtner A., Ripke S., Freilinger T., Lichtner P., Muller-Myhsok B., Wichmann H.E., Meitinger T. & Dichgans M. (2008) Genetic variation in soluble epoxide hydrolase (EPHX2) is associated with an increased risk of ischemic stroke in white Europeans. *Stroke* **39**, 1593-1596.

Hamm R.J., Pike B.R., O'Dell D.M., Lyeth B.G. & Jenkins L.W. (1994) The rotarod test: an evaluation of its effectiveness in assessing motor deficits following traumatic brain injury. *Journal of Neurotrauma* **11**, 187-196.

Harizi H., Corcuff J.B. & Gualde N. (2008) Arachidonic-acid-derived eicosanoids: roles in biology and immunopathology. *Trends in Molecular Medicine* **14**, 461-469.

Herrero M.E., Arand M., Hengstler J.G. & Oesch F. (1997) Recombinant expression of human microsomal epoxide hydrolase protects V79 Chinese hamster cells from styrene oxide- but not from ethylene oxide-induced DNA strand breaks. *Environmental and Molecular Mutagenesis* **30**, 429-439.

Hew B. (2019) ETH Diss. No. 25662: Substrate identification and functional analysis of α/β hydrolase fold epoxide hydrolases. p. 1-99. ETH, Zurich.

Holler R., Arand M., Mecky A., Oesch F. & Friedberg T. (1997) The membrane anchor of microsomal epoxide hydrolase from human, rat, and rabbit displays an unexpected membrane topology. *Biochemical and Biophysical Research Communications* **236**, 754-759.

Hoofnagle A.N., Whiteaker J.R., Carr S.A., Kuhn E., Liu T., Massoni S.A., Thomas S.N., Townsend R.R., Zimmerman L.J. & Boja E. (2016) Recommendations for the generation, quantification, storage, and handling of peptides used for mass spectrometry–based assays. *Clinical Chemistry* **62**, 48-69.

Hoopes S.L., Gruzdev A., Edin M.L., Graves J.P., Bradbury J.A., Flake G.P., Lih F.B., DeGraff L.M. & Zeldin D.C. (2017) Generation and characterization of epoxide hydrolase 3 (EPHX3)-deficient mice. *PloS One* **12**, e0175348.

Hou H.-H., Hammock B.D., Su K.-H., Morisseau C., Kou Y.R., Imaoka S., Oguro A., Shyue S.-K., Zhao J.-F. & Lee T.-S. (2012) N-terminal domain of soluble epoxide hydrolase negatively regulates the VEGF-mediated activation of endothelial nitric oxide synthase. *Cardiovascular Research* **93**, 120-129.

Hu C., Busuttil R.W. & Lipshutz G.S. (2010) RH10 provides superior transgene expression in mice when compared with natural AAV serotypes for neonatal gene therapy. *The Journal of Gene Medicine* **12**, 766-778.

Hung Y.W., Hung S.W., Wu Y.C., Wong L.K., Lai M.T., Shih Y.H., Lee T.S. & Lin Y.Y. (2015) Soluble epoxide hydrolase activity regulates inflammatory responses and seizure generation in two mouse models of temporal lobe epilepsy. *Brain, Behavior, and Immunity* **43**, 118-129.

Hvorecny K.L., Bahl C.D., Kitamura S., Lee K.S.S., Hammock B.D., Morisseau C. & Madden D.R. (2017) Active-Site Flexibility and Substrate Specificity in a Bacterial Virulence Factor: Crystallographic Snapshots of an Epoxide Hydrolase. *Structure* **25**, 697-707.e694.

Hvorecny K.L., Dolben E., Moreau-Marquis S., Hampton T.H., Shabaneh T.B., Flitter B.A., Bahl C.D., Bomberger J.M., Levy B.D., Stanton B.A., Hogan D.A. & Madden D.R. (2018) An epoxide hydrolase secreted by Pseudomonas aeruginosa decreases mucociliary transport and hinders bacterial clearance from the lung. *American Journal of Physiology: Lung Cellular and Molecular Physiology* **314**, L150-L156.

Inceoglu B., Zolkowska D., Yoo H.J., Wagner K.M., Yang J., Hackett E., Hwang S.H., Lee K.S., Rogawski M.A., Morisseau C. & Hammock B.D. (2013) Epoxy fatty acids and inhibition of the soluble epoxide hydrolase selectively modulate GABA mediated neurotransmission to delay onset of seizures. *PloS One* **8**, e80922.

Kalia L.V. & Lang A.E. (2015) Parkinson's disease. *Lancet* **386**, 896-912.

Kaneko-Ishino T., Kuroiwa Y., Miyoshi N., Kohda T., Suzuki R., Yokoyama M., Viville S., Barton S.C., Ishino F. & Surani M.A. (1995) Peg1/Mest imprinted gene on chromosome 6 identified by cDNA subtraction hybridization. *Nature Genetics* **11**, 52-59.

Kaplitt M.G., Leone P., Samulski R.J., Xiao X., Pfaff D.W., O'Malley K.L. & During M.J. (1994) Long-term gene expression and phenotypic correction using adeno-associated virus vectors in the mammalian brain. *Nature Genetics* **8**, 148.

Kerr B.M., Rettie A.E., Eddy A.C., Loiseau P., Guyot M., Wilensky A.J. & Levy R.H. (1989) Inhibition of human liver microsomal epoxide hydrolase by valproate and valpromide: in vitro/in vivo correlation. *Clinical Pharmacology and Therapeutics* **46**, 82-93.

Kitamura S., Hvorecny K.L., Niu J., Hammock B.D., Madden D.R. & Morisseau C. (2016) Rational Design of Potent and Selective Inhibitors of an Epoxide Hydrolase Virulence Factor from Pseudomonas aeruginosa. *Journal of Medicinal Chemistry* **59**, 4790-4799.

Kobayashi S., Kohda T., Miyoshi N., Kuroiwa Y., Aisaka K., Tsutsumi O., Kaneko-Ishino T. & Ishino F. (1997) Human PEG1/MEST, an imprinted gene on chromosome 7. *Human Molecular Genetics* **6**, 781-786.

Kollipara L. & Zahedi R.P. (2013) Protein carbamylation: in vivo modification or in vitro artefact? *Proteomics* **13**, 941-944.

Kosaka K., Suzuki K., Hayakawa M., Sugiyama S. & Ozawa T. (1994) Leukotoxin, a linoleate epoxide: its implication in the late death of patients with extensive burns. *Molecular and Cellular Biochemistry* **139**, 141-148.

Kovalchuk S.I., Anikanov N.A., Ivanova O.M., Ziganshin R.H. & Govorun V.M. (2015) Bovine serum albumin as a universal suppressor of non-specific peptide binding in vials prior to nano-chromatography coupled mass-spectrometry analysis. *Analytica Chimica Acta* **893**, 57-64.

Kozak M. (1984) Point mutations close to the AUG initiator codon affect the efficiency of translation of rat preproinsulin in vivo. *Nature* **308**, 241.

Kramer J. & Proschak E. (2017) Phosphatase activity of soluble epoxide hydrolase. *Prostaglandins and Other Lipid Mediators* **133**, 88-92.

Lacourciere G.M. & Armstrong R.N. (1993) The catalytic mechanism of microsomal epoxide hydrolase involves an ester intermediate. *Journal of the American Chemical Society* **115**, 10466-10467.

Lambert J.-P., Ivosev G., Couzens A.L., Larsen B., Taipale M., Lin Z.-Y., Zhong Q., Lindquist S., Vidal M. & Aebersold R. (2013) Mapping differential interactomes by affinity purification coupled with data-independent mass spectrometry acquisition. *Nature methods* **10**, 1239.

Laughlin L.T., Tzeng H.F., Lin S. & Armstrong R.N. (1998) Mechanism of microsomal epoxide hydrolase. Semifunctional site-specific mutants affecting the alkylation half-reaction. *Biochemistry* **37**, 2897-2904.

Laurenzana E.M., Hassett C. & Omiecinski C.J. (1998) Post-transcriptional regulation of human microsomal epoxide hydrolase. *Pharmacogenetics* **8**, 157-167.

Lee J.P., Yang S.H., Kim D.K., Lee H., Kim B., Cho J.Y., Yu K.S., Paik J.H., Kim M., Lim C.S. & Kim Y.S. (2011) In vivo activity of epoxide hydrolase according to sequence variation affects the progression of human IgA nephropathy. *American Journal of Physiology: Renal Physiology* **300**, F1283-1290.

Lefebvre L., Viville S., Barton S.C., Ishino F., Keverne E.B. & Surani M.A. (1998) Abnormal maternal behaviour and growth retardation associated with loss of the imprinted gene Mest. *Nature Genetics* **20**, 163.

Liu M., Hunter R., Nguyen X.V., Kim H.C. & Bing G. (2008) Microsomal epoxide hydrolase deletion enhances tyrosine hydroxylase phosphorylation in mice after MPTP treatment. *Journal of Neuroscience Research* **86**, 2792-2801.

Liu Y., Zhang Y., Schmelzer K., Lee T.S., Fang X., Zhu Y., Spector A.A., Gill S., Morisseau C., Hammock B.D. & Shyy J.Y. (2005) The antiinflammatory effect of laminar flow: the role of PPARgamma, epoxyeicosatrienoic acids, and soluble epoxide hydrolase. *Proceedings of the National Academy of Sciences of the United States of America* **102**, 16747-16752.

Lo W.D., Qu G., Sferra T.J., Clark R., Chen R. & Johnson P.R. (1999) Adeno-associated virus-mediated gene transfer to the brain: duration and modulation of expression. *Human Gene Therapy* **10**, 201-213.

Lord C.C., Thomas G. & Brown J.M. (2013) Mammalian alpha beta hydrolase domain (ABHD) proteins: Lipid metabolizing enzymes at the interface of cell signaling and energy metabolism. *Biochimica et Biophysica Acta* **1831**, 792-802.

Luria A., Weldon S.M., Kabcenell A.K., Ingraham R.H., Matera D., Jiang H., Gill R., Morisseau C., Newman J.W. & Hammock B.D. (2007) Compensatory mechanism for homeostatic blood pressure regulation in Ephx2 gene-disrupted mice. *Journal of Biological Chemistry* **282**, 2891-2898.

MacEachran D.P., Ye S., Bomberger J.M., Hogan D.A., Swiatecka-Urban A., Stanton B.A. & O'Toole G.A. (2007) The Pseudomonas aeruginosa secreted protein PA2934 decreases apical membrane

expression of the cystic fibrosis transmembrane conductance regulator. *Infection and Immunity* **75**, 3902-3912.

Madacki J., Laval F., Grzegorzewicz A., Lemassu A., Zahorszka M., Arand M., McNeil M., Daffe M., Jackson M., Laneelle M.A. & Kordulakova J. (2018) Impact of the epoxide hydrolase EphD on the metabolism of mycolic acids in mycobacteria. *Journal of Biological Chemistry* **293**, 5172-5184.

Manza L.L., Stamer S.L., Ham A.J., Codreanu S.G. & Liebler D.C. (2005) Sample preparation and digestion for proteomic analyses using spin filters. *Proteomics* **5**, 1742-1745.

Marowsky A., Burgener J., Falck J., Fritschy J.-M. & Arand M. (2009a) Distribution of soluble and microsomal epoxide hydrolase in the mouse brain and its contribution to cerebral epoxyeicosatrienoic acid metabolism. *Neuroscience* **163**, 646-661.

Marowsky A., Burgener J., Falck J.R., Fritschy J.M. & Arand M. (2009b) Distribution of soluble and microsomal epoxide hydrolase in the mouse brain and its contribution to cerebral epoxyeicosatrienoic acid metabolism. *Neuroscience* **163**, 646-661.

Marowsky A., Haenel K., Bockamp E., Heck R., Rutishauser S., Mule N., Kindler D., Rudin M. & Arand M. (2016) Genetic enhancement of microsomal epoxide hydrolase improves metabolic detoxification but impairs cerebral blood flow regulation. *Archives of Toxicology* **90**, 3017-3027.

Marowsky A., Meyer I., Erismann-Ebner K., Pellegrini G., Mule N. & Arand M. (2017) Beyond detoxification: a role for mouse mEH in the hepatic metabolism of endogenous lipids. *Archives of Toxicology* **91**, 3571-3585.

Mastakov M.Y., Baer K., Symes C.W., Leichtlein C.B., Kotin R.M. & During M.J. (2002) Immunological aspects of recombinant adeno-associated virus delivery to the mammalian brain. *Journal of Virology* **76**, 8446-8454.

Mayer W., Hemberger M., Frank H.G., Grummer R., Winterhager E., Kaufmann P. & Fundele R. (2000) Expression of the imprinted genes MEST/Mest in human and murine placenta suggests a role in angiogenesis. *Developmental Dynamics* **217**, 1-10.

Miyata M., Kudo G., Lee Y.H., Yang T.J., Gelboin H.V., Fernandez-Salguero P., Kimura S. & Gonzalez F.J. (1999) Targeted disruption of the microsomal epoxide hydrolase gene. Microsomal epoxide hydrolase is required for the carcinogenic activity of 7,12-dimethylbenz[a]anthracene. *Journal of Biological Chemistry* **274**, 23963-23968.

Moghaddam M.F., Grant D.F., Cheek J.M., Greene J.F., Williamson K.C. & Hammock B.D. (1997) Bioactivation of leukotoxins to their toxic diols by epoxide hydrolase. *Nature Medicine* **3**, 562-566.

Morisseau C. (2013) Role of epoxide hydrolases in lipid metabolism. *Biochimie* **95**, 91-95.

Morisseau C. & Hammock B.D. (2013) Impact of soluble epoxide hydrolase and epoxyeicosanoids on human health. *Annual Review of Pharmacology and Toxicology* **53**, 37-58.

Mrsny R.J., Gewirtz A.T., Siccardi D., Savidge T., Hurley B.P., Madara J.L. & McCormick B.A. (2004) Identification of hepoxilin A3 in inflammatory events: a required role in neutrophil migration across intestinal epithelia. *Proceedings of the National Academy of Sciences of the United States of America* **101**, 7421-7426.

Mule N.K., Orjuela Leon A.C., Falck J.R., Arand M. & Marowsky A. (2017) 11,12 -Epoxyeicosatrienoic acid (11,12 EET) reduces excitability and excitatory transmission in the hippocampus. *Neuropharmacology* **123**, 310-321.

Muller F., Arand M., Frank H., Seidel A., Hinz W., Winkler L., Hanel K., Blee E., Beetham J.K., Hammock B.D. & Oesch F. (1997) Visualization of a covalent intermediate between microsomal epoxide

hydrolase, but not cholesterol epoxide hydrolase, and their substrates. *European Journal of Biochemistry* **245**, 490-496.

Nardini M. & Dijkstra B.W. (1999) Alpha/beta hydrolase fold enzymes: the family keeps growing. *Current Opinion in Structural Biology* **9**, 732-737.

Nardini M., Ridder I.S., Rozeboom H.J., Kalk K.H., Rink R., Janssen D.B. & Dijkstra B.W. (1999) The X-ray Structure of Epoxide Hydrolase from Agrobacterium radiobacter AD1 An enzyme to detoxify harmful epoxides. *Journal of Biological Chemistry* **274**, 14579-14586.

Naso M.F., Tomkowicz B., Perry W.L., 3rd & Strohl W.R. (2017) Adeno-Associated Virus (AAV) as a Vector for Gene Therapy. *Biodrugs* **31**, 317-334.

Neckar J., Kopkan L., Huskova Z., Kolar F., Papousek F., Kramer H.J., Hwang S.H., Hammock B.D., Imig J.D., Maly J., Netuka I., Ostadal B. & Cervenka L. (2012) Inhibition of soluble epoxide hydrolase by cis-4-[4-(3-adamantan-1-ylureido)cyclohexyl-oxy]benzoic acid exhibits antihypertensive and cardioprotective actions in transgenic rats with angiotensin II-dependent hypertension. *Clinical Science (London, England: 1979)* **122**, 513-525.

Newman J.W., Morisseau C. & Hammock B.D. (2005) Epoxide hydrolases: their roles and interactions with lipid metabolism. *Progress in Lipid Research* **44**, 1-51.

Nikonova L., Koza R.A., Mendoza T., Chao P.M., Curley J.P. & Kozak L.P. (2008) Mesoderm-specific transcript is associated with fat mass expansion in response to a positive energy balance. *FASEB Journal* **22**, 3925-3937.

Oesch F. (1974) Purification and specificity of a human microsomal epoxide hydratase. *Biochemical Journal* **139**, 77-88.

Oesch F., Hengstler J.G. & Arand M. (2004) Detoxication Strategy of Epoxide Hydrolase—The Basis for a Novel Threshold for Definable Genotoxic Carcinogens. *Nonlinearity in Biology, Toxicology, Medicine* **2**, 15401420490426963.

Oesch F., Herrero M.E., Hengstler J.G., Lohmann M. & Arand M. (2000) Metabolic detoxification: implications for thresholds. *Toxicologic Pathology* **28**, 382-387.

Ohtoshi K., Kaneto H., Node K., Nakamura Y., Shiraiwa T., Matsuhisa M. & Yamasaki Y. (2005) Association of soluble epoxide hydrolase gene polymorphism with insulin resistance in type 2 diabetic patients. *Biochemical and Biophysical Research Communications* **331**, 347-350.

Ojala D.S., Amara D.P. & Schaffer D.V. (2015) Adeno-associated virus vectors and neurological gene therapy. *Neuroscientist* **21**, 84-98.

Ollis D.L., Cheah E., Cygler M., Dijkstra B., Frolow F., Franken S.M., Harel M., Remington S.J., Silman I., Schrag J. & et al. (1992) The alpha/beta hydrolase fold. *Protein Engineering* **5**, 197-211.

Orjuela Leon A.C., Marwosky A. & Arand M. (2017) Evidence for a complex formation between CYP2J5 and mEH in living cells by FRET analysis of membrane protein interaction in the endoplasmic reticulum (FAMPIR). *Archives of Toxicology* **91**, 3561-3570.

Pacifici G.M., Temellini A., Giuliani L., Rane A., Thomas H. & Oesch F. (1988) Cytosolic epoxide hydrolase in humans: development and tissue distribution. *Archives of Toxicology* **62**, 254-257.

Panigrahy D., Edin M.L., Lee C.R., Huang S., Bielenberg D.R., Butterfield C.E., Barnés C.M., Mammoto A., Mammoto T. & Luria A. (2012) Epoxyeicosanoids stimulate multiorgan metastasis and tumor dormancy escape in mice. *The Journal of Clinical Investigation* **122**, 178-191.

Parkins M.D., Somayaji R. & Waters V.J. (2018) Epidemiology, Biology, and Impact of Clonal Pseudomonas aeruginosa Infections in Cystic Fibrosis. *Clinical Microbiology Reviews* **31**.

Paterna J.C., Moccetti T., Mura A., Feldon J. & Bueler H. (2000) Influence of promoter and WHV post-transcriptional regulatory element on AAV-mediated transgene expression in the rat brain. *Gene Therapy* **7**, 1304-1311.

Planagumà A., Pfeffer M.A., Rubin G., Croze R., Uddin M., Serhan C.N. & Levy B.D. (2010) Lovastatin decreases acute mucosal inflammation via 15-epi-lipoxin A4. *Mucosal Immunology* **3**, 270-279.

Przybyla-Zawislak B.D., Srivastava P.K., Vazquez-Matias J., Mohrenweiser H.W., Maxwell J.E., Hammock B.D., Bradbury J.A., Enayetallah A.E., Zeldin D.C. & Grant D.F. (2003) Polymorphisms in human soluble epoxide hydrolase. *Molecular Pharmacology* **64**, 482-490.

Sado T., Nakajima N., Tada M. & Takagi N. (1993) A Novel Mesoderm-Specific cDNA Isolated from a Mouse Embryonal Carcinoma Cell Line: (embryonal carcinoma cell/cDNA/in situ hybridization/mesoderm/mouse embryo). *Development, Growth & Differentiation* **35**, 551-560.

Saenz-Mendez P., Katz A., Perez-Kempner M.L., Ventura O.N. & Vazquez M. (2017) Structural insights into human microsomal epoxide hydrolase by combined homology modeling, molecular dynamics simulations, and molecular docking calculations. *Proteins* **85**, 720-730.

Salganik M., Hirsch M.L. & Samulski R.J. (2015) Adeno-associated Virus as a Mammalian DNA Vector. *Microbiology Spectrum* **3**.

Sari I., Pinarbasi H., Pinarbasi E. & Yildiz C. (2017) Association between the soluble epoxide hydrolase gene and preeclampsia. *Hypertension in Pregnancy* **36**, 315-325.

Scott L.J. (2015) Alipogene tiparvovec: a review of its use in adults with familial lipoprotein lipase deficiency. *Drugs* **75**, 175-182.

Sechi S. & Chait B.T. (1998) Modification of cysteine residues by alkylation. A tool in peptide mapping and protein identification. *Analytical Chemistry* **70**, 5150-5158.

Shimada T. (2006) Xenobiotic-metabolizing enzymes involved in activation and detoxification of carcinogenic polycyclic aromatic hydrocarbons. *Drug Metabolism and Pharmacokinetics* **21**, 257-276.

Sinal C.J., Miyata M., Tohkin M., Nagata K., Bend J.R. & Gonzalez F.J. (2000) Targeted disruption of soluble epoxide hydrolase reveals a role in blood pressure regulation. *Journal of Biological Chemistry* **275**, 40504-40510.

Sisignano M., Park C.K., Angioni C., Zhang D.D., von Hehn C., Cobos E.J., Ghasemlou N., Xu Z.Z., Kumaran V., Lu R., Grant A., Fischer M.J., Schmidtko A., Reeh P., Ji R.R., Woolf C.J., Geisslinger G., Scholich K. & Brenneis C. (2012) 5,6-EET is released upon neuronal activity and induces mechanical pain hypersensitivity via TRPA1 on central afferent terminals. *Journal of Neuroscience* **32**, 6364-6372.

Smith K.R., Pinkerton K.E., Watanabe T., Pedersen T.L., Ma S.J. & Hammock B.D. (2005) Attenuation of tobacco smoke-induced lung inflammation by treatment with a soluble epoxide hydrolase inhibitor. *Proceedings of the National Academy of Sciences of the United States of America* **102**, 2186-2191.

Snyder R., Chepiga T., Yang C.S., Thomas H., Platt K. & Oesch F. (1993) Benzene metabolism by reconstituted cytochromes P450 2B1 and 2E1 and its modulation by cytochrome b5, microsomal epoxide hydrolase, and glutathione transferases: evidence for an important role of microsomal epoxide hydrolase in the formation of hydroquinone. *Toxicology and Applied Pharmacology* **122**, 172-181.

Swiatecka-Urban A., Moreau-Marquis S., Maceachran D.P., Connolly J.P., Stanton C.R., Su J.R., Barnaby R., O'toole G.A. & Stanton B.A. (2006) Pseudomonas aeruginosa inhibits endocytic recycling of CFTR in polarized human airway epithelial cells. *American Journal of Physiology: Cell Physiology* **290**, C862-872.

Takahashi M., Kamei Y. & Ezaki O. (2005) Mest/Peg1 imprinted gene enlarges adipocytes and is a marker of adipocyte size. *American Journal of Physiology: Endocrinology and Metabolism* **288**, E117-124.

Tieu K. (2011) A guide to neurotoxic animal models of Parkinson's disease. *Cold Spring Harbor Perspectives in Medicine* **1**, a009316.

van der Werf M.J., Overkamp K.M. & de Bont J.A. (1998) Limonene-1, 2-epoxide hydrolase fromRhodococcus erythropolis DCL14 belongs to a novel class of epoxide hydrolases. *Journal of Bacteriology* **180**, 5052-5057.

Vo T.T.L., Jang W.J. & Jeong C.H. (2018) Leukotriene A4 hydrolase: an emerging target of natural products for cancer chemoprevention and chemotherapy. *Annals of the New York Academy of Sciences*.

Wagner K.M., McReynolds C.B., Schmidt W.K. & Hammock B.D. (2017) Soluble epoxide hydrolase as a therapeutic target for pain, inflammatory and neurodegenerative diseases. *Pharmacology and Therapeutics* **180**, 62-76.

Wang L., Luo G., Zhang L.F. & Geng H.X. (2018) Neuroprotective effects of epoxyeicosatrienoic acids. *Prostaglandins and Other Lipid Mediators* **138**, 9-14.

Wang Z., Fang Y., Teague J., Wong H., Morisseau C., Hammock B.D., Rock D.A. & Wang Z. (2017) In Vitro Metabolism of Oprozomib, an Oral Proteasome Inhibitor: Role of Epoxide Hydrolases and Cytochrome P450s. *Drug Metabolism and Disposition: The Biological Fate of Chemicals* **45**, 712-720.

Wickliffe J.K., Ammenheuser M.M., Salazar J.J., Abdel-Rahman S.Z., Hastings-Smith D.A., Postlethwait E.M., Lloyd R.S. & Ward J.B. (2003) A model of sensitivity: 1,3-butadiene increases mutant frequencies and genomic damage in mice lacking a functional microsomal epoxide hydrolase gene. *Environmental and Molecular Mutagenesis* **42**, 106-110.

Wisniewski J.R., Zougman A., Nagaraj N. & Mann M. (2009) Universal sample preparation method for proteome analysis. *Nature Methods* **6**, 359-362.

Wu Z., Asokan A. & Samulski R.J. (2006) Adeno-associated virus serotypes: vector toolkit for human gene therapy. *Molecular Therapy* **14**, 316-327.

Yamaguchi H. & Shen J. (2013) Histological Analysis of Neurodegeneration in the Mouse Brain In: *Necrosis: Methods and Protocols* (eds. by McCall K & Klein C). Humana Press.

Yamanashi H., Boeglin W.E., Morisseau C., Davis R.W., Sulikowski G.A., Hammock B.D. & Brash A.R. (2018) Catalytic activities of mammalian epoxide hydrolases with cis and trans fatty acid epoxides relevant to skin barrier function. *Journal of Lipid Research*, jlr. M082701.

Yang L., Cheriyan J., Gutterman D.D., Mayer R.J., Ament Z., Griffin J.L., Lazaar A.L., Newby D.E., Tal-Singer R. & Wilkinson I.B. (2017) Mechanisms of Vascular Dysfunction in COPD and Effects of a Novel Soluble Epoxide Hydrolase Inhibitor in Smokers. *Chest* **151**, 555-563.

Ye S., MacEachran D.P., Hamilton J.W., O'Toole G.A. & Stanton B.A. (2008) Chemotoxicity of doxorubicin and surface expression of P-glycoprotein (MDR1) is regulated by the Pseudomonas aeruginosa toxin Cif. *American Journal of Physiology: Cell Physiology* **295**, C807-818.

Zeldin D.C., Kobayashi J., Falck J.R., Winder B.S., Hammock B.D., Snapper J.R. & Capdevila J.H. (1993) Regio-and enantiofacial selectivity of epoxyeicosatrienoic acid hydration by cytosolic epoxide hydrolase. *Journal of Biological Chemistry* **268**, 6402-6407.

Zhang W., Yang A.L., Liao J., Li H., Dong H., Chung Y.T., Bai H., Matkowskyj K.A., Hammock B.D. & Yang G.Y. (2012) Soluble epoxide hydrolase gene deficiency or inhibition attenuates chronic active inflammatory bowel disease in IL-10(-/-) mice. *Digestive Diseases and Sciences* **57**, 2580-2591.

Zincarelli C., Soltys S., Rengo G. & Rabinowitz J.E. (2008) Analysis of AAV serotypes 1-9 mediated gene expression and tropism in mice after systemic injection. *Molecular Therapy* **16**, 1073-1080.

Zou J., Hallberg B.M., Bergfors T., Oesch F., Arand M., Mowbray S.L. & Jones T.A. (2000) Structure of Aspergillus niger epoxide hydrolase at 1.8 A resolution: implications for the structure and function of the mammalian microsomal class of epoxide hydrolases. *Structure* **8**, 111-122.

ACKNOWLEDGMENTS

I want to thank all the people who supported me and contributed in different ways to my thesis:

First, I want to thank Erni who gave me the opportunity to work on this project in his lab and was always supportive. You gave me freedom to be creative and learn and showed me the way when I needed it. Your passion for science always inspired me!

Thank you, Bettina, I would not be here without you! Thank you for always being here for me, for the discussions, advice, your amazing capacity of not forgetting important things and reminding me, for listening and making lab life fun! Thank you for all the activities outside the lab, skiing, bodycombat, hikes, BBQs, dinners and parties. Two Musketeers until the end and beyond!

Thanks to the members of my committee, Uli Zeilhofer and Ursula Quitterer.

I want to thank all previous and current Toxies – for discussions, advice and support in the lab and for fun, skiing, hiking and great evenings outside the lab. Special thanks to Kira for your unbelievable endurance in proofreading and advice for all types of (life) problems and Beau for your valuable inputs and help with my thesis and your enthusiasm for science but also sports, events and our Institute. Thank you, Pascal, for all the runs, pizzas, fun and your proofreading!

A big thank you to Sandra, Michi, Martina, Marco, Thomas and all other members of the Krämer lab, for the opportunity to use your machines and for your tremendous support with the analysis.

Thank you, Mohammad, Karen, Ladina, Rebecca and Tilo for your help with animal experiments and tissue stainings.

Thanks to all members of the Butterfly Office, especially Rebecca, Karen, Ben, Mohammad, and Tina for the warm atmosphere, your help in the lab and all our amazing activities outside the lab!

Thanks to all my friends who supported me during the last five years, in particular Basil, Maxime, Nicole, Lukas, Valerie, Almuth, Regula, Prisca, and Flo!

Finally, I want to thank my parents, Sandra&Markus, Vanina&Diego and Gregor for your support, for listening and for your advice! The last five years would not have been possible without you! Special Thanks to Vanina for her tremendous help with scientific and all my other problems.

CURRICULUM VITAE

PERSONAL DATA

Surname	DENGLER
First name	Monika
Date of birth	18. August, 1988
Citizen of	Oberegg AI
Nationality	Swiss

EDUCATION

02/2014 – 01/2019	**PhD studies at the Institute of Pharmacology and Toxicology**, University of Zurich, group of Prof. Dr. Michael Arand PhD committee: Prof. Dr. Hanns Ulrich Zeilhofer, Prof. Dr. Michael Arand, Prof. Dr. Ursula Quitterer
09/2011 – 09/2013	**Master studies in Pharmaceutical Science,** ETH Zurich Master thesis at the Institute of Pharmaceutical Science, ETH Zurich, group of Prof. Dr. Michael Arand "Expression and Analysis of the Substrate Specificity of the CFTR Inhibitory Factor Cif"
09/2011 – 12/2011	Research project at the Institute of Medical Microbiology, University of Zurich, group of Prof. Dr. Brigitte Berger-Bächi "Analysis of *Staphylococcus aureus* isolates from the ANTIRESDEV study focusing on antibiotic resistance and fitness"
02/2011 – 06/2011	Exchange semester at the University of Copenhagen, Denmark
10/2007 – 09/2010	**Bachelor studies in Pharmaceutical Science,** ETH Zurich
08/2003 – 09/2007	Kantonsschule St. Gallen (high school), Major in Biology and Chemistry

POSTERS and PRESENTATIONS

38th Colloquium on Toxicology, Swiss Society of Toxicology, May 16th, 2017, Basel, Switzerland
Presentation: A bacterial epoxide hydrolase as a pathogenicity factor. M. Dengler, M. Arand.

Third Symposium of the Drug Discovery Network Zurich, DDNZ, February 10th, 2017, ETH Zurich, Switzerland. Poster: ABHD5, a potential "retard" epoxide hydrolase involved in lipolysis and skin barrier formation. P. Matthieu, M. Dengler, M. Arand

RETREATS

Retreat of the Doctoral Program Predictive Toxicology, September 11th – 12th, Vitzau, Switzerland. Presentation: A bacterial epoxide hydrolase as a pathogenicity factor – the case of Cif

Retreat of the Doctoral Program Predictive Toxicology, November 5th – 6th, Engelberg, Switzerland. Presentation: Deciphering the (patho)physiologic role of epoxide hydrolases by *ex vivo* cartography of their substrate landscape – LC-MS/MS

Retreat of the Doctoral Program Predictive Toxicology, Juni 27th – 28th, Itigen, Switzerland. Presentation: Deciphering the (patho)physiologic role of epoxide hydrolases by *ex vivo* cartography of their substrate landscape – LC-MS/MS

Retreat of the Doctoral Program Predictive Toxicology, June 1st – 2nd, Stoos, Switzerland. Presentation: Deciphering the (patho)physiologic role of epoxide hydrolases by *ex vivo* cartography of their substrate landscape

CONTINUING EDUCATION

Training program to become European Registered Toxicologist, Deutsche Gesellschaft für experimentelle und klinische Pharmakologie und Toxikologie:

Grundlagen der Organtoxikologie und –pathologie I, 16.-20.6.2014, Erfurt
Fremdstoffmetabolismus/Toxikokinetik, 25.-29.8.2014, Zurich
Safety Pharmacology, 2.-6.2.2015, Basel
Grundlagen der Organtoxikologie und –pathologie II, 23.-27.2.2015, Erfurt
Molekulare Zelltoxikologie, 16.-20.3.2015, Neuherberg
LTK Modul 1, FELASA Category B, 10.-19.8.2015, Zurich
Lebensmitteltoxikologie, 10.-14.10.2016, Hannover
Epidemiologische Methoden, 6.-10.3.2017, Hannover
Klinische Toxikologie, 11.-15.9.2017, Berlin
Chemische Kanzerogenese und Mutagenese, 27.11. – 2.12.2017, Neuherberg